Assessment of land-use/land-cover changes impact on Land surface temperature using Geospatial Technology: a case of Addis Ababa including Sheger City, Ethiopia

Barklegn Sebsibe Belayneh

A Thesis Submitted to the Department of Geomatics Engineering
School of Civil Engineering and Architecture

Presented in Partial Fulfillment of the Requirement for the Degree of Master's in Geo-Informatics

Office of Graduate Studies

Adama Science and Technology University

June, 2024
Adama, Ethiopia

Assessment of land-use/land-cover changes impact on Land surface temperature using Geospatial Technology: a case of Addis Ababa including Sheger City, Ethiopia

Barklegn Sebsibe Belayneh

Advisor
Roba Gemechu (PhD)

A Thesis Submitted to the Department of Geomatics Engineering
School of Civil Engineering and Architecture

Presented in Partial Fulfillment of the Requirement for the Degree of Master's in Geo-Informatics

Office of Graduate Studies

Adama Science and Technology University

June, 2024
Adama, Ethiopia

Approval Sheet

I the advisors of the thesis entitled "Assessment of land-use/land-cover changes impact on Land surface temperature using Geospatial Technology: a case of Addis Ababa including Sheger City, Ethiopia" and developed by Barklegn Sebsibe, here by certify that the recommendation and suggestions made by the board of examiners are appropriately incorporated into the final version of the thesis.

Roba Gemechu (PhD)		
Major Advisor/Supervisor	Signature	Date

We, the undersigned, members of the Board of Examiners of the thesis by Barklegn Sebsibe have read and evaluated the thesis entitled "Assessment of land-use/land-cover changes impact on Land surface temperature using Geospatial Technology: a case of Addis Ababa including Sheger City, Ethiopa" and examined the candidate during open defense. This is, therefore, to certify that the thesis is accepted for partial fulfillment of the requirement of the degree of Master of Science in Geo-informatics.

Dejene Tesema (PhD)		
ChairPerson	Signature	Date
Getachew Brhanemeskel (PhD)		
Internal Examiner	Signature	Date
Asfaw Mohamed (PhD)		
External Examiner	Signature	Date

Final approval and acceptance of the thesis is contingent upon submission of its final copy to the Office of Postgraduate Studies (OPGS) through the Department Graduate Council (DGC) and School Graduate Committee (SGC).

Department Head	Signature	Date
School Dean	Signature	Date
Office of Postgraduate Studies, Dean	Signature	Date

Declaration

I hereby declare that this Master Thesis entitled "Assessment of land-use/land-cover changes impact on Land surface temperature using Geospatial Technology: a case of Addis Ababa including Sheger City, Ethiopia" is my original work. That is, it has not been submitted for the award of any academic degree, diploma or certificate in any other university. All sources of materials that are used for this thesis have been duly acknowledged through citation.

Barklegn Sebsibe Belayneh

Name of student	Signature	Date

Recommendation

I, the advisor(s) of this thesis, hereby certify that I/we have read the revised version of the thesis entitled “Assessment of land-use/land-cover changes impact on Land surface temperature using Geospatial Technology: a case of Addis Ababa including Sheger City, Ethiopia” prepared under my guidance by Barklegn Sebsibe. Therefore, I recommend the submission of revised version of the thesis to the department following the applicable procedures.

Roba Gemechu (PhD)

____________________	____________________	______________
Major Advisor/Supervisor	Signature	Date

Acknowledgement

Firstly, I extend my deepest gratitude to Almighty God, the Lord of all, for my health and for making all things possible throughout my life. I am immensely thankful to my advisor, Roba Gemechu (PhD), whose guidance, supervision, support, and insightful feedback have been invaluable during the completion of this thesis. I am also appreciative of the staff at the Ethiopian National Meteorology Agency for providing all the essential data and information about the study area. I would like to acknowledge the Space Science and Geospatial Institute for their prompt provision of DEM data. Lastly, I must express my profound appreciation to my parents, friends, and course instructors, whose constant encouragement has sustained me throughout my thesis work.

Table of Contents

List of Table

List of Figures

List of Acronyms

DEM	Digital Elevation Model
DIP	Digital Image Processing
DN	Digital Number
ENVI	Environment for Visualizing Images
ERDAS	Earth Resources Data Analysis System
ETM+	Enhanced Thematic Mapper Plus
ESS	Ethiopia Statistical Service
FAO	Food and Agricultural Organization
GIS	Geographic Information System
GPS	Global Positioning System
LST	Land Surface Temperature
LU/LC	Land Use/Land Cover
LU/LCC	Land Use/Land Cover Change
NDVI	Normalized Difference Vegetation Index
NDBI	Normalized Difference Built-up Index
NDBaI	Normalized Difference Bareness Index
NDWI	Normalized Difference Water Index
OLI	Operational Land Imager
QGIS	Quantum GIS
TIRS	Thermal Infrared Sensor
TM	Thematic Mapper
TOA	Top of Atmosphere
UHI	Urban Heat Island
UNEP	United Nations Environmental Program
USGS	United States Geological Survey
UTM	Universal Transverse Mercator

Abstract

Changes in land-use and land-cover are major environmental issues that significantly impact urbanization and agricultural growth. There has been a notable and consistent rise in LST over the years, posing a significant challenge globally. This study explores how changes in land-use and land-cover affect LST. The study took place in Addis Ababa including Sheger, utilizing Geospatial technologies to extract LU/LC, LST, NDVI, NDBI, NDBaI, and NDWI using images from Landsat TM of 1991 and 2001, and Landsat 8 OLI/TIRS images of 2013 and 2023. These tools proved effective for mapping and quantifying changes in LU/LC and their impact on land surface temperatures. The study area's land surface temperature was determined using a split-window algorithm and utilized zonal statistics in a tabular format to correlate LU/LC classifications with LST. The evaluation and analysis of changes in land use and land cover from 1991 to 2023 were conducted with geospatial tools and corroborated through field data. Findings from the LU/LC analysis revealed that over 56% of the area was occupied by cropland throughout the study period (1991–2023), while built-up areas accounted for over 23%. The research showed that regions which exhibited lower Land Surface Temperatures (LST) in 1991 transitioned to higher LST by the years 2001, 2013, and 2023. This shift was primarily attributed to various changes in LU/LC, notably the expansion of Built-up area and reduction of vegetation covers in the area. The study revealing a strong negative correlation between LST with both NDVI and NDWI. Conversely, LST displayed a strong positive correlation with NDBI and NDBaI. The findings on LST revealed that the northwestern region, including Menagesha Suba and Entoto Park, in addition to the areas around Lake Geferesa and Legedadi, experienced relatively low temperatures ranging from 7ºC to 18ºC, attributed to high NDVI values. Conversely, the southeastern and eastern parts of the city recorded significantly higher LST values, peaking at 42ºC. Thus, a visual analysis of images from 1991, 2001, 2013, and 2023 reveals that the types of land use/land cover, along with the status of NDVI, NDBI, NDBaI, and NDWI, significantly influence the variability of LST values. Finally, this study suggests that geospatial technologies are essential tools for decision-makers, providing a timely and cost-effective approach to analyze and evaluate LST. These technologies also facilitate the study of LST's implications for local environments, such as the prevalence of heat waves and droughts.

Keywords: LST, NDVI.

CHAPTER I

1. INTRODUCTION

1.1. Background of the study

The Earth has undergone constant transformation over an extended period, grappling with the persistent challenge of a substantial rise in Land Surface Temperature (LST) on an annual basis. Modifications in land use and land cover (LU/LC), resulting from both natural forces and human activities, have significantly influenced climate patterns and various aspects of the Earth on both a global and regional scale (Ramachandra et al., 2012).

In contemporary times, the phenomenon of global warming is causing extensive alterations in land use and land cover (LU/LC), exerting profound impacts on various facets of the natural environment. Worldwide, shifts in LU/LC are contributing to environmental transformations, including fluctuations in the rainy season, rising sea levels, and elevated land surface temperatures (LST). The significant changes in LU/LC are primarily driven by the growing human population's demand for land for settlement and agriculture. Given that land is a finite and irreplaceable natural resource, its utilization must align with its capacity, taking into account the broader climate conditions and environmental considerations (FAO/UNEP, 1999). The expansion of the human population is leading to the conversion of natural landscapes into human-altered environments.

Land use change such as expansion of human settlements, the demand for farmland, and the development of industrial and large urban areas are significant contributors to the conversion of the natural setting, this shift from permeable and moist land uses to impermeable and dry ones, characterized by the use of paving and building materials, can adversely impact Land Surface Temperature and the overall energy budget, as highlighted by (Guo et al., 2012). Additionally, these changes have profound effects on various characteristics like surface infiltration, evaporation, runoff rates and drainage systems. Hence, there is a critical need for comprehensive studies that provide detailed information on the spatial-temporal dynamics of LU/LC and the pace of these changes. One of the primary environmental challenges in both Urban and Rural settings involves the rise in LST resulting from the transformation of vegetated areas into settlements, bare land, and farming fields.

The measurement of LST is a crucial aspect, and various sensors like AVHRR, MODIS, Landsat-5 Thematic Mapper, Landsat-7 Enhanced Thematic Mapper Plus, and Landsat-8 Thermal Infrared Sensor. Utilize thermal bands to assess this variable (Gebrekidan, 2016). LST, essentially the land's temperature, is determined through sunlight exposure (Kumar and Singh, 2016). It is also described as the temperature of the Earth's surface skin and reflects the perceived heat of the Earth's surface based on either direct measurements or information obtained through remote sensing methods (Kayet el al., 2016). As per (Rajeshwari and Mani, 2014), LST denotes the temperature given off by the Earth's surface, measured in Kelvin or Celsius. In the context of remote sensing, LST refers to the radiometric Temperatures emitted by land surfaces and detected by a sensor at specific perspectives on observation (Prata and Caselles, 1995; Schmugge et al., 1998). Its values are notably affected by the escalating presence of Greenhouse gases present in the atmosphere alterations in LST are intertwined with various factors, including alterations in land-use, seasonal fluctuations in precipitation, meteorological circumstances, and socio-economic progress (Jiang and Guangjin, 2010).

Urban thermal patterns are shaped by both the Earth's surface features and human socio-economic activities, while rural areas are influenced by land-use and agricultural practices (Yue et al., 2007). The thermal environment serves as a crucial indicator for characterizing both urban vegetation and the overall environment. Although the total energy balance in rural and urban areas is analogous, distinctions exist in the proportion of shortwave and longwave Radiation (orsolya et al., 2016).

In Africa, the rapid pace of urbanization, deforestation, and agricultural expansion is dramatically transforming the natural landscape, leading to substantial alterations in the Earth's surface characteristics. These changes intensify the urban heat island effect, accelerate climate change, and impact local weather patterns. As urban areas grow and vegetation diminishes, land surface temperatures (LST) rise, which has serious consequences for human health, biodiversity, and sustainable development (Balogun et al., 2018; Li et al., 2019). Ethiopia, in particular, has witnessed environmental degradation since the initiation of agricultural activities (Oysolya et al., 2016). The future poses challenges such as a growing population, high population pressure, reduced agricultural production, shrinking land holdings, soil fertility decline, and a Growing need for fuel and construction materials. These factors are anticipated to impact Ethiopia, leading to modifications and conversions of the environment that will affect ecology and exert pressure on the society's living standards. (Asubonteng, 2007) emphasizes that changes in land use and rapid alterations in land cover have significant implications for human survival. The primary drivers of alterations in land cover are predominantly attributed to fire, as indicated by (Nunes et al., 2005), and the clearing of forests for agricultural and settlement purposes, including urban expansion. These Changes in Land Cover not only disrupt biogeochemical cycling but also contribute to global warming, soil erosion, and shifts in land-use patterns as noted by (Huang and Siegert, 2006).

Addis Ababa, Ethiopia's capital, is undergoing rapid urbanization and significant land use and land cover (LULC) changes, which are profoundly impacting the city's land surface temperature (LST). The transformation from vegetative and agricultural lands to impervious surfaces such as buildings and roads has intensified the urban heat island effect, leading to higher temperatures within the city compared to its rural surroundings. This increase in LST poses serious challenges, including adverse effects on human health, such as heat stress and heat-related illnesses, as well as negative impacts on biodiversity and ecosystem services. The reduction in green spaces exacerbates these issues, contributing to more pronounced temperature extremes and variability. Additionally, these changes can alter local weather patterns and accelerate climate change, further complicating the city's sustainability and resilience efforts (Worku et al., 2020; Balogun et al., 2018; Li et al., 2019)

RS and GIS, along with geospatial tools, are currently offering innovative solutions for enhanced environmental management. Utilizing satellite data enables a comprehensive examination of the Earth's system, allowing the observation of patterns and changes at various scales from local to global over time. This study seeks to assess, analyze, and map the LU/LC and LST status in Addis Ababa including Sheger City, Ethiopia, leveraging the capabilities of RS and GIS. These technologies are also applied to evaluate and process meteorological data, including rainfall and temperature, providing valuable information for relevant authorities to incorporate into environmental management practices.

1.2. Statement of the problem

The rate of global climate change is causing concern, with both urban and rural area experiencing a steady rise in temperatures (Naissan and Lily, 2016). The rapid urbanization and land-use/land-cover changes in Ethiopia have led to significant alterations in the land surface temperature, contributing to the emergence of urban heat islands and potential adverse effects on the local climate (Guha, Govil, & Mukherjee, 2017).

In Addis Ababa including Sheger City, the LST has shown a consistent rise across different seasons. The expansion of urban areas, coupled with the conversion of vegetated and agricultural lands into built-up environments, has been associated with notable changes in land surface temperature (Fikru et al., 2023). These LULC changes often result in increased LST, contributing to the urban heat island effect, which exacerbates thermal discomfort, energy consumption for cooling, and can adversely impact human health (Dessie & Kinney, 2021). Despite these known effects, there is a paucity of comprehensive studies examining the specific impact of LULC changes on LST in Addis Ababa. This gap in research underscores the need for an in-depth assessment of how recent Built-up expansion and associated LULC changes are influencing LST patterns in the city. Such an assessment is crucial for informing sustainable urban planning and mitigating the adverse effects of the UHI phenomenon.

Although several studies were conducted on assessment of LULC change impact on LST, some studies used a limited number of sample points for correlation analysis, resulting in inflated maximum values due to poor sample distribution. While these researchers utilized Data from remote sensing generate surface temperature maps, they failed to statistically analyze which LU/LC factors contribute most to the increase in LST. Additionally, they lacked confidence intervals to validate their results. Many studies focus only on examining the relationships between LULC, LST, and NDVI. As Sheger City is newly established, no prior Studies have been carried out on this topic. This study aims to address these gaps by integrating various geospatial software and statistically analyzing the data using SPSS, to investigate and gain deeper insights into LU/LCC patterns and their correlation with LST, NDVI, NDBI, NDBaI and NDWI in Addis Ababa including Sheger city.

The main reason for carrying out this study in Addis Ababa including Sheger City stems from their unique characteristics, which include a range of climate conditions, different topographic patterns, and a broad range of land-use/land-cover situations.

1.3. Objectives of the study

1.3.1. General objective

The general objective of this thesis is Assessment of land-use/land-cover changes impact on land surface temperature using Geospatial Technology: a case of Addis Ababa including Sheger City, Ethiopia.

1.3.2. Specific Objectives

To accomplish the general objective, three specific objectives were developed. These include:

- To map land-use/land-cover, LST, NDVI, NDBI, NDBAI, and NDWI;
- to Analyze the correlation among LULC, LST, NDVI, NDBI, NDBAI, and NDWI across the years 1991, 2001, 2013, and 2023;
- to identify hotspots areas with significant land surface temperature anomalies resulting from LU/LCC.

1.4. Research Questions

Comprehending the influence of LU/LC and vegetation on LST holds significance for effective strategies for managing and planning land aimed at mitigating LST and adapting the study area to climate change challenges. All actions aligned with the stated general and specific objectives should be consistent with the following research question.

I. What is the relation between LULC, LST, NDVI, NDBI, NDBAI and NDWI in the study area?
II. What are the spatiotemporal patterns of LU/LCC in the Study Area?
III. What is the effect of LU/LC dynamics on LST change in the study area?

1.5. Scope of the study

This study was conducted in Addis Ababa including Sheger City, Ethiopia, where various land-use/land-cover patterns exist and have undergone changes over time. The Land Use/Land Cover in the study areas has exhibited fluctuations, leading to a corresponding rise in Land Surface Temperature in the city.The objectives of this study are to comprehend and analyze the trends in LU/LC changes, establish the relationship between LU/LC, LST, NDVI, NDBI, NDBaI and NDWI, and assess the impact of LU/LC dynamics on LST changes.

To achieve this, LST values for every LU/LC class will be evaluated, and the LU/LC classification will be substantiated through on-site field verification. The escalating LST poses environmental challenges, including Climate and seasonal fluctuations variations. Mismanagement of land for Built-up and cropland aggravate these issues, potentially causing adverse effects on the environment. Addressing this concern is crucial, and the outcomes of this study aim to provide valuable information to decision-makers by identifying different LU/LC classes and their changes.

1.6. Significance of the study

The study holds significance in various ways. Firstly, it provides valuable insights into the evolving patterns of LU/LC and LST within the study area. Secondly, the findings serve as crucial information for government policymakers, as well as those involved in management of land in urban and rural areas, as well as the management of natural resources and environmental expertise. These stakeholders can utilize the study's results to inform their decision-making processes regarding the dynamic changes in LU/LC and LST over time. Moreover, the study can serve as a foundational resource for future research endeavors. Researchers can refer to the analysis conducted in this study as a starting point for further investigations.

1.7. Limitations of the study

The temperature and rainfall data collected from the National Meteorological Agency contains some missing or null daily temperature and rainfall records. These gaps may affect the quality of the current findings related to atmospheric temperature.

1.8. Thesis Paper Organizations

This thesis comprises five chapters, each serving distinct purposes. Beginning with the introductory chapter, it addresses the background, problem statement, study objectives, research Questions, scope, significance, and limitations. Following this, the subsequent chapter delves into literature reviews. The third chapter express the study area, data and software utilized, methodologies, and various analyses such as land-use/land-cover change detection, calculation of Normalized Difference Vegetation Index, Land Surface Temperature, Urban Hotspot Area, as well as Zonal statistics and Spatial interpolation. As for the fourth chapter, it presents the results and discussions derived from the thesis's entirety. Finally, the concluding chapter summarize the thesis with its conclusions and recommendations.

CHAPTER II

2. LITERATURE REVIEW

In this chapter, complexity theory, urban system theory, fundamental notions and definitions of LULC, LST, NDVI, NDBI, NDBaI, NDWI, RS, and GIS are introduced. Additionally, an investigation is conducted into the outcomes of prior research conducted across various regions.

2.1. Complexity Theory

Complexity theory provides an insightful framework for examining the intricate and often unpredictable dynamics within urban systems, especially regarding changes in LULC and their effects on LST. This theory posits that urban areas function as complex adaptive systems characterized by numerous interrelated components that continuously evolve over time.

- Non-Linearity and Feedback Loops: Urban systems display non-linear behaviors where minor changes in one area can result in significant and often unpredictable impacts elsewhere. For instance, converting green spaces into impervious surfaces can create heat islands, which then feedback into the system by modifying local microclimates and influencing subsequent urban development patterns (Batty, 2007; Grimm et al., 2008) (Copernicus Climate) (NASA Earth Observatory). This non-linearity indicates that the effects of LULC changes on LST can be disproportionately large and complex to forecast.
- Emergent Properties: Complexity theory emphasizes the concept of emergence, where the behavior of an entire system cannot be fully understood by examining its individual components alone. For instance, the urban heat island effect arises from the combined impact of various land cover changes, such as deforestation and urban expansion. These emergent properties are essential for comprehending how urbanization affects LST and why effective mitigation strategies must consider the broader urban context instead of isolated actions (Bettencourt et al., 2007; Copernicus Climate; NASA Earth Observatory).
- Adaptation and Resilience: Urban systems continuously adapt to environmental changes, but such adaptations can sometimes aggravate existing issues. For example, as cities grow, they often respond by expanding infrastructure and increasing impervious surfaces, which can intensify the urban heat island effect.

Complexity theory helps to understand these adaptive behaviors and informs resilience planning by promoting sustainable urban practices that reduce negative impacts on land surface temperature (Alberti, 2008; Copernicus Climate; NASA Earth Observatory).

2.2. Urban System Theory

Urban system theory offers a conceptual framework for comprehending the spatial and functional dynamics of cities and how these dynamics affect LST through changes in LULC. This theory highlights the interconnections between various urban subsystems, including transportation, housing, and green spaces, and their combined influence on the urban environment.

- Spatial Configuration and Urban Form: The spatial arrangement of urban areas significantly impacts LST. Urban system theory underscores the role of urban form whether compact or sprawling in determining the extent of impervious surfaces and green spaces. Compact urban forms are generally associated with lower LST due to higher efficiency in land use and greater potential for green infrastructure integration (Newman & Kenworthy, 1999).
- Functional Interdependencies: Urban areas consist of various interdependent functions, including residential, commercial, industrial, and recreational activities. Changes in land use for one function can have cascading effects on others. For example, converting agricultural land to residential use not only increases land surface temperature (LST) due to the loss of vegetation but also alters water runoff patterns, air quality, and local climate. Urban system theory helps in understanding these interdependencies and planning for balanced land use to mitigate LST increases (Seto et al., 2012; Copernicus Climate; NASA Earth Observatory).
- Policy and Governance: Effective governance and policy-making are crucial components of urban system theory. Urban policies that promote sustainable land use, such as zoning regulations, green building codes, and urban green space preservation, can mitigate the impacts of LULC changes on LST. Urban system theory underscores the importance of integrated and coherent policies that address the multifaceted nature of urban environments (UN-Habitat, 2016).

2.3. The notion of changes in LU/LC

Activities conducted by humans such as deforestation, agriculture, and urbanization have significantly altered the Earth's surface over the past decades. The term Land Use/Land Cover (LU/LC) is commonly used in research to describe the changes, but it's important to note that LU/LC have distinct meanings. Land cover refers to the physical features observed on the Earth's surface, encompassing water bodies, soil, vegetation and hard surfaces. In comparison, land use pertains to how humans exploit and utilize the land for purposes like agriculture, settlements, forestry, and pasture, influencing processes such as hydrology, biogeochemistry and biodiversity. In this context, changes in the landscape's surface component are acknowledged only if the appearance differs between two successive observations. The Food and Agriculture Organization (FAO) describes land use as the preparations, actions, and resources undertaken by people in a specific type of land cover either induce alter or preserve it. According to definitions provided by (Di Gregorio and Jansen, 2000), and (FAO, 1999), variations in LU/LC can occur due to human-induced factors, leading to significant socio-ecological consequences and negative feedback resulting from ecosystem service degradation. (Lambin and Meyfroidt, 2010) note that transitions in LU/LC are often triggered by severe ecosystem service degradation or Changes and innovations in the social and economic spheres.

2.4. The factors contributing to alterations in LU/LC

Alterations in land utilization serve as a reflection of humanity's historical trajectory and potentially foreshadow its future. These alterations are shaped by a myriad of factors entwined with human population expansion, economic progress, technological advancements, and environmental shifts (Houghton, 1994). The transformation of land cover—where the land shifts from one type to another—and the adjustments made within a specific category constitute the essence of land-use change, typically originating at the elevation of land plots as perceived by land administrators opt for a shift to a different land utilization type (Meyer and Tuner, 1992). A pivotal element driving land-use/land-cover (LU/LC) change is population growth. Humans stand as a crucial natural resource, their relationship with the environment intricately linked and interdependent for sustainable development (Santa, 2011). Nevertheless, the significance of land use underscores the vital role of land as a fundamental yet finite resource in various human endeavors such as agriculture, forestry, energy production, industry, recreation, water catchment, settlement and storage (http://www.ciesin.org/docs/002-105/002-105b.html).Over the past three centuries, Earth's cultivated land area has expanded by over 45%, surging From 2.65 million square kilometers to 15 million square kilometers. Simultaneously, other natural resources, particularly forests, have dwindled because of the growth of agricultural land and urbanization (Santa, 2011). The prevalent deforestation in numerous developing nations is commonly linked to the tandem challenges regard to increase in population and poverty (Mather and Needle, 2000).

Land-use and land-cover changes have emerged as significant global challenges, playing a pivotal role in driving widespread environmental transformations (FAO, 1999). These alterations, characterized by the expansion of agricultural land in rural areas, deforestation, urbanization, and various Natural events and human actions, contribute to substantial modifications in worldwide systems and processes. Throughout history, a primary catalyst for land-use changes has been the extensive growth of agricultural land on an international level (Houghton, 1994). Climate change denotes a lasting shift in the climate of a region. Key indicators of climate change encompass an increased frequency of droughts, rising global temperatures, heightened occurrences of tropical cyclones, floods, diminished annual rainfall, reductions covered in ice over the mountains, and escalating sea levels (Alemayehu, 2008). The Environmental Protection Agency of the United States (USEPA, 2004) has identified general causes of land-use/land-cover changes as:

I. Natural phenomena, including alterations in climate and the atmosphere, as well as occurrences like wildfires and pest invasions.
II. The immediate impact of human actions, like building roads, unauthorized housing construction, and the clearing of trees through deforestation.
III. The repercussions of human actions include indirect outcomes, such as the redirection of water causing a decrease in the water table.

2.5. Ethiopia undergoes alterations in LU/LC

In Ethiopia, the availability of natural resources varies, and their management varies significantly across different regions. This diversity is due to differences in topography, biogeography and climate. LU/LCC are increasing due to human activities, and these changes also impact humans (Agarwal et al., 2002). The dynamics of land use and land cover modify the availability of various natural resources such as water, plants, soil, livestock feed, and others (Ali, 2009). Previous research indicated that Ethiopia has experienced significant land use and land cover changes across various regions, with cultivated land expanding at the cost of forested areas, even into hilly terrain, due to land scarcity Especially in Ethiopia's highlands, there is a long-standing history of human settlement and agricultural practices which has continued up to the present day. Highland areas experiencing population growth, leading to the depletion of natural resources and unsustainable practices (Miheretu and Yimer, 2017).

2.6. Geographic Information System

A GIS is a specialized system crafted to collect, store, and process, analyze, oversee, and display data with spatial or geographic attributes (Coppin and Bauer, 1996). GIS data can be broadly categorized into spatial and non-spatial types, where spatial data possesses location values, and non-spatial data typically describe spatial information in tabular form. In the words of (Burrough, 1990), GIS data encompasses three dimensions: spatial (geographic), temporal (time), and attribute. Some individuals view a GIS as a combination of hardware and software tools that facilitate the analysis and processing of information (Maguire, 1991). Contrary to a mere digital repository of spatial elements such as points, areas and lines, GIS is also proficient in spatial analysis, examining relationships between these objects based on their position and shape (Maguire, 1991). (Foresman, 1998) notes that the convergence of computing technology and mapmaking in the 1960s opened up possibilities beyond traditional cartography, introducing techniques like map superimposition and overlay to diverse fields. This integration of climate, terrain, environment, agronomic, social, economic and institutional data empowers both managers and scientists with a potent modeling tool, allowing for comprehensive analysis and decision-making.

2.7. Remote Sensing

RS involves acquiring information without direct physical contact (Lillesand and Kiefer, 2000). In contemporary usage, the term primarily refers to the technical methods of collecting data from airborne and space-based sources. Although Monitoring the Earth using airborne platforms has a history spanning 150 years, significant advancements and innovations have occurred mostly in the last few decades (Zubair, 2006). The utilization of balloons for earth observation in the 1860s marked a crucial milestone in the evolution of RS (Lillesand and Kiefer, 2000). Data can be acquired through natural observation with the naked eye or using instruments like cameras that measure radiation (radiometric). Satellite-based remote sensing important in providing valuable information for assessing Many different features of the atmosphere environment, meteorology, climatology, agronomy, ecology, and environmental protection (Kern, 2011). At its core, remote sensing involves the measurement and recording of electromagnetic radiation that is emitted or reflected by the Earth's surface (Hardegree, 2006). This technique allows for the investigation and understanding of the patterns of LU/LCC over time.

2.8. GIS and RS role to Detect Changes in LU/LC

The utilization of RS and GIS methods is widespread globally when investigating historical transformations in LU/LC and analyzing land surface temperature. Remote sensing has proven effective in detecting various features for Examples vegetation, air pollution, and LST, providing a wealth of data at the earth surface for detailed analysis and change detection through airborne and space borne means (Zha, 2012; Weng, 2004). Additionally, comprehending the correlation between LU/LC and LST is crucial for effective land management. The technology offers a diverse range of data, including historical information, and with reduced data costs and enhanced resolution from satellite systems, RS is poised to have an even more significant impact on detecting LU/LCC. Landsat instruments, including the Landsat Multispectral Scanner (MSS) and the Landsat Thematic Mapper (TM), along with image classification techniques, enable the analysis of land-use/land-cover changes over time (Gumindoga, 2010). Beginning in 1972, Landsat satellites have consistently supplied comprehensive, worldwide coverage through high-resolution multispectral imagery. Their extensive track record and dependability have established them as a widely utilized resource for capturing LU/LCC over time, as noted by Turner et al. in 2003. The launch of Landsat 7 with ETM+ sensors in 1999 further signifies the evolution of this satellite system. (Macleod and Congation, 1998) identify four crucial Elements related to detecting change in LU/LC that play a crucial role in the surveillance of natural resources.

- Identifying the features of the alteration.
- Identification and discovery of the alterations that have taken place.
- Determining the size or scope of the alteration
- Evaluating and examining the spatial arrangement of alterations.

The fundamental principle behind employing RS data used for change detection involves identifying modifications in land cover lead to corresponding modifications in values of radiance, which are detectable through remote sensing technology.

2.9. Urban heat island

The UHI refers to a metropolitan or urban area that experiences notably higher temperatures compared to the rural regions that encircle it, primarily as a result of human activities. The phrase 'heat island' characterizes developed areas that exhibit elevated temperatures in contrast to nearby non-urban regions (Sobrino et al., 2012). The UHI phenomenon occurs when both temperatures of the air and surfaces in urban zones become significantly higher than those observed in adjacent areas. Land-cover change has emerged as a pivotal element in contemporary approaches to Supervising the use of natural assets and environmental monitoring (Sobrino et al., 2012). The IPCC, which stands for the Intergovernmental Panel on Climate Change Report highlights that climate change has played a substantial role in the considerable rise of the global mean temperature (IPCC, 2014). Several contributing factors significantly contribute to the formation of the urban heat island, including the use of low albedo materials, obstruction of wind flow, presence of air pollutants, human congregation, reduction of tree cover, and increased reliance on air conditioning (Nuruzzaman, 2015).

2.10. Temperature of the Earth's land surface

Land surface temperature, as defined by (Kayet et al., 2016), refers to the temperature at the Earth's surface, often described as the skin temperature of the Earth's. The perception of the "surface" varies when observed from a satellite, depending on the location and time, as highlighted by (Kumar and Singh, 2016). The utilization of RS and geospatial tools is pivotal in the quantitative assessment of LST. (Khin et al., 2012) note that LST is obtained through the geometrically adjusted Landsat TIRS band 6, as well as Landsat 8 TIRS bands 10 and 11. The process of determining the LST for a specific area involves considering its brightness temperature and ground surface radiative emission. (Md Shahid, Rajeshwari and Mani, 2014) emphasize utilizing the split window algorithm in calculating land surface emissivity. (Kerr et al., 2004) stress that LST provides valuable information regarding the disparity between the surface equilibrium states, which is vital for various applications. (Paramasivam, 2016) offers an additional definition, characterizing LST As the surveillance of surface temperature through pixel-derived observations through remote sensing. The temperature of urban land surfaces exhibits specific characteristics determined by its surface energy balance. This balance is influenced by various properties, including sky, wind conditions and orientation exposure to sunlight, radiative capacity for reflecting solar and infrared radiation, infrared emission capability, surface moisture availability for evaporation, and surface roughness (Voogt, 2000). Changes in LU/LC contribute to alterations in LST, prompting Managers in urban and rural areas assess urban surface temperature and its effect on the adjacent rural areas. This evaluation is crucial for urban planning and overall land management (Becker et al., 1990).

2.11. Normalized Difference Vegetation Index

The NDVI is a metric Derived from reflectance measurements within the near-infrared (NIR) and red portions of the spectrum, as outlined by Burgan and Hartford in 1993. To compute NDVI, one subtracts the value of the red band from the near-infrared, then divides the result through the total of the near-infrared and red band values. The resulting NDVI the values vary between -1 and 1. Negative values indicate the presence of water, clouds, snow, non-reflective surfaces, and other non-vegetated areas, with positive values signify vegetated areas and reflective surfaces regions. Vegetation exhibits a direct correlation with the moisture, thermal and radiative properties of the Earth's surface, influencing LST as discussed by (Weng, 2004). Alongside NDVI, the Normalized Difference Moisture Index (NDMI) serves as another way to measure the urban heat island effect on the surface in Landsat satellite images. NDMI is calculated using the formula (NIR-IR)/(NIR+IR), evaluating the moisture content of landscape elements, particularly in soils, rocks, and vegetation. A value greater than 0.1, depicted by light colors, indicates a high humidity level, while Values near -1, represented by dark colors, signify a low humidity level, as explained by Mihai in 2012.

Previously, researchers from various locations outside Ethiopia conducted studies on the correlation between LU/LCC and their effect on LST. However, within Ethiopia, there are relevant papers addressing the same topic. One such example is (Gebrekidan, 2016), who explored the modeling using satellite data to measure land surface temperature in Addis Ababa. This research was presented at the United Nations Conference Centre, Africa hall in Addis Ababa, Ethiopia during the ESRI conference on Education GIS in Eastern Africa took place. On September 23-24, 2016. Gebrekidan's study specifically concentrated on modeling the LST of Addis Ababa city, utilizing Landsat 5 & 8 data spanning from 1985 to 2015. The results of the study revealed a negative correlation between the NDVI and LST. The study underscores the importance of implementing urban greening initiatives and increasing vegetation cover to sustain the city's ecosystem and mitigate the UHI effect.

(Streutker, 2003) states that a promising approach for examining urban surface temperature involves the utilization of remote sensing or airborne technology. The assessment of LST through RS data is prevalent, especially in research focused on evapotranspiration and processes related to desertification. Additionally, (Walsh et al., 2011) asserted that anthropogenic factors such as urban structures (e.g., buildings, roads, and infrastructure) contribute to the rise in atmospheric temperature. The widespread application of LST in environmental studies has elevated remote sensing of LST to a significant academic concern during the last few decades. Undoubtedly, land surface temperature, as highlighted by (Buyadi et al., 2013), stands out as one of the crucial parameters Shaping the exchanges and movements between the Earth's surface and the air in surface-atmosphere dynamics.

2.12. Normalized Difference Built-up Index

The NDBI is a remote sensing metric, serves to identify and measure built-up regions within an image. Derived from a formula incorporating SWIR (Shortwave Infrared) and NIR (Near Infrared) spectral reflectance values, NDBI typically yields a range between -1 and 1. Elevated values signify a greater presence of built-up areas, while negative values denote non-built-up regions. This index holds significant relevance in urban research, aiding in the Assessment of urban growth, tracking changes in built-up areas over time, and scrutinizing urban growth patterns. Its utility extends to the study of urban heat islands, environmental surveillance, and evaluating the effects of urbanization on natural ecosystems. Numerous researchers have utilized NDBI as a critical tool in urban research. For example, (Smith et al., 2018) employed NDBI for examining urban expansion patterns and Monitoring alterations in urban development over time, showcasing its effectiveness in evaluating urban growth dynamics and its implications for urban planning. The correlation between LST and NDBI has been extensively investigated within UHI studies. (Chen et al., 2019) explored the relationship between NDBI values and LST variations to identify intensity of urban heat islands in urban regions, illustrating the usefulness of NDBI in quantifying the impacts of UHI and guiding mitigation strategies. Furthermore, NDBI has found application in environmental monitoring and management endeavors. (Li et al.,2020) employed NDBI to evaluate the influence of urbanization on ecological landscapes and habitat fragmentation, underscoring the necessity of integrating NDBI analysis into environmental assessments to address the detrimental impacts of urban expansion on natural ecosystems.

2.13. Normalized Difference Bareness Index

The NDBaI serves as a remote sensing metric for gauging the prevalence of bare expanses within a given region. It holds particular significance within urban and suburban areas settings, where the distinction between developed areas and open terrain holds critical importance across a spectrum of uses including urban heat island analysis, land use planning and urban growth monitoring. Expressed as $NDBaI$= ($SWIR$−TIRS)/ ($SWIR$+TIRS), the NDBaI formula quantifies the difference between thermal infrared (TIRS) and short-wave infrared (SWIR) spectral reflectance. It leverages the insight that vegetation typically shows significant presence in the near-infrared spectrum while absorbing in the short-wave infrared spectrum. Conversely, barren surfaces such as soil, pavement, and rooftops exhibit minimal near-infrared reflectance but relatively higher reflectance in the short-wave infrared range. By normalizing the discrepancy between these two bands, NDBaI enhances the differentiation between vegetated and barren surfaces. Index the values vary between -1 and 1, where positive values denote areas dominated by bare surfaces, negative values signify areas abundant in vegetation, and values near zero suggest a balanced coexistence of both. NDBaI's computation can draw upon diverse remote sensing datasets, including multispectral satellite imagery or aerial sensors. Its application facilitates the mapping and characterization of barren terrain, streamlining evaluations of land cover dynamics, urban expansion, and environmental surveillance across natural and urban landscapes alike. In their study, (Ghosh, Swati, et al., 2015) delve into the efficacy of diverse remote sensing indices, such as NDBaI, in evaluating the impacts of urban heat islands (UHIs). Emphasizing the pivotal role of NDBaI in quantifying bare surfaces within urban settings, the review underscores its importance in comprehending UHI dynamics. In (Bhandari, Subodh, et al., 2016) utilize NDBaI alongside other remote sensing indices to examine the urban development trends in Western Kathmandu, Nepal. By employing NDBaI, they can pinpoint bare surfaces and constructed areas, thereby aiding in the Assessment of urban growth and alterations in land usage over time. Meanwhile, (Weng, Qihao, and Doug Spillum, 1999) introduce a methodology for tracking LU/LCC within urban environments using remote sensing data. Their study harnesses NDBaI to identify bare surfaces, thus enriching the understanding of urban land cover dynamics and enhancing the accuracy of change detection analyses.

2.14. Normalized Difference Water Index

The NDWI stands as a prevalent spectral index in remote sensing, serving to detect the existence of water bodies in images. Its computation involves utilizing reflectance data from two distinct spectral bands, typically near-infrared (NIR) and either green or shortwave infrared (SWIR), contingent on the particular application and available bands. The NDWI formula is expressed as follows: $NDWI$= (Green−NIR)/(Green+NIR). NIR denotes the reflectance value in the near-infrared spectrum, while Green represents the corresponding value in the green band. NDWI values typically span Ranging between -1 and 1, with values that are more elevated signaling a greater probability of water presence, and smaller numbers signifying the absence of water features. NDWI offers distinct advantages due to water bodies' tendency to exhibit high NIR reflectance owing to water absorption characteristics, in contrast to non-water features such as soil and vegetation, which typically possess lower NIR reflectance. Through a comparison of NIR and SWIR band reflectance values, NDWI effectively accentuates water bodies, showcasing a substantial disparity in reflectance when juxtaposed with surrounding land features. The widespread adoption of NDWI across various domains, encompassing hydrological studies, land cover mapping, and environmental monitoring, underscores its efficacy in delineating water bodies from remotely sensed imagery. In 1996, McFeeters introduced the NDWI as a means of identifying water bodies visible in images captured remotely, showcasing its efficacy in discerning water bodies from other types of land cover. This seminal work laid the groundwork for the widespread utilization of NDWI in hydrological studies and land cover mapping. Nearly a decade later, in 2006, Xu proposed adjustments to the NDWI algorithm aimed at heightening its sensitivity to open water features, particularly in scenarios where water bodies lack clear contrast with their surroundings.

2.15. LU/LCC and its impact on LST

The escalation of LST can be attributed to significant factors such as LU/LCC. Numerous researchers concur that alterations in land use and the unregulated utilization of land resources contribute to the rise in land surface temperature. (Oluseyi et al., 2011) have explored spatial correlations, highlighting changes in specific LU/LC. Their study focuses on the variations in LST from 1995 to 2006 in Anyigba Town, Kogi State, Nigeria. The findings reveal a 1ºC rise in surface temperature for vacant land, built-up areas, and streams, where cultivated land and plants experienced respective increases of 0.95ºC. The influence of land use and land cover changes on land surface temperature varies across different latitudes, exemplified in the tropical temperate regions of South Asia and East Asia (Shukla, 1990). Investigating the connection between changes in land use, land degradation and biodiversity in East Africa, (Matimal et al., 2009) demonstrate transformations of land cover into grazing crop land and built-up areas. (Yue et al., 2007) utilized integrated remote sensing techniques to assess the correlation between NDVI and LST in Shanghai, employing Landsat7 ETM+ data. Their findings indicate distinctive influences of various Land Use/Land Cover (LU/LC) classes on both LST and NDVI, as determined by the ETM+ sensor within the urban setting of Shanghai.

2.16. Empirical literature review

(Bülent Karaku, 2019) aims to investigate how changes in Land Use/Land Cover (LULC) affect Land Surface Temperature (LST) in Sivas City Center and nearby areas. Understanding LULC changes is crucial in urban planning. LST and UHI are key factors linked to these changes and should be considered in such studies. RS and GIS are commonly employed to gather such data. Karaku's study analyzed Landsat satellite images from 1989 to 2015 to explore the correlation between LULC, NDVI, and LST, revealing the intensity of UHI. The study clearly indicated a rise in urban and agricultural areas alongside a decline in barren land over time. Changes in Land Surface Temperature (LST) were linked to factors like construction materials, greenery, geography, and topography. Urban and barren lands exhibited the highest LST, with urban areas showing fluctuating temperatures while rural areas tended to cool. The increase in urban areas led to a noticeable UHI effect.

Similarly, (Suzana Binti Abu Bakar et al., 2016) studies to explore the link between LST and LU/LC on Langkawi Island. They analyzed satellite imagery from 2002 to 2015, employing indices like NDVI, NDBI, and MNDWI alongside classifiers like MLC and SVM. SVM exhibited higher accuracy (90%) compared to MLC (86.62%). Results indicated a rise in temperature with increased impervious surfaces and a decline in vegetated areas. The study suggests using NDVI, NDBI, and MNDWI as indicators to monitor Land Surface Temperature influenced by LU/LCC.

In (G. Worku et al.,2021) aims to estimates changes in vegetation and Land Surface Temperature (LST) in Addis Ababa, Ethiopia, using satellite data from Landsat TM (1985) and Landsat 8 OLI (2015). The analysis employed supervised image classification and the maximum likelihood algorithm to assess land use/land cover changes. Results indicated a significant reduction in vegetation cover and a rapid increase in built-up areas, from 18.23% in 1985 to 33.86% in 2015. This urban expansion led to a 3-8°C increase in LST in central areas and regions with low vegetation cover. A negative correlation was found between the Normalized Difference Vegetation Index (NDVI) and LST across all sub-cities. The findings highlight the importance of strategies to mitigate urban heat stress.

Similarly, (Tafesse, 2017) explored how changes in land use affect land surface temperature (LST) in Adama Zuria Woreda. Employing GIS and RS techniques, he analyzed data from Landsat imagery from the years 1989, 1999, and 2016. The study revealed that farmland dominated the area, with more than 60% Coverage, then shrub land at over 12%. Results indicated a shift towards higher LST, attributed to decreased vegetation cover. Correlation analysis between land cover classes and LST, using zonal statistics, showed a negative relationship with NDVI, with R2 values of 96%, 97.5%, and 98.5% for 1989, 1999 and 2016 respectively. Areas with high NDVI exhibited lower LST values, while those with low NDVI had higher LST values, demonstrating the significant role of land cover and vegetation status in LST variability over time but he uses only 10 samples for computing correlation among LST and NDVI.

Previously, research both at the global and national levels used geospatial techniques to identify and analyzed the impact of land use land cover change in land surface temperature, their methodologies and findings differ. Some studies used a limited number of sample points for correlation analysis, resulting in inflated maximum values due to poor sample distribution. While these researchers utilized Data from remote sensing generate surface temperature maps, they failed to statistically analyze which LU/LC factors contribute most to the increase in LST. Additionally, they lacked confidence intervals to validate their results. Many studies focus only on examining the relationships between LULC, LST, and NDVI. Some researchers relied on outdated data and software for analyzing surface temperature variations. As Sheger City is newly established, no prior Studies have been carried out on this topic. Therefore, this study aims to address these gaps by integrating various geospatial software and statistically analyzing the data using SPSS. It seeks to analyze correlations between different land use classes and variables such as LST, NDVI, NDBI, NDBaI, and NDWI using 188 well-distributed samples.

CHAPTER III

3. METHODOLOGY

3.1. Description of the study area

3.1.1. Location

Addis Ababa including sheger city serves as the political, economic, and cultural center of the country. The geographical location of the study area is 08º 46′ – 09º 14′ N and 38º 30′ – 39º 02′ E. From the entire extent of the study area (2,038.56km^2), Addis Ababa city covers 21.10% (430.26km^2) and Sheger city area covers 78.90% (1608.30km^2).

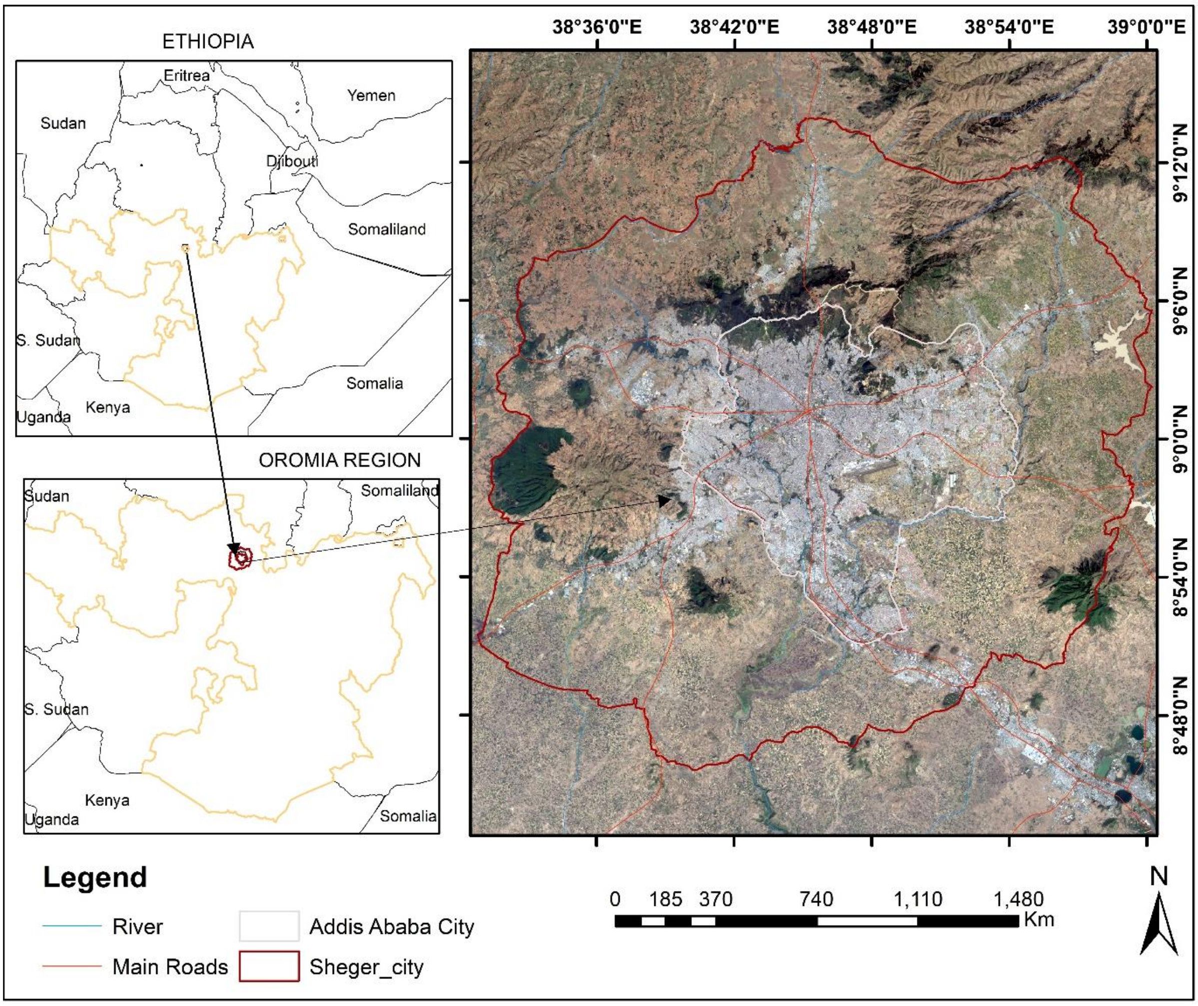

Figure 3.1 Study area map.

3.1.2. Topography

The study area elevation ranges from 1,950m to 3,390m above mean sea level. The southern part of the study area, including the Akaki Kality area, has a lower elevation whilst the northern part of the study area including mount Entoto and the western part of the study area Suba Menagesha Forest has a higher elevation. The central part has a medium elevation when compared to the other parts. Figure 3.2 shows the elevation map of the study area extracted from 20m DEM (SSGI).

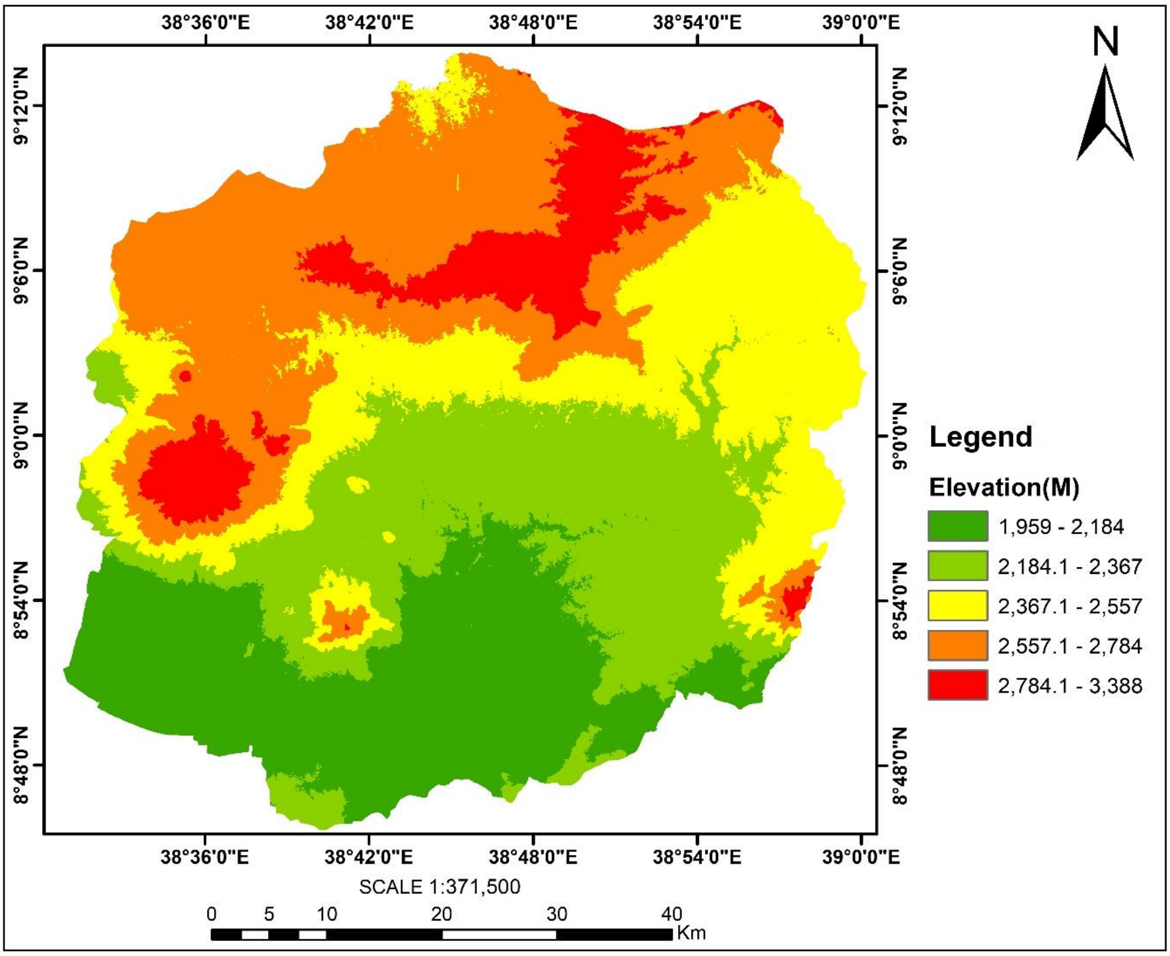

Figure 3.2 Elevation map of the study area.

3.1.3. Climate

I. Rainfall

A comprehensive analysis of rainfall data spanning from 1991 to 2023, collected from multiple meteorological stations including Addis Ababa Bole, Addis Ababa Obs, Aleltu, Enchini, Guranda Meta, Sendafa, Zequala, and Boneya, indicates an average annual precipitation of 1242.14 mm. The highest monthly average rainfall recorded was 288.83 mm in July, as illustrated in Figure 3.3. Typically, the peak rainy season occurs in March, June, July, August, and September. In contrast, January, October, November, and December are generally dry months. Temperature-wise, may is usually the warmest month, while July tends to be the coolest. Of all the months, December consistently has the least amount of rainfall.

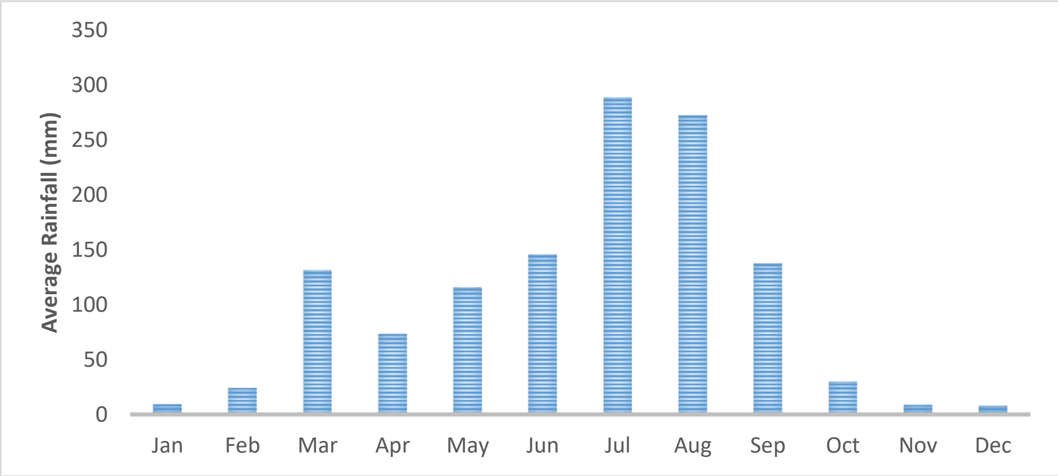

Figure 3.3: Distribution of the average monthly rainfall in the study area.

II. Temperature

The average yearly temperature in Addis Ababa, including Sheger City, is 24.72°C. Has a subtropical climate influenced by its altitude, the regions situated at elevations from 1,950 to 3,390 meters above sea level. In the study area, May is the warmest month, reaching an average peak temperature of 29.5°C. Further details can be found in Figure 3.4.

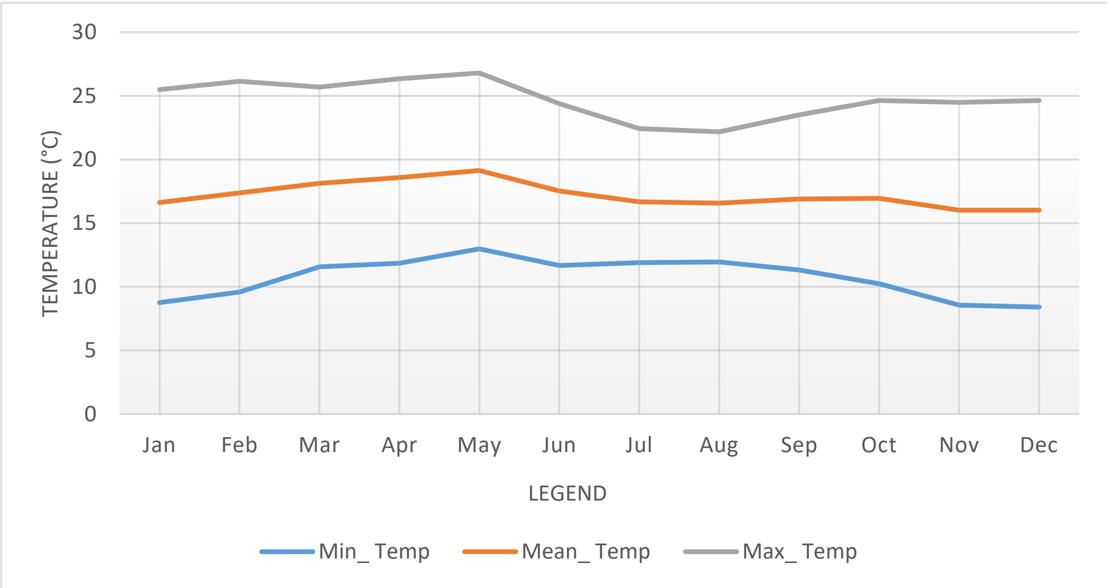

Figure 3.4: Maximum, mean and Minimum Monthly Temperature during 1991–2023.

3.1.4. Population

The population of Addis Ababa including sheger city in 2007 was three million two hundred seventy-eight thousand four hundred fifty (3,278,450). After eight years, the population number increased by 72.47% and reached three four million five hundred twenty-three thousand six hundred twelve (4,523,612) in the year 2022 projected (CSA, 2022).

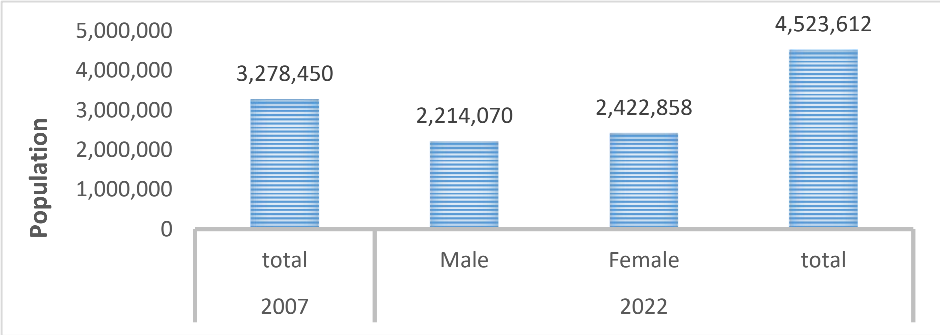

Figure 3.5: Population of study area

3.2. Research Approach and Design

This study utilized quantitative research approach to assess the impact of LULC changes on LST, first acquire high-resolution, multi-temporal satellite imagery Landsat, and relevant ancillary data such as meteorological records and topographical maps. Used supervised classification techniques, categorize land cover types and validate the classifications with ground truth data. LST extracted from thermal infrared bands using split-window algorithms, validated against in-situ measurements. Change detection methods, including post-classification comparison and image differencing, identify LULC changes over time. Statistical analyses, such as Pearson correlations and regression models, are quantify the relationship between LULC changes and LST. Spatial analysis using GIS tools will visualize and analyze the spatial patterns of LST variations, employed techniques like hotspot and cluster analysis to identify significant changes. This comprehensive approach ensures a robust understanding of how LULC changes influence LST, providing valuable insights for urban planning and environmental management.

3.3. Data and software

This research utilized both primary and secondary data sources. The primary data, which mainly consisted of satellite data, was the most crucial. The secondary data, referred to as ancillary data, was gathered from various governmental and non-governmental organizations, along with published sources.

3.3.1. Primary data

The main data set comprises Landsat satellite imagery sourced from the USGS, including Thematic Mapper (TM) images from 1991 and 2001, as well as images from the operational land imager/thermal infrared Sensor (OLI/TIRS) for the years 2013 and 2023. Additionally, digital elevation model (DEM) data with a 20m x 20m resolution was utilized to map the area's elevation. Field data, consisting of GPS coordinates for various LU/LC classes, verification.

3.3.2. Satellite image data acquisition

Images from Landsat 5 TM for the years 1991 and 2001, and Landsat 8 OLI/TIRS for the years 2013 and 2023, were collected. These cloud-free images covered the study area on path 168 and row 054 and were downloaded from the Earth Explorer website of the United States geological survey (USGS). The data utilizes the World Geodetic System 1984 (WGS84) projection. The remote sensing images were employed to assess Land Surface Temperature (LST), Normalized Difference Vegetation Index (NDVI), Normalized Difference Built-up Index (NDBI), Normalized Difference Bareness Index (NDBAI), Normalized Difference Water Index (NDWI), and Land Use and Land Cover (LULC) of Addis Ababa including Sheger city. These are detailed in Table 3.1 and the multispectral bands are depicted in Figure 3.6.

Table 3.1: Satellite image used in the study.

Date of Acquisition YYYY/MM/DD	Sensor	Path	Row	Multispectral Band	Thermal Band	Spectral range(μm)	Spatial Resolution	Source
1991/01/19 2001/12/16	TM	168	054	1 to5 and7	6	10.40-12.50	120m	USGS
2013/12/01 2023/11/27	OLI & TIR			1 to7 and9	10 and 11	10.60-12.51	100m	

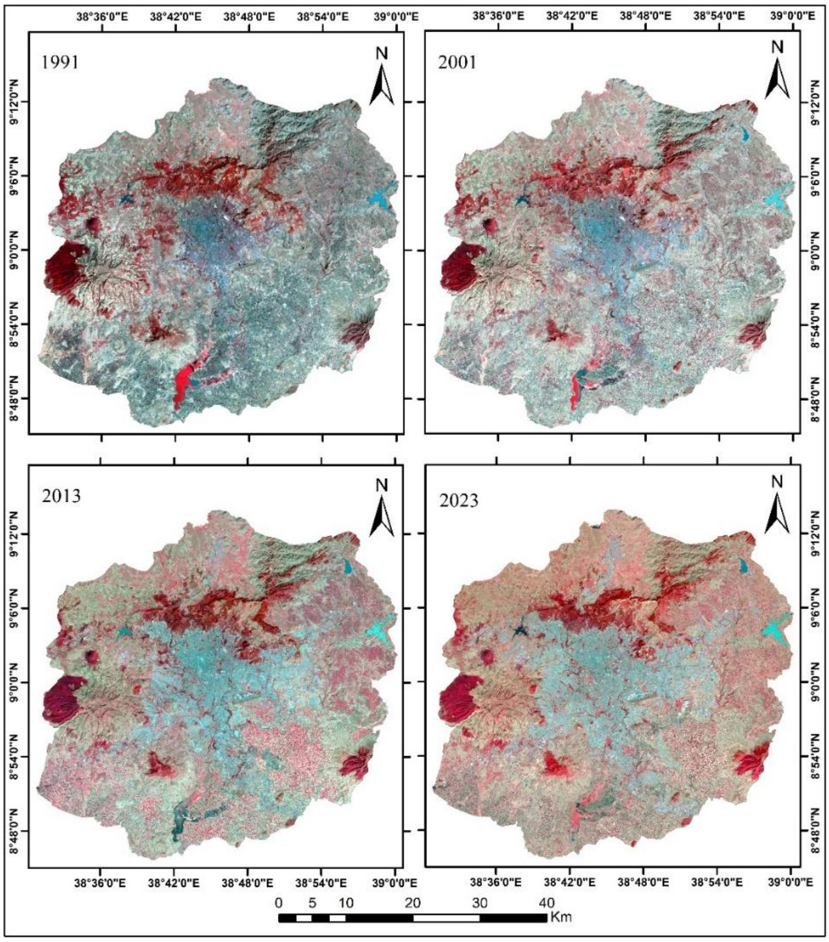

Figure 3.6: Landsat Images of Study Area.

I. Landsat Thematic Mapper (TM)

The thematic mapper (TM) sensor, operational from March 1, 1984, to June 5, 2013, was mounted on a satellite with a repeat cycle of every 16 days. This sensor features seven spectral bands, including three in the visible spectrum and four in the infrared spectrum. Notably, Band 6 is designed to detect thermal infrared radiation, which is used for measuring surface temperatures. For more detailed information, refer to Table 3.2.

Table 3.2: Description of Landsat 5 thematic mapper.

Sensor	**Band**	**Band name**	**Wavelength (µm)**	**Resolution (m)**	**Repeat cycle**
Landsat5	1	Visible Blue	0.45 – 0.52	30	
Thematic	2	Visible Green	0.52 – 0.60	30	
Mapper	3	Visible Red	0.63 – 0.69	30	16 days
(TM)	4	NIR	0.76 – 0.90	30	
	5	SWIR 1	1.55 – 1.75	30	
	6	Thermal	10.40 – 12.50	30(120)	
	7	SWIR 2	2.08 – 2.35	30	

II. Landsat 8 operational land imager and thermal infrared sensor Capabilities

The images feature nine spectral bands; bands 1 through 7, 9, and the thermal infrared sensor (TIRS), which includes bands 10 and 11, all have a spatial resolution of 30 meters. The newly added band 1, also known as ultra-blue, is beneficial for studying coastal areas and aerosols. Additionally, the new band 9 is effective in detecting cirrus clouds. Landsat 8 was launched on February 11, 2013, as detailed in Table 3.3. The OLI on Landsat 8 is designed to capture high-resolution images across multiple spectral bands, from the visible to the near-infrared and shortwave infrared regions. Key features of the OLI include:

- Spectral Bands: The OLI includes nine spectral bands, which provide detailed information across different wavelengths. This includes a deep blue band for coastal and aerosol studies, and a cirrus band for cloud detection.
- Spatial Resolution: The OLI offers a spatial resolution of 30 meters for most bands, with a 15-meter resolution for the panchromatic band. This high resolution is ideal for detailed land cover and land use analysis.

- Radiometric Resolution: The instrument captures data with a 12-bit radiometric resolution, allowing for finer distinctions between different surface features and conditions.

Table 3.3: Descriptions of Landsat 8 OLI and TIRS

Sensor	Band	Band name	Wavelength (μm)	Resolution (m)	Repeat cycle
	1	Coastal	0.43 – 0.45	30	
	2	Blue	0.45 – 0.51	30	
Landsat8	3	Green	0.53 – 0.59	30	
OLI/TIRS	4	Red	0.63 – 0.67	30	
	5	NIR	0.85 – 0.88	30	
	6	SWIR 1	1.57 – 1.65	30	16 days
	7	SWIR 2	2.11 – 2.29	30	
	8	Pan	0.50 – 0.68	15	
	9	Cirrus	1.36 – 1.38	30	
	10	TIRS 1	10.60 – 11.19	30 (100)	
	11	TIRS 2	11.50 – 12.51	30 (100)	

3.3.3. Field data

The research utilized field data derived from GPS coordinates to precisely validate the classified image of the LU/LC into various categories. Randomly generated GPS points were collected along with photographs that demonstrated the different LU/LC classes. This field data facilitated the evaluation of accuracy for. The validation process, anchored on ground truth verification.

3.3.4. Secondary data

This study utilized secondary data, including meteorological information like average monthly temperatures and rainfall from the period 1991 to 2023. These data sets were employed for both evaluation and validation purposes. Additionally, the research incorporated a geological map provided by the Geological Institute of Ethiopian, which helped in assessing the geological characteristics of the area. Population statistics from the Ethiopia Statistical Service (ESS) from 2007 were also analyzed to gauge the demographic conditions of the study area.

3.3.5. Description of data and data source

The data utilized in this study, both primary and secondary, was sourced from various locations as detailed in Table 3.4

Table 3.4: Description of Data and data sources

Data Description	Data source
(Study Area) Boundary	ESS,2021
River and Roads	ESS,2021
Elevation and Slope	DEM 20m SSGI
Temperature and Rainfall	National Metrological Agency
Population	ESS,2007
Satellite Image 1991 Landsat5 TM 2001 Landsat5 TM 2013 Landsat 8 OLI/TIRS 2023 Landsat 8 OLI/TIRS	USGS 1991,2001,2013 and 2023
Ground truth 2023	Field survey

3.3.6. Software Packages and Instruments

Table 3.5: Software packages and Instruments used

Software packages	Purposes
ArcGIS Pro	Data analysis and Map preparation
ERDAS IMAGINE 2014	For LULC classification
Google Earth Pro	For reference in accuracy assessment
Quantum GIS 3.10	For downloading and processing Landsat Data
SPSS 22.0	For correlation and regression analysis
Microsoft Office 2016	For statistical Data analysis and presentation
Handheld GPS	To collect ground truth data for accuracy assessment

3.4. Methods

In this research, the approach to meeting the study goals started with obtaining Landsat images for the years 1991, 2001, 2013, and 2023 from the Earth Explorer website (USGS). These specific years were selected due to the availability of data. The images were acquired during the dry season and were free of cloud cover.

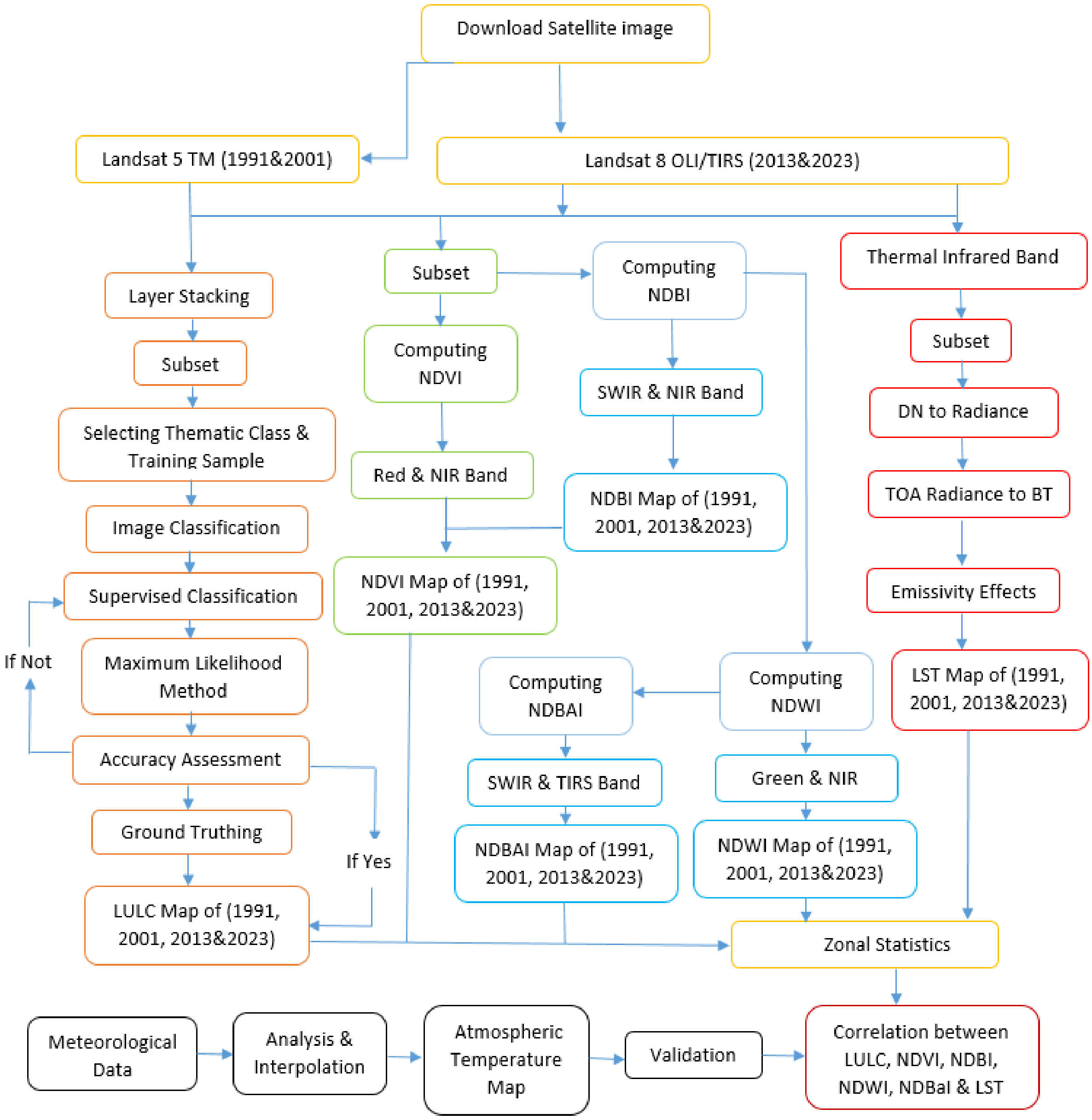

Figure 3.7 Methodological flow chart of the study.

3.4.1. Preparing and Analyzing Data

Satellite images naturally exhibit various imperfections such as distortion, noise, haze, and striping. Consequently, it is essential to preprocess these images before any further analysis. The preprocessing steps performed included Importing, Layer Stacking and cropping the image to fit the boundaries of Addis Ababa including Sheger city. This was followed by geometric and radiometric corrections, stripe removal, pan sharpening, and other enhancement techniques to improve image quality. Radiometric correction specifically involves eliminating atmospheric noise to better represent true ground conditions as detected by the sensors. All these steps were undertaken to enhance the clarity and detail of the image, making it easier to distinguish between different features in the scene.

3.4.2. Processing of Digital Images

A digital image is essentially a numerical depiction, consisting of binary data that represents a two-dimensional image. This type of image is created by sampling and quantizing visual scenes into elements known as pixels. DIP refers to the techniques used to manipulate and interpret these images using computers. Historically, in the field of remote sensing, digital image processing has primarily focused on two key application areas: enhancing image quality for visual interpretation by humans and refining the image data for interpretation aided by computers. The core activities involved in DIP aim to improve the spectral distinctiveness of objects within the image.

3.4.3. Image enhancement

Image enhancement refers to the process of manipulating image data to optimize its presentation or recording for further visual analysis. Typically, this process includes methods that amplify the visual contrast among different elements within an image (Billah and Rahman, 2004). The primary goal of image enhancement is to enhance the clarity of information in images for human observers or to refine the data for subsequent automated image processing applications.

3.4.4. Image classification

In remote sensing, the purpose of image classification is to derive thematic information from an image containing multiple bands by categorizing it into different information classes. This process involves analyzing the image based on the reflectance properties of objects to achieve specific objectives. Essentially, it translates image data into thematic categories. Techniques of digital image classification group pixels into LU/LC classes based on the statistics of their reflectance. Pixels are organized into clusters according to their reflectance characteristics. Users determine the number of clusters that is wanted and select the spectral bands to analyze. Using these parameters, the image classification software then creates these clusters. In this study, supervised classification techniques are employed.

I. Supervised classification

Supervised classification is commonly employed in the quantitative analysis of remote sensing data (RS) imagery based on their reflectance characteristics. This method utilizes spectral signatures from training samples to categorize images. The image classification Toolbar facilitates the creation of these training samples to denote various classes. In supervised classification, specific information classes (such as different types of land cover) can be identified in the image. For each year, the supervised classification process involves categorizing pixels by utilizing training areas for each LU/LC class. Following the designation of training areas for each class, the classification is executed. For LU/LC types like bare land, cropland, shrub land and built-up areas, forests, wetlands, and water bodies, 10 training sites are used. These areas in digital images are labeled as signatures representing individual identities, and field truth verification is employed to accurately represent LU/LC classes (Coppin and Bauer, 1996).

Utilizing Bands 1 to 5 and 7 of the Multispectral Bands for TM from the years 1991 and 2001, as well as bands 2 to 7 for OLI in 2013 and 2023, the land-use and land-cover patterns in the preprocessed images were identified through supervised classification using the likelihood classification algorithm in ERDAS Imagine 2014. In this method, the types of LU/LC classes were defined by the user employing image processing techniques. The study identified seven primary classes in Addis Ababa including Sheger city: cropland, bare land, built-up areas, shrub land, forest land, water bodies and wetland. The benefits of supervised classification included the ability to develop specific information classes, perform self-assessment with training sites, and reuse these training sites for further analysis. However, challenges such as discrepancies between information classes and spectral classes, as well as variation in the homogeneity and uniformity of the information classes, were noted.

II. Maximum likelihood classification

Maximum likelihood classification (MLC) is a widely recognized method in remote sensing that classifies pixels into corresponding classes or categories based on their statistical probability. This approach, which uses a statistical decision-making measure, is particularly useful for classifying pixels with overlapping signatures, assigning them to the category where they have the highest likelihood of belonging. MLC is generally more precise than parallelepiped classification, though it requires more time to compute. The MLC tool takes into account the variances in class signatures when allocating each pixel to a class as represented in the signature file.

III. Ground truth

A ground truthing exercise took place in the study area to validate various land use/land cover (LU/LC) class. The LU/LC classes observed included cropland, shrub land, forest, wetland, water bodies, bare land, and built-up areas. These categories were instrumental in developing the map legends. Assisted by GPS, training datasets necessary for image classification were collected. Additionally, during these ground Truthing efforts, photographs and coordinates of specific scenes representing the sampled land use land cover classes were recorded.

3.4.5. Classification accuracy assessment

Evaluating the accuracy of a classification involves gathering original data or having prior knowledge of certain areas of the terrain for comparison purposes. This comparison is done between the classification map derived from remote sensing and a presumed accurate map, which might still contain some errors.

The map believed to be accurate might have been generated through direct on-site inspection or more commonly by interpreting data from remote sensing that was collected at a higher scale or resolution. To evaluate its accuracy, the map created from remote sensing analysis is compared to a reference map that uses different sources of information. A field survey utilizing handheld Global Positioning System (GPS) devices identified approximately 70 points in the study area. This survey, along with Google Earth, served as the basis for assessing the accuracy of the Land-use/Land-cover (LU/LC) classification. The classification's accuracy results for the years 1991, 2001, 2013, and 2023 are detailed. The various land-use and land-cover classes are described in Table 3.6.

Table 3.6: Description of the study area land use/land cover class.

LU/LC classes	Code	Description
Shrubs Land	SL	Regions filled with shrubs, bushes, and small trees that offer minimal usable timber, interspersed with patches of grass and less than dense forests.
Crop Land	CL	Regions utilized for the farming of both annual and perennial crops, as well as the surrounding rural areas.
Built-up	BU	Regions utilized for residential, commercial, and industrial buildings, including areas designated for transportation such as roads, mixed-use urban developments, and other infrastructure.
Water Body	WB	Regions encompassing small natural and artificial dams, such as ponds, lakes, and rivers.
Wetland	WL	Regions where water saturates the soil, remaining at or near the surface throughout the year or intermittently during different times, including the growing season.
Forest Land	FL	A forest is an area densely populated with trees and serves as a natural habitat for diverse forms of life such as plants, animals, and microorganisms.
Bare land	BL	Regions characterized by thin soil, sand, and rocks, encompass deserts, dry salt flats, beaches, sand dunes, exposed rock formations, strip mines, quarries, and gravel pits. These areas are largely dominated by rocky outcrops, and lands that have been eroded or degraded.

To identify and categorize the land use/land cover (LU/LC) of the study area, it is essential to have prior knowledge about the region. Field observations revealed seven principal LU/LC classes. The process used to classify LU/LC from a Landsat image is detailed in Figure 3.8.

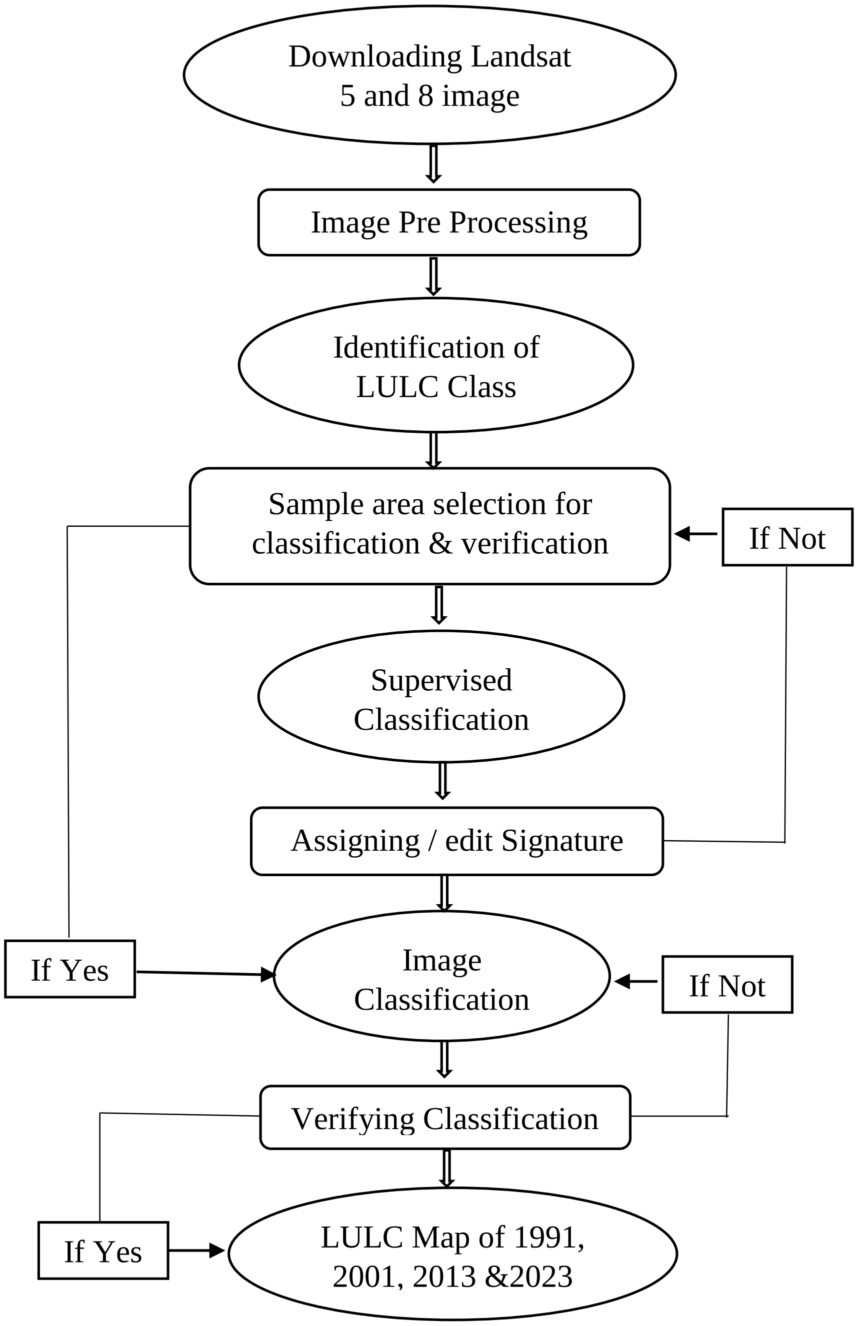

Figure 3.8: LU/LC Classification Procedures and methods used.

3.5. Detecting changes in land use and land cover

Detection of changes in land use and land cover (LU/LCC) was conducted using satellite images from the years 1991, 2001, 2013, and 2023. By employing GIS and the intersection method, thematic images from these years were analyzed for differences. The process involved first mapping the most recent satellite imagery from 2023 and then progressively mapping earlier years, concluding with the 1991 imagery. Post-classification, as noted by Chen (2000), is a prevalent technique utilized for detecting such changes. The analytical procedure incorporated integrating technical methodologies within the ArcGIS software to assess LU/LCC. A key part of this analysis was creating a table that showed the area in square kilometers and the percentage of change for each land use and cover class across the years 1991, 2001, 2013, and 2023. This involved employing specific calculation formulas (eq.3.1) as outlined by (Lambin et al, 2001).

$$Percentage\ change = \frac{\text{observed change}}{\text{sum of area}} * 100 \qquad \text{Eq. (3.1)}$$

3.6. Calculation of NDVI, LST, NDBI, NDBaI and NDWI.

3.6.1. Calculation of Normalized Difference Vegetation Index

(Farooq, 2012) explains that NDVI (Normalized Difference Vegetation Index) is connected to the presence of vegetation because areas with dense vegetation exhibit stronger reflection in the near-infrared spectrum. He notes that green foliage typically reflects less than 20% of light in the 0.5 to 0.7 micrometer range, but around 60% in the 0.7 to 1.0 Micrometer range. The NDVI values range from -1 to 1 and are derived from spectral reflectance data in the visible (RED) and near-infrared (NIR) spectrums, processed using ArcGISpro Software. The index is calculated based on the following formula:

$$NDVI = \frac{\text{NIR}-\text{Red}}{\text{NIR}+\text{Red}} \qquad \text{Eq. (3.2)}$$

NDVI stands for Normalized Difference Vegetation Index. In this context, NIR refers to the near-infrared, which is band 4, and R denotes band 3, the red band. Equation 3.2 applies this calculation for the NDVI using the TM sensor for the years 1991 and 2001, as well as the OLI sensor for 2013 and 2023. However, for the Landsat 8 satellite, the NIR is designated as band 5, while the red band shifts to band 4, as noted by (Weng et al, 2004).

The calculation of fractional Vegetation Cover (FVC) was performed using Equation 3.3.

$$FVC = \frac{\text{NDVI}-\text{NDVIs}}{\text{NDVIv}-\text{NDVIs}} \qquad \text{Eq. (3.3)}$$

Where,

FVC= Fractional Vegetation Cover

NDVI= Normalized Difference Vegetation Index

The equation mentioned above (FVC) was utilized to calculate the fraction of an area covered by vegetation using the NDVI value.

NDVIs = is NDVI for Soil and NDVIv = NDVI for vegetation

Equation 3.4 was utilized to determine the Vegetation Proportion, which is essential for calculating the land surface emissivity (LSE) of Landsat 8.

$Pv = (\frac{NDVI - NDVImin}{NDVImax - NDVImin})^2$ Eq. (3.4)

Where,

Pv= Proportion of Vegetation

NDVI= Normalize Difference Vegetation Index

NDVI min= Normalized Difference Vegetation Index Minimum Value

NDVI max= Normalized Difference Vegetation Index Maximum Value

3.6.2. Calculation of land surface temperature

Determining the temperature of the land's surface involves several stages.

To determine the LSE, understanding the intrinsic properties of the earth's surface is crucial, as these affect the conversion of thermal radiance into LST (sobrino et al., 2014). Table 3.7 lists the emissivity constants for both vegetation and soil.

Table 3.7: The emissivity constant value for Landsat 8.

Emissivity	Band 10	Band 11
es	0.971	0.977
ev	0.987	0.989

The equations labeled 3.5, 3.6, and 3.7 are utilized to calculate the Land Surface Emissivity, the average Land Surface Temperature, and the variation in land surface Emissivity for Bands 10 and 11, respectively.

$LSE = 0.004\mathrm{Pv} + 0.986$ Eq. (3.5)

$Mean\ of\ LST = \frac{LST10 + LST11}{2}$ Eq. (3.6)

Difference of Land Surface Emissivity (LSE) = LSE10 - LSE11 Eq. (3.7)

3.6.3. Radiometric correction

Radiometric correction involves transforming digital numbers from remote sensing data into spectral radiance values for comparison purposes. According to (Parente, 2013), image processing techniques that correct errors by converting digital numbers to radiance and subsequently to reflectance fall under the category of radiometric correction. Equation (3.8) is utilized to facilitate the conversion of Digital numbers to spectral radiance.

$\mathrm{L}\,\lambda = \mathrm{Lmin} + (\mathrm{Lmax} - \mathrm{Lmin}) * \mathrm{DN}/255$ Eq. (3.8)

Where,

L λ=Spectral radiance

Lmin= Spectral Radiance of DN value 1

Lmax= Spectral radiance of DN value of 255

DN= Digital Number

Equation 3.8 the above, was used to convert digital Number in to Spectral radiance

3.6.4. Conversion at Sensor Spectral radiance

In radiometric calibration, the pixel values denoted by Q in the raw and unprocessed image date from remote sensing were converted into absolute radiance values. Equation 3.9 facilitated this conversion, scaling the Sensor spectral radiance or satellite data into an 8-bit format.

$$L\lambda = \left(\frac{Lmax\lambda - \text{min}\lambda}{Qcalmax - Qcalmin}\right)(Qcai - Qcalmin) + Lmin\lambda \qquad \text{Eq. (3.9)}$$

Where,

L λ=Spectral radiance at sensors aperture or the calculated radiance associated to the ground area enclosed in the Pixel and referred to λ wavelength range of specific band.

Lmaxλ=Spectral at Sensor Radiance that is Scaled to Qcalmax

Lminλ= Spectral at Sensor Radiance that is Scaled to Qcalmin

Qcalmax=Maximum Quantized Calibrated Pixel Values Corresponding to Lmaxλ

Qcalmin=Minimum Quantized Calibrated Pixel Values Corresponding to Lminλ

Qcal= Quantized Calibrated Pixel Values (DN)

3.6.5. Conversion of top of atmosphere (TOA) reflectance

Data from the Landsat Thematic Mapper, showing top of atmosphere reflectance, requires correction and processing. This is necessary due to changes in the solar zenith angle caused by the timing differences in data acquisition. The resulting output is then calibrated to reflectance values. To calculate the top of atmosphere reflectance, Equation 3.10 was employed.

$$\text{P}\lambda = \frac{\pi.\text{L}\lambda.\text{d}^2}{\text{ESUN}\lambda 2.COS\theta s} \qquad \text{Eq. (3.10)}$$

Where,

Pλ=planetary top of atmosphere (TOA) reflectance, which has no unit or it is unit less

π=mathematical constant approximately equal to 3.14159. It is also unit less

Lλ=spectral radiance at the sensors aperture

d=earth -sun distance/distance from the earth to the sun astronomical units

ESUNλ=mean exoatmospheric solar irradiation (from Meta data)

ɵ = Solar zenith angle

3.6.6. Conversion of radiance into brightness temperature

Thermal infrared data can be transformed from atmospheric reflectance (Lλ) into effective sensor brightness temperature (TB) using thermal constants found in the metadata file. For remote sensing data, such as Landsat imagery, thermal band 6 on both the Thematic Mapper and Enhanced Thematic Mapper Plus needs to be converted from at-sensor spectral radiance to effective at-sensor brightness temperature. Brightness temperature represents the radiance that moves upward from the Earth's atmosphere. To convert spectral radiance (Lλ) to brightness temperature (TB), Equation 3.11 from (Rajeshwari and Mani, 2014) was utilized.

$$TB = \frac{K2}{\left(Ln\frac{K1}{L\lambda}\right)+1} \qquad \text{Eq. (3.11)}$$

Where,

TB=effective at satellite brightness temperature (unit in Kelvin)

K2=calibration constant 2

Ln=natural logarithm

K1=calibration constant 1

λ=spectral radiance at sensors aperture

Landsat 8 includes two thermal bands, namely band 10 and band 11. Table 3.8 presents the calibration constants utilized in the calculation of brightness temperature.

Table 3.8: Thermal band calibration constant of Landsat 8.

Satellite	sensors	Categories	Band 10	Band 11
Landsat 8	OLI/TIRS	K1	774.8853	480.8883
		K2	1321.0789	1201.1442
		Radiance_ MULT_BAND	0.0003342	0.0003342
		Radiance_ADD_BAND	0.10	0.10

LST was obtained from Landsat TIRS data using bands 10 and 11 through the split window algorithm, first introduced by McMillin in 1975. The equation is shown as follows (eq. 3.12).

$$LST = TB10 + C1\,(TB10 - TB11) + C2\,(TB10 - TB11)2 + C0 + (C3 + C4W)\,(1 - m) + (C5 + C6W)\,\Delta m \qquad \text{Eq. (3.12)}$$

Where,

LST=Land Surface Temperature

C0 up to C6=Split Window Coefficient Value

TB10=Brightness Temperature of band 10

TB11=Brightness Temperature of band11

m=Mean Land Surface Emissivity of thermal infrared bands (mean of band 10 and band11)

W=Atmospheric water vapor content (0.005) from Earth science reference table (ESRT) Relative humidity table.

Δ m=Difference in Land Surface Emissivity (LSE)

While calculating the Land Surface Temperature (LST) of a specified area, Landsat 8 thermal bands (referenced in Table 3.9) were utilized.

Table 3.9: Split window algorithm constant value.

Constant	Value
C0	-0.268
C1	1.378
C2	0.138
C3	54.3
C4	-2.238
C5	-129.2
C6	16.4

The calibration constant for Landsat 5 differs from that of Landsat 8. For Landsat 5, Table 3.10 was utilized.

Table 3.10: Thematic mapper (TM) thermal band calibration constant.

satellite	sensors	constant	value
Landsat 5	TM	K1	607.76
		K2	1260.56

Temperature was transformed from degrees Kelvin to degrees Celsius by using the formula in equation 3.13, which involves subtracting 272.15 from the Kelvin measurement.

$$C = K - 272.15 \qquad \text{Eq. (3.13)}$$

Where,

C: result in degree Celsius

K: result in degree Kelvin

Generally, to compute the Land Surface Temperature (LST) using the TM sensor, subtract 272.15 from the result obtained by applying the formula for effective satellite temperature, which is given in Kelvin.

3.7. Calculation of Normalized Difference Build-Up Index

The Normalized Difference Build-Up Index has been developed by (Zha et al., 2003) in order to identify the built-up areas. NDBI is expressed by the following formula based on Short Wave1-infrared: (band 5 for Landsat 5 and 7, Band 6 for Landsat 8) and Near-infrared bands (band 4 for Landsat 5 and 7, band 5 for Landsat 8) satellites (Eq. (3.5))

$$NDBI = \frac{(\text{SWIR})1 - \text{NIR}}{(\text{SWIR})1 + \text{NIR}} \qquad \text{Eq. (3.14)}$$

3.8. Calculation of Normalized Difference Bareness Index

When estimating the thermal environment, NDBaI was chosen to represent barren terrain areas, which often show large variances in thermal characteristics (Zhifeng and Jianjun, 2012). It is estimated using the reflectance of Short Wave1-infrared (band 5 for Landsat 5 and 7, Band 6 for Landsat 8) and thermal infrared (band 6 for Landsat 5 and 7, band 10 and 11 for Landsat 8) satellites (Eq. (3.4))

$$NDBaI = \frac{(\text{SWIR})1 - \text{TIRS}}{(\text{SWIR})1 + \text{TIRS}} \qquad \text{Eq. (3.15)}$$

3.9. Calculation of Normalized Difference Water Index

The NDWI was introduced by (McFeeters, S. K., 1996). The use of the Normalized Difference Water Index (NDWI) in the delineation of open water features. This formula highlights the difference in reflectance between the green and near-infrared bands, which is sensitive to the presence of water in vegetation. Green (band 2 for Landsat 5 and Band 3 for Landsat 8) and near-infrared bands (band 4 for Landsat 5 and band 5 for Landsat 8) satellites (Eq. (3.4))

$$NDWI = \frac{\text{Green} - \text{NIR}}{\text{Green} + \text{NIR}} \qquad \text{Eq. (3.16)}$$

3.10. Calculation of Urban Hotspot Area

Urban hotspot and Non-urban hotspot were identified by the range of Land Surface Temperature determinate by the following equations (Ma, Kuang, &Huang, 2010; Guha, Govil, & Mukherjee, 2017):

$$\text{UHS:} \quad LST > \mu + 2 * \delta$$

$$\text{Non-UHS:} \quad LST < \mu + 2 * \delta \qquad \text{Eq. (3.17)}$$

Where

μ and δ are the Mean and Standard deviation of LST in the study area, respectively.

3.11. Zonal statistics

A zone is defined by all the contiguous areas in the input that share the same value. The zonal statistics function collects and summarizes the values from a raster within the boundaries defined by another dataset, which can be either raster or vector, and outputs the results in a table format. Land Use/Land Cover (LU/LC), Normalized Difference Vegetation Index (NDVI), Normalized Difference Built-up Index (NDBI), Normalized Difference Bareness Index (NDBaI), Normalized Difference Water Index (NDWI), and Land Surface Temperature (LST) maps were created for the years 1991, 2001, 2013, and 2023. To explore the spatial variations in LST in relation to different LU/LC, the data was analyzed using the zonal statistics tool in ArcGISPro.

Additionally, summarized data for LU/LC, NDVI, NDBI, NDBaI, NDWI, and LST were further analyzed using Excel. Zonal statistics as a table is a crucial method for investigating the relationships between LU/LC and indices such as NDVI, NDBI, NDBaI, NDWI, and LST.

3.12. Spatial interpolation

Spatial interpolation involves estimating values at unknown locations based on known values from surrounding points. For instance, this method can be used to create maps showing rainfall and temperature for a specific area using data from nearby weather stations. In this study, we used meteorological data to interpolate and analyze results in comparison with Land Surface Temperature (LST) values obtained from Landsat's thermal infrared bands. The Inverse Distance Weighted (IDW) method was utilized to interpolate temperature data. The IDW method is an interpolation technique where sample points are assigned weights that decrease with increasing distance from the point of interpolation.

Inverse Distance Weighted (IDW) is one of the most straightforward and deterministic interpolation methods. Deterministic models such as IDW, rectangular grids, natural neighbors, and splines employ interpolation techniques. These techniques utilize vector points with known values to predict values at unknown locations, thereby generating a raster surface that spans the entire area (Legates and Wilmont, 1990). The benefits of using IDW interpolation include: The integration of various distances into the estimation process, the ability to finely control the influence of these distances through weighting and the method is both rapid and straightforward to compute.

In this study, temperature data were interpolated from sample points using the ArcGISPro platform, and the resulting interpolated maps were subsequently used for validation.

3.13. Correlation analysis

In correlation analysis, R and R^2 are statistical measures used to quantify the strength and direction of the relationship between two variables. R, also known as the Pearson correlation coefficient, measures the strength and direction of the linear relationship between two continuous variables.

It ranges from -1 to 1, where 1 indicates a perfect positive linear relationship, -1 indicates a perfect negative linear relationship, and 0 indicates no linear relationship. Positive values (0 to 1) mean that as one variable increases, the other variable tends to increase. Negative values (0 to -1) mean that as one variable increases, the other variable tends to decrease. The closer R is to 1 or -1, the stronger the linear relationship between the variables.

R^2 is the square of the correlation coefficient R. It represents the proportion of the variance in the dependent variable that is predictable from the independent variable(s) and ranges from 0 to 1. A value of 0 indicates that the independent variable explains none of the variance in the dependent variable, while a value of 1 indicates that the independent variable explains all of the variance in the dependent variable. As noted by (Ratner, 2009) more details on the degree of relationship are presented in Table 4.11.

Table 3.11: Degree of relationship

Correlation strength	Correlation direction	Description
-1 – -0.5	Negative	Strong Negative relationship
-0.5 – -0.3	Negative	Moderate Negative relationship
-0.3 – -0.1	Negative	Small Negative relationship
0	Neutral/ No	No relationship
0.1 – 0.3	Positive	Small Positive relationship
0.3 – 0.5	Positive	Moderate Positive relationship
0.5 – 1	Positive	Strong Positive relationship

CHAPTER IV

4. RESULTS AND DISCUSSIONS

4.1. Land-use/land-cover in 1991, 2001, 2013 and 2023

The 1991 land-use/land-cover (LU/LC) classification revealed that Cropland and shrub land were the predominant categories, together making up 73.37% of the total area. Out of the entire area of 2038.56 km², Cropland represented 1,173.58 km² (57.57%) and shrub land covered 322.09 km² (15.80%). The remaining land class, which included bare land, forest, built-up areas, wetlands, and water bodies, accounted for 542.9 km² (26.63%) of the area. Of all the categories, water bodies occupied the least amount of space. Analysis of the 2001 imagery reveals that croplands were the predominant land use/land cover (LU/LC) type in the study area, covering an extensive area of 1,392.63 km², which constitutes 68.31% of the total. Forest lands were the next significant class, covering 223.63km² or 10.97% of the area. Other LU/LC class, including bare land, shrub land, built-up areas, wetlands, and water bodies, collectively made up 20.72% of the landscape. Of all categories in 2001, wetlands occupied the smallest area. A 2013 study revealed that cropland covered the majority of the land in the study area, measuring 1,296.67 km² or 63.61%. Built-up areas were the next significant class, occupying 371.69 km², which is 18.23% of the area. The remaining land classes, including bare land, forest land, shrub land, wetlands, and water bodies, collectively made up 18.16% of the total land. Among these, wetlands occupied the smallest area compared to all other class. The 2023 classification of land use and land cover (LU/LC) showed that cropland and built-up areas were the predominant class, together comprising 80.58% of the total area. Specifically, cropland covered 1,154.58 km², or 56.64%, and built-up areas covered 487.96 km², or 23.94%. Other LU/LC class included bare land, forest, shrub land, wetland, and water bodies, collectively making up 19.42% of the area. Notably, the cropland area saw a slight decrease of 0.93% since 1991. Cropland remains the principal land use and cover type in terms of area, followed by built-up areas. Detailed statistics for each class and the LU/LC map for the period are provided in Table 4.1 and Figure 4.1.

Table 4.1: LU/LC area coverage of the Study Area.

No	Class Name	1991		2001		2013		2023	
		Area (km2)	(%)	Area (km2)	(%)	Area (km2)	(%)	Area (km2)	(%)
1	Waterbody	4.65	0.23	5.79	0.28	6.19	0.30	6.89	0.34
2	Built-up	160.15	7.86	169.68	8.32	371.69	18.23	487.96	23.94
3	Shrub Land	322.09	15.80	87.64	4.30	164.78	8.08	178.02	8.73
4	Bare Land	171.21	8.40	158.07	7.75	27.51	1.35	12.06	0.59
5	Forestland	204.72	10.04	223.63	10.97	171.31	8.40	198.30	9.73
6	Cropland	1,173.58	57.57	1,392.63	68.31	1,296.67	63.61	1,154.58	56.64
7	Wetland	2.17	0.11	1.11	0.05	0.42	0.02	0.75	0.04
	Total	**2,038.56**	**100**	**2,038.56**	**100**	**2,038.56**	**100**	**2,038.56**	**100**

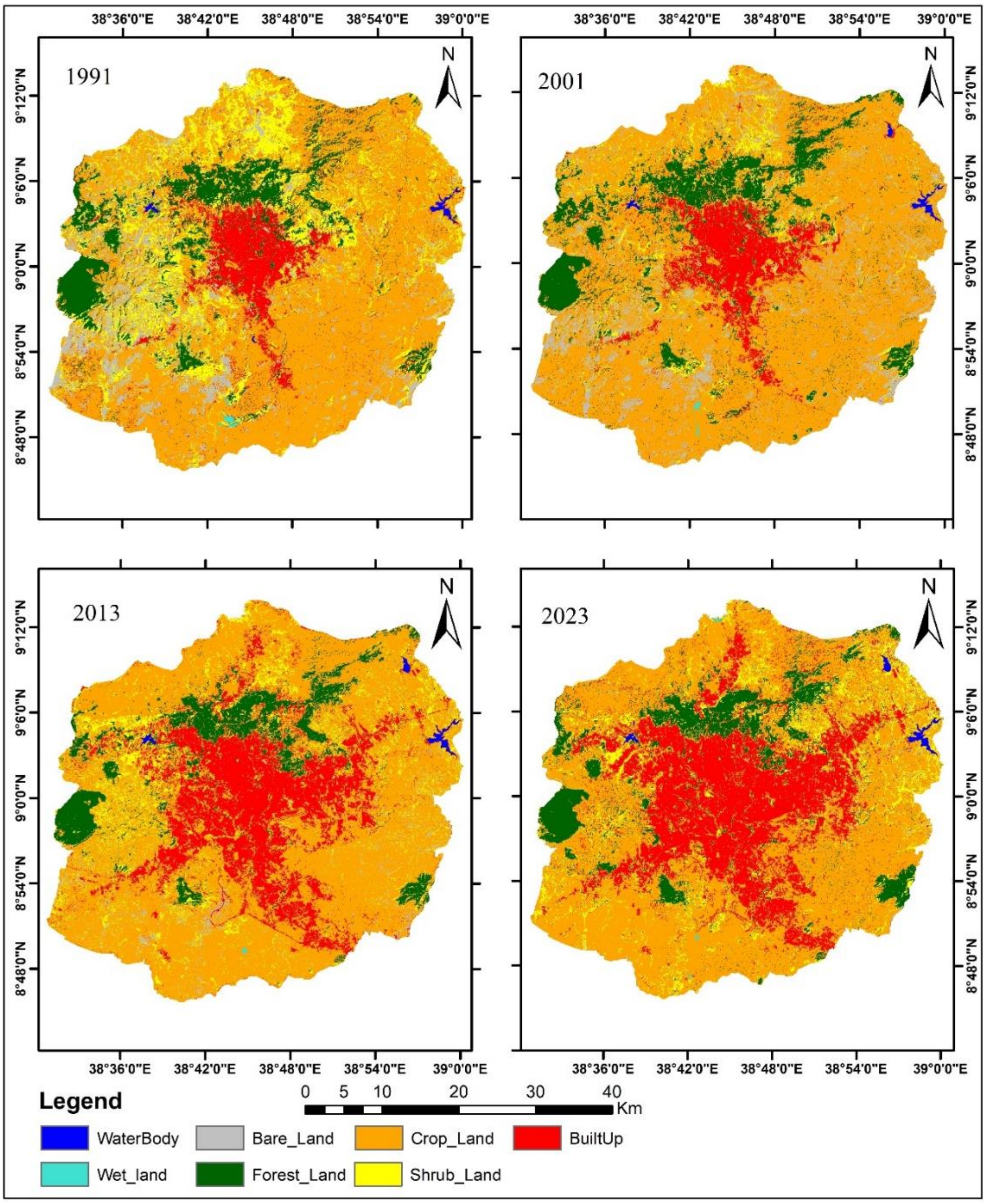

Figure 4.1: LU/LC maps of the study area.

From 1991 to 2023, cropland was the most extensive land use/land cover type in the study area. Starting at 1,173.58 km^2 in 1991, cropland area expanded to 1,392.63 km^2 by 2001. However, there was a slight reduction to 1,296.67 km^2 by 2013, and it further decreased to 1,154.58 km^2 by 2023, as shown in Figure 4.2.

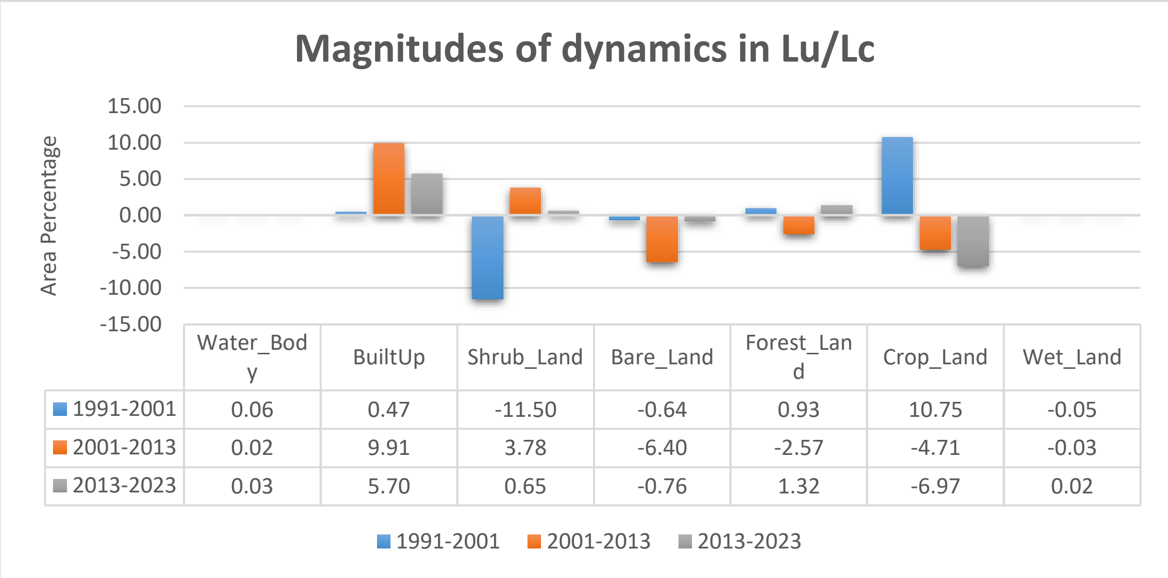

Figure 4.2: Magnitudes of dynamics of LU/LC.

4.2. Spatial extent of land-use/land-cover

The land-use and land-cover (LU/LC) patterns within the study area have undergone significant transformations from 1991 to 2023. The majority of the land, over 70%, was consistently dominated by cropland and shrub land across the study period in all seven major LU/LC classes. The built-up area showed a noticeable increase, rising from 7.86% in 1991 to 8.32% in 2001, reaching 18.23% by 2013, and further expanding to 23.94% by 2023. Similarly, the coverage of water bodies also grew during this period, escalating from 0.23% in 1991 to 0.28% in 2001, then to 0.30% in 2013, and finally to 0.34% in 2023. From 1991 to 2023, the percentage of forested areas experienced variations, starting at 10.04% in 1991, rising to 10.97% by 2001, dropping to 8.40% by 2013, and climbing to 9.73% by 2023. Similarly, shrub land percentages fluctuated, beginning at 15.80% in 1991, falling sharply to 4.30% by 2001, then increasing to 8.08% by 2013 and rising slightly to 8.73% by 2023. Cropland showed an initial increase from 57.57% in 1991 to 68.31% in 2001, followed by a decrease to 63.61% in 2013 and further declining to 56.64% by 2023. Both wetland and bare land percentages continuously decreased throughout the period from 1991 to 2023. In 1991, wetlands covered 0.11% of the area, which declined to 0.05% by 2001, further dropped to 0.02% by 2013, and slightly increased to 0.04% by 2023. Bare land accounted for 8.40% in 1991, which decreased to 7.75% by 2001, fell sharply to 1.35% by 2013, and further reduced to 0.59% by 2023 (Table 4.2).

Table 4.2: Land-use/land-cover coverage and net changes during 1991–2023.

No	Class Name	1991		2001		2013		2023		Net Change 1991-2023, Km2
		Area(Km2)	(%)	Area(Km2)	(%)	Area(Km2)	(%)	Area(Km2)	(%)	
1	Water body	4.65	0.23	5.79	0.28	6.19	0.30	6.89	0.34	**2.24**
2	Built-up	160.15	7.86	169.68	8.32	371.69	18.23	487.96	23.94	**327.81**
3	Shrub Land	322.09	15.80	87.64	4.30	164.78	8.08	178.02	8.73	**-144.07**
4	Bare Land	171.21	8.40	158.07	7.75	27.51	1.35	12.06	0.59	**-159.15**
5	Forest land	204.72	10.04	223.63	10.97	171.31	8.40	198.30	9.73	**-6.42**
6	Crop land	1,173.58	57.57	1,392.63	68.31	1,296.67	63.61	1,154.58	56.64	**-19.00**
7	Wet land	2.17	0.11	1.11	0.05	0.42	0.02	0.75	0.04	**-1.41**
	Total	2,038.56	100	2,038.56	100	2,038.56	100	2,038.56	100	

The study area's analysis of land use/land cover changes revealed a decrease in bare land and wetland areas by 159.15 km² and 1.41 km², respectively. Meanwhile, other class exhibited trends of both growth and variability in their spatial coverage. These LU/LC changes is illustrated in Figure 4.3.

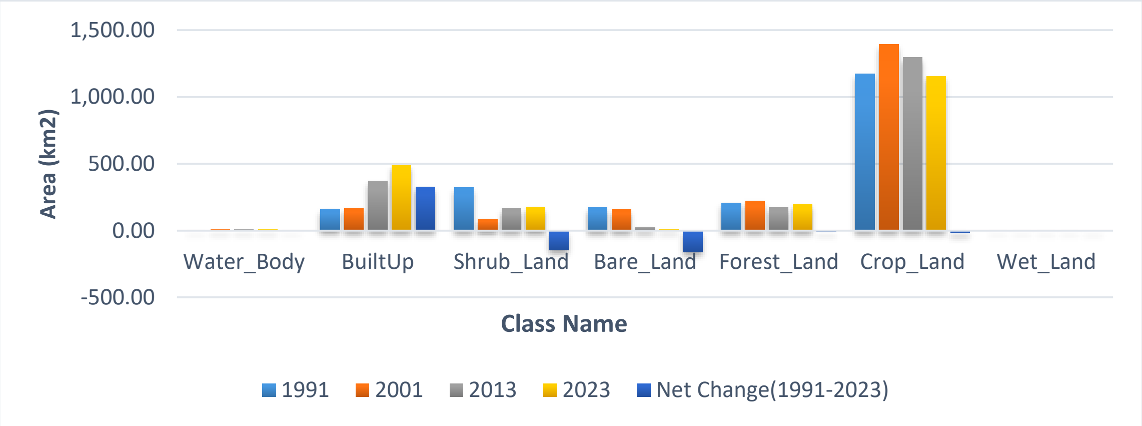

Figure 4.3: LU/LC changes during 1991– 2023 in the study area.

4.3. Monitoring changes in land use and land cover

The method of change detection through post-classification comparison demonstrated that various land use and land cover (LULC) class experienced changes in the study area over the observed period. The conversion matrix tables, processed using ArcGIS Pro, illustrate the relative changes for each LULC class from 1991 to 2023.

Over the past three decades leading up to 2023, the LULC pattern in the study area has experienced rapid changes, as indicated by the shifts in area coverage among various LULC classes. Throughout the study period, bare land and wetland consistently decreased, while forest land, shrub land, and crop land exhibited fluctuations. Conversely, settlement areas and water bodies showed a steady increase. From the initial to the final year, 40.40 km^2 of bare land was converted to built-up areas, 101.20 km^2 to crop land, 2.51 km^2 to forest land, 24.82 km^2 to shrub land, 0.05 km^2 to water bodies, and 0.05 km^2 to wetland, with 2.18 km^2 remaining unchanged as bare land. A built-up area of 0.32 km^2 was converted to bare land, while 32.04 km^2 was transformed into cropland. Additionally, 5.21 km^2 became forest land, 3.16 km^2 was changed to shrub land, 0.45 km^2 to a water body, and 0.01 km^2 to wetlands. The remaining 118.96 km^2 of built-up area remains unchanged.

A 6.72 km^2 of cropland has been converted to bare land, 236.77 km^2 has been transformed into built-up areas, 39.31 km^2 has changed to forest land, 76.63 km^2 to shrub land, 1.88 km^2 to water bodies, and 0.44 km^2 to wetlands. The remaining 811.83 km^2 of cropland remains unchanged. The forestland undergone significant changes, with 0.23 km^2 being converted to bare land, 22.52 km^2 transformed into built-up areas, 48.91 km^2 turned into cropland, and 7.24 km^2 changed to shrub land. Additionally, 0.10 km^2 became a water body, 0.01 km^2 was converted to wetlands, while the remaining 125.72 km^2 of forestland remained unchanged. from 2.63km2 of shrub land transitioning to bare land, 69.27km2 evolving into built-up areas, 158.46km2 dedicated to crop land, 25.48km2 designated as forest land, 0.15km2 transformed into water bodies, and 0.22km2 converted into wetlands. The remaining 65.88km2 remained unchanged Shrub land.

The waterbody is not transitioned into bare land and wetland, while 0.02km2 shifted into built-up areas. Crop land expanded to cover 0.30km2, while forest land remained at 0.04km2. Additionally, 0.02km2 converted to shrub land, leaving the remaining 4.26km2 unchanged as waterbody. The landscape undergone transformations from a wetland is not transitioned into bare land and water bodies, while 0.01km^2 evolved into built-up areas. Additionally, 1.84km^2 transitioned into crop lands, 0.02km^2 transformed into forested areas, and 0.27km^2 developed into shrub lands. The remaining 0.03km^2 retained its original state as unchanged wetland. Detailed statistics of Post-classification analysis and the LU/LC change map for the period are provided in Table 4.3 and Figure 4.4.

Table 4.3. Post-classification analysis of the study area from (1991-2023).

		Final Year_2023							
	Class Name	**Bare Land** Area (Km2)	**Built-up** Area (Km2)	**Crop land** Area (Km2)	**Forest land** Area (Km2)	**Shrub Land** Area (Km2)	**Water body** Area (Km2)	**Wet land** Area (Km2)	**Class Total**
Initial Year _1991	Bare Land	2.18 18.04%	40.40 8.28%	101.20 8.77%	2.51 1.26%	24.82 13.94%	0.05 0.74%	0.05 6.72%	**171.21**
	Built-up	0.32 2.61%	118.96 24.38%	32.04 2.77%	5.21 2.63%	3.16 1.78%	0.45 6.47%	0.01 0.95%	**160.15**
	Cropland	6.72 55.70%	236.77 48.52%	811.83 70.31%	39.31 19.82%	76.63 43.05%	1.88 27.28%	0.44 58.10%	**1,173.58**
	Forestland	0.23 1.88%	22.52 4.61%	48.91 4.24%	125.72 63.40%	7.24 4.06%	0.10 1.49%	0.01 0.81%	**204.72**
	Shrub Land	2.63 21.77%	69.27 14.20%	158.46 13.72%	25.48 12.85%	65.88 37.01%	0.15 2.13%	0.22 29.68%	**322.09**
	Waterbody	0.00 0.00%	0.02 0.00%	0.30 0.03%	0.04 0.02%	0.02 0.01%	4.26 61.88%	0.00 0.07%	**4.65**
	Wetland	0.00 0.00%	0.01 0.00%	1.84 0.16%	0.02 0.01%	0.27 0.15%	0.00 0.00%	0.03 3.67%	**2.17**
	Class Total	**12.06**	**487.96**	**1,154.58**	**198.30**	**178.02**	**6.89**	**0.75**	**2,038.56**

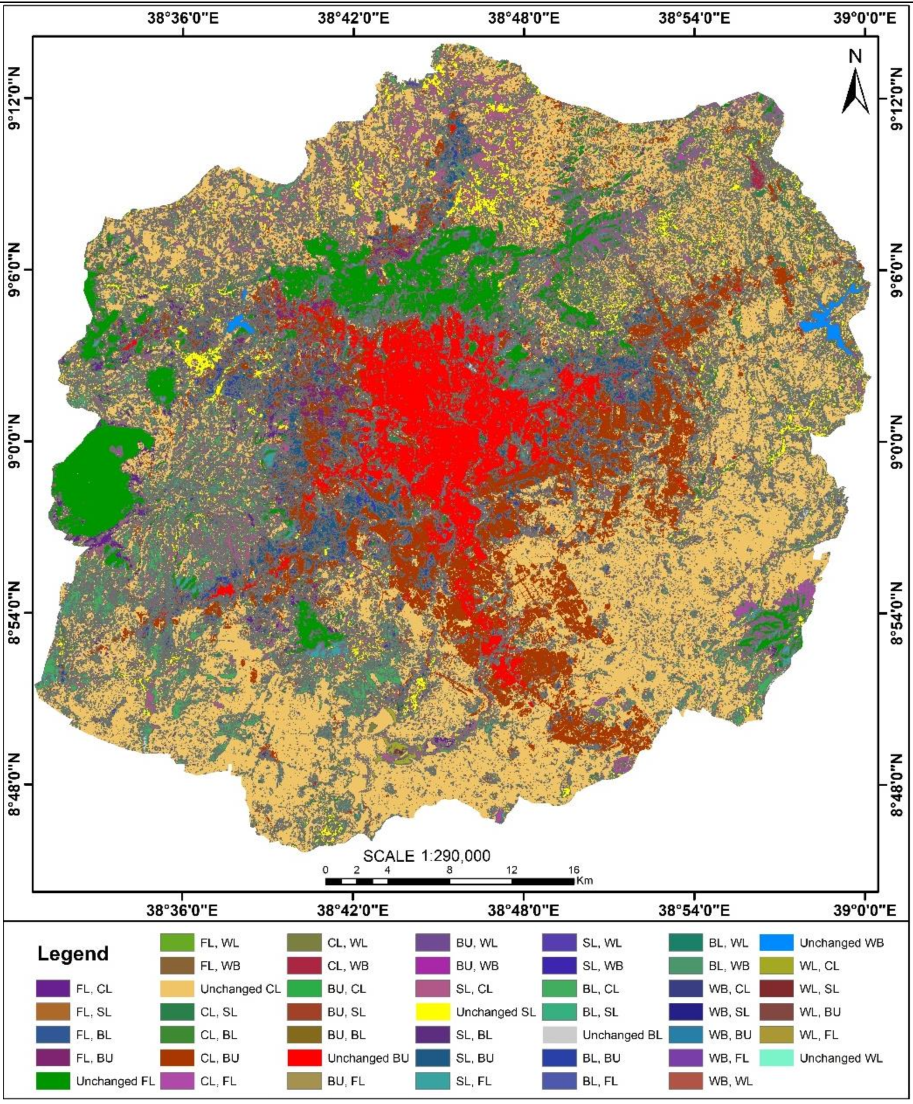

Figure4.4: Land use Land Cover Map of study Area from 1991-2023.

4.4. Expansion of Built-up from 1991 to 2023

An overlay analysis comparing satellite images from 1991, 2001, 2013, and 2023 of Addis Ababa including Sheger City shows that croplands, shrub land, forests, and bare lands have increasingly been transformed into urban built-up areas in various parts of the city. The built-up area saw a steady increase from the starting year to the ending year, with increments of 160.15km2, 169.68km2, 317.69km2, and 487.96km2 respectively. These alterations were derived from converting 40.40km2 of bare land, 236.77km2 of crop land, 22.52km2 of forest land, and 69.27km2 of shrub land to Built-up. The expansion of built-up areas into other land use and land cover class is illustrated in Figure 4.5.

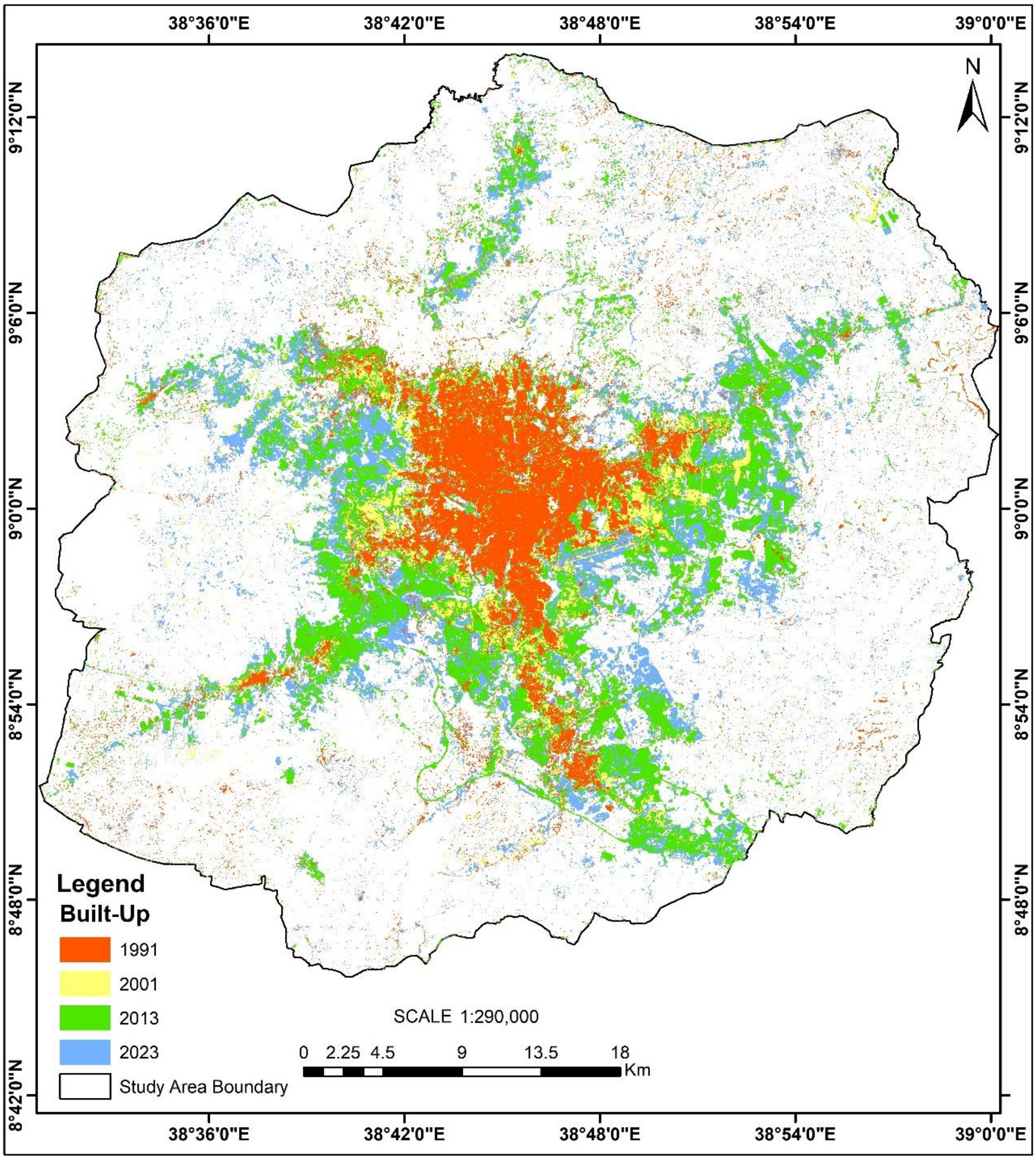

Figure 4.5: The pattern of built-up growth in study area from 1991 to 2023.

4.5. Accuracy assessment

The evaluation of land use/land cover (LU/LC) accuracy for the years 1991, 2001, 2013, and 2023 showed overall classification accuracies of 89.00%, 90.00%, 90.00%, and 91.00% respectively. The Kappa statistic for 1991 was 0.8716. In subsequent years, the Kappa values were 0.8857 for 2001, 0.8861 for 2013, and 0.9000 for 2023. Detailed data on producer and user accuracy can be found in Table 4.4.

Table 4.4: Accuracy assessment statistics for the years 1991, 2001, 2013, and 2023.

	1991		2001		2013		2023	
Class Name	producers accuracy	users accuracy	producers accuracy	users accuracy	producers accuracy	users accuracy	producers accuracy	users accuracy
Wetland	81.82%	90.00%	88.89%	80.00%	90.00%	90.00%	100.00%	100.00%
Waterbody	88.89%	80.00%	88.89%	80.00%	90.91%	100.00%	90.91%	100.00%
Shrub Land	90.91%	100.00%	83.33%	100.00%	100.00%	70.00%	100.00%	90.00%
Bare Land	90.00%	90.00%	83.33%	100.00%	90.91%	100.00%	90.00%	90.00%
Forestland	88.89%	80.00%	100.00%	90.00%	90.91%	100.00%	90.00%	90.00%
Cropland	88.89%	80.00%	90.00%	90.00%	88.89%	80.00%	72.73%	80.00%
Built-up	90.00%	90.00%	88.89%	80.00%	100.00%	80.00%	88.89%	80.00%
Overall accuracy	89%		90%		90%		91%	
Kappa	0.8716		0.8857		0.8861		0.90	

4.6. Normalized Difference Vegetation Index

This research found that vegetation cover was notably higher in the years 1991 and 2001, reaching peak NDVI values of 0.74 and 0.76, respectively, indicating robust vegetation health. However, there was a decline in vegetation cover in 2013, with the NDVI dropping to 0.59, followed by a recovery in 2023, when the NDVI increased to 0.63. The findings for the years 1991, 2001, 2013, and 2023 are detailed in Figure 4.5. The analysis revealed that the northern, northwest, and southwest regions of the study area consistently exhibited higher NDVI values. Additionally, Entoto Park and Suba Menagesha Park registered the highest NDVI values throughout the study period. However built-up areas, water bodies, and many areas in the eastern region typically exhibit lower NDVI values. As shown in Figure 4.6, there has been a gradual decline in vegetation cover with an increase in areas devoid of vegetation over the time of the study. Nonetheless, in 2023, there was a slight increase in vegetative cover due to the Green Legacy initiative. Table 4.5 presents the statistical data on NDVI values for the years 1991, 2001, 2013, and 2023.

Table 4.5: Statistical data on NDVI values for the years 1991, 2001, 2013, and 2023.

Year	Min	Max	Mean	Std
1991	-0.42	0.74	0.14	0.11
2001	-0.54	0.76	0.18	0.12
2013	-0.22	0.59	0.22	0.83
2023	-0.27	0.63	0.20	8.23

Where, Min = Minimum, Max = Maximum, Std = Standard deviation

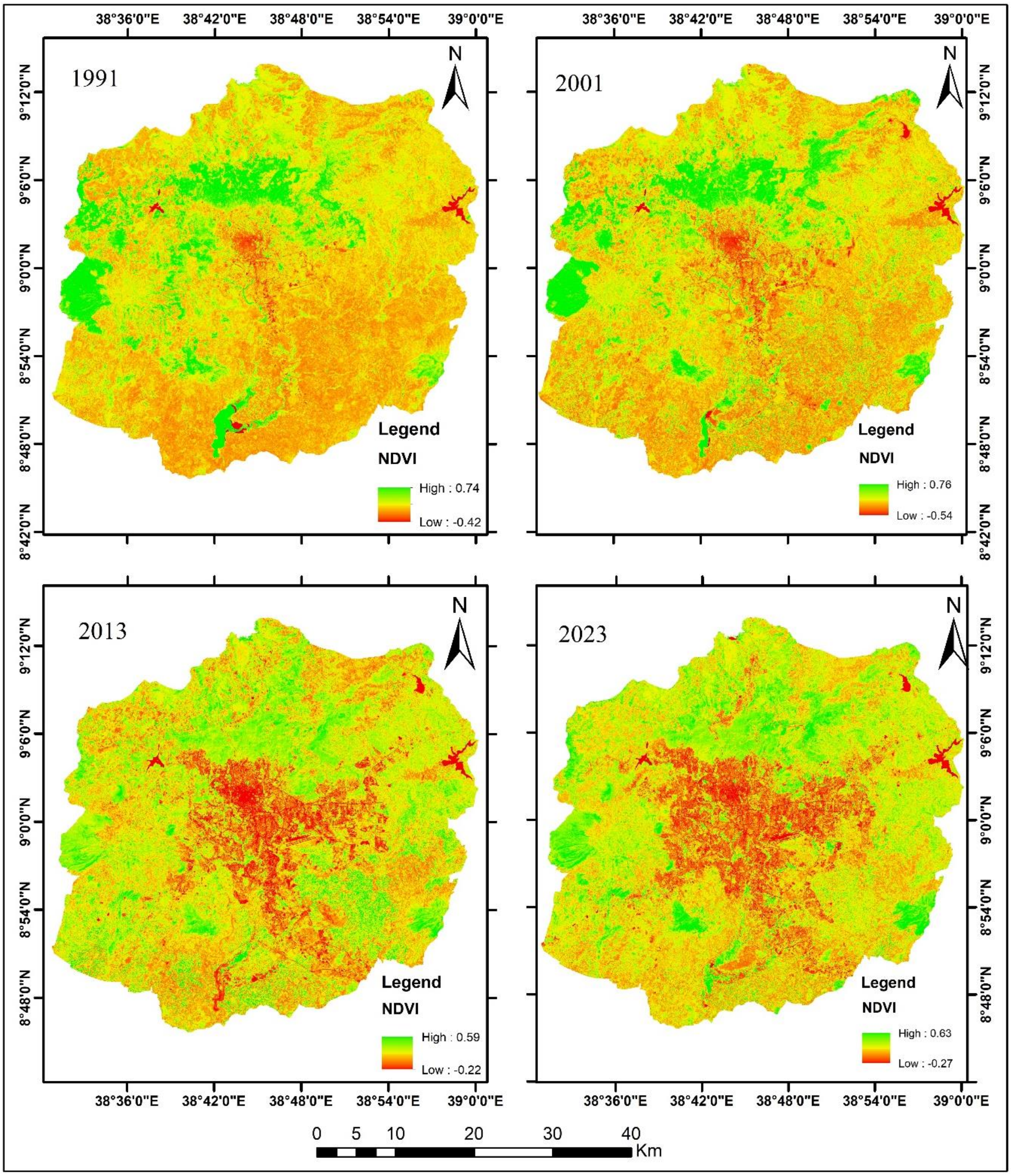

Figure 4.6: Maps of NDVI for the study area in the years 1991, 2001, 2013, and 2023.

4.6.1. Zonal statistical relation between LU/LC and NDVI

Maps of the normalized difference vegetation index (NDVI), derived from the near-infrared and red bands during the study periods, show that various land use/land cover (LU/LC) types exhibit distinct NDVI values. NDVI, which reflects vegetation health, differs across locations according to the intensity of vegetation present. Areas classified as forest land, shrub land, and cropland consistently display higher NDVI values compared to other categories, as illustrated in Figure 4.7.

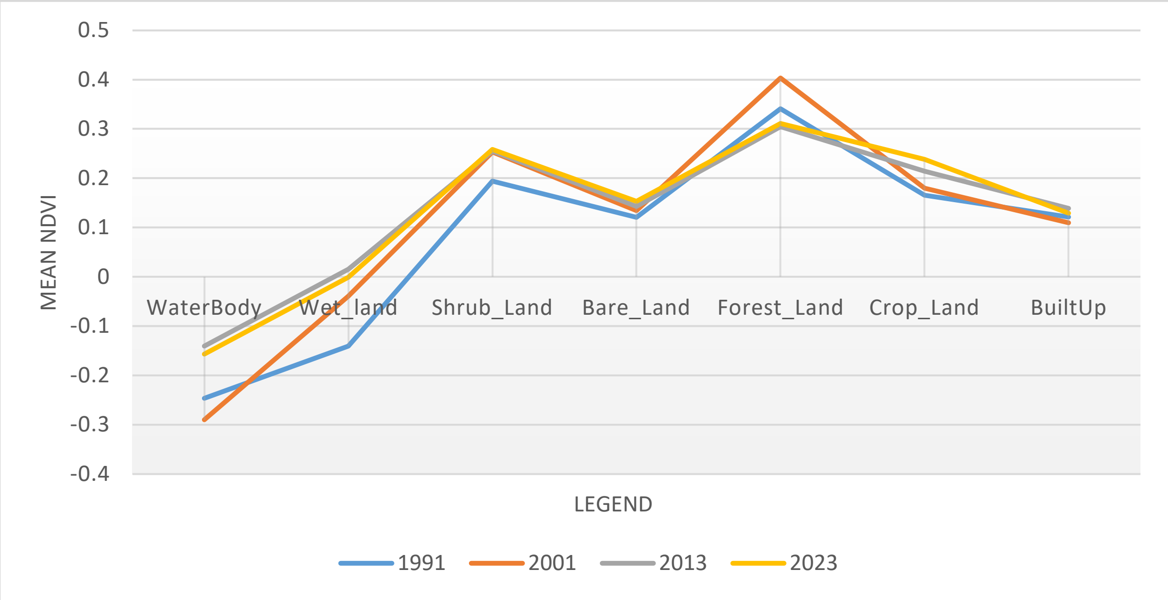

Figure 4.7: Zonal Statistical analysis of NDVI for the years 1991, 2001, 2013, and 2023 across various LU/LC classes in the study area.

4.7. Normalized Difference Built-up index

In 2001 and 2023, the built-up areas reached their peaks with Normalized Difference Built-Up Index (NDBI) values of 0.49 and 0.64, respectively, indicating extensive urban development. In contrast, the NDBI values were slightly lower in 1991 and 2013, recorded at 0.43 and 0.47, respectively. Figure 4.5 illustrates the NDBI results for these years, showing variations in urban expansion over time. The results of the Normalized Difference Built-up Index (NDBI) for the years 1991, 2001, 2013, and 2023 indicate higher NDBI values in the central region of the study area, extending in all directions. In contrast, the forested areas and other parts outside the central region exhibit relatively low NDBI values. Figure 4.8 illustrates that built-up areas have expanded while non-built-up zones have steadily decreased throughout the study period. Additionally, Table 4.6 presents statistical data on the Normalized Difference Built-up Index (NDBI) for the years 1991, 2001, 2013, and 2023.

Table 4.6: Statistical data on NDBI values for the years 1991, 2001, 2013, and 2023.

Year	Min	Max	Mean	Std
1991	-0.81	0.43	-0.16	0.12
2001	-0.90	0.49	-0.20	0.14
2013	-0.56	0.47	-0.17	9.68
2023	-0.59	0.64	-0.14	9.34

Where, Min = Minimum, Max = Maximum, Std = Standard deviation

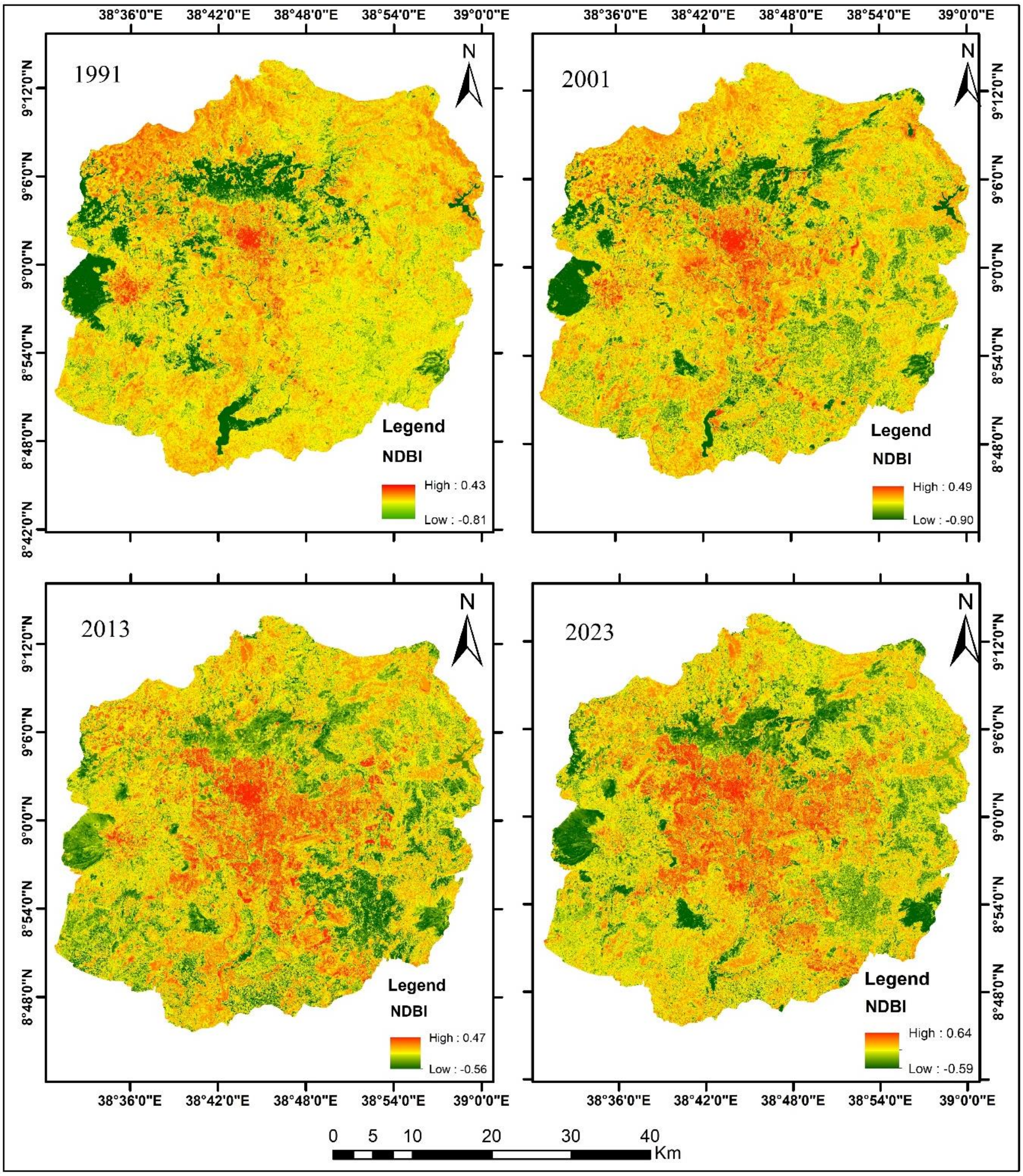

Figure 4.8: Maps of NDBI for the study area in the years 1991, 2001, 2013, and 2023.

4.7.1. Zonal statistical relation between LU/LC and NDBI

Maps of the Normalized Difference Built-up Index (NDBI) derived from short wave infrared and near infrared data during the study periods show that various land use/land cover (LU/LC) types exhibit distinct NDBI values. The NDBI, which indicates the presence of built-up areas, fluctuates across different locations depending on the intensity of built-up areas at each site. Built-up areas and bare land typically register the highest NDBI values compared to other categories (Figure.4.9).

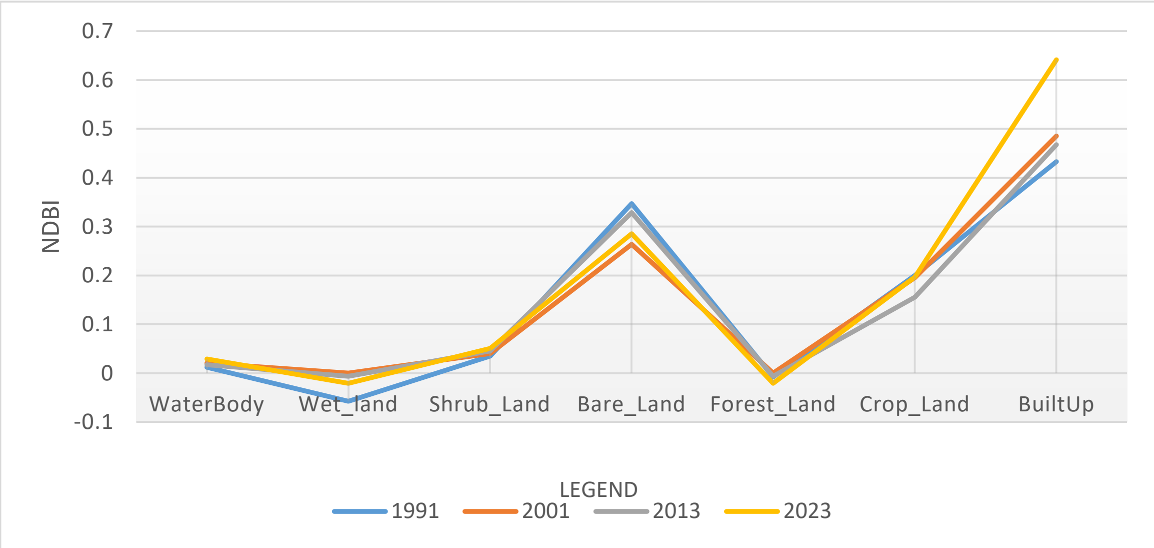

Figure 4.9: Zonal Statistical analysis of NDBI for the years 1991, 2001, 2013, and 2023 across various LU/LC classes in the study area.

4.8. Normalized Difference Bareness Index

In 2013 and 2023, the bare areas reached their peak with NDBaI values of 0.42 and 0.39, respectively, indicating significant barrenness. Earlier years, such as 1991 and 2001, also showed notable bareness with NDBaI values of 0.36 and 0.34, respectively. These figures suggest a high degree of land exposure, though not to the same extent as the latter years. The data for the Normalized Difference Bareness Index (NDBaI) from 1991, 2001, 2013, and 2023 is presented in Figure 4.10. The results of the Normalized Difference Bareness Index (NDBaI) from the years 1991, 2001, 2013, and 2023 indicate that the northern, northwest, and southwest regions of the study area exhibited higher NDBaI values. Conversely, the built-up areas, Entoto Park, and Suba Menagesha Park recorded the lowest NDBaI values. According to Figure 4.9, there has been a gradual decrease in bareness and an increase in non-bare areas throughout the study period. Furthermore, Table 4.7 provides statistical data on the NDBaI values for the years 1991, 2001, 2013, and 2023.

Table 4.7: Statistical data on NDBaI values for the years 1991, 2001, 2013, and 2023.

Year	Min	Max	Mean	Std
1991	-0.84	0.36	-0.19	0.12
2001	-0.94	0.34	-0.21	0.13
2013	-0.68	0.42	-0.36	6.62
2023	-0.71	0.39	-0.38	6.44

Where, Min = Minimum, Max = Maximum, Std = Standard deviation

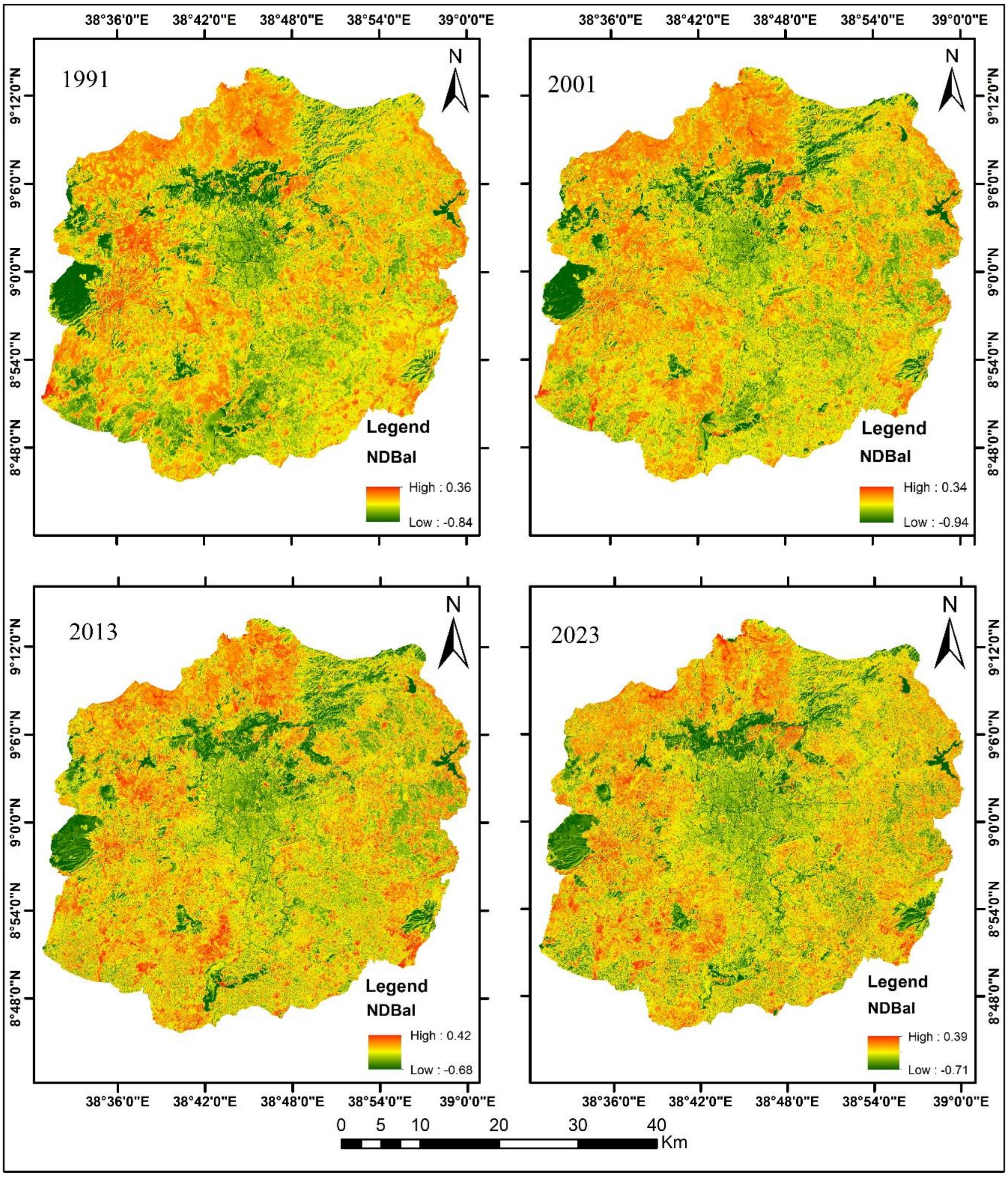

Figure 4.10: Maps of NDBaI or the study area in the years 1991, 2001, 2013, and 2023.

4.8.1. Zonal statistical relation between LU/LC and NDBaI

Maps of the Normalized Difference Bareness Index (NDBaI) derived from short wave infrared and thermal band. Data during the study periods show that various land use/land cover (LU/LC) types exhibit distinct NDBaI values. The NDBaI, which indicates the presence of bareness areas, fluctuates across different locations depending on the intensity of bareness areas at each site. Bare areas and cropland land typically register the highest NDBaI values compared to other categories (Figure.4.11).cropland shows relatively higher value related to other class because of the image is captured when crops harvested.

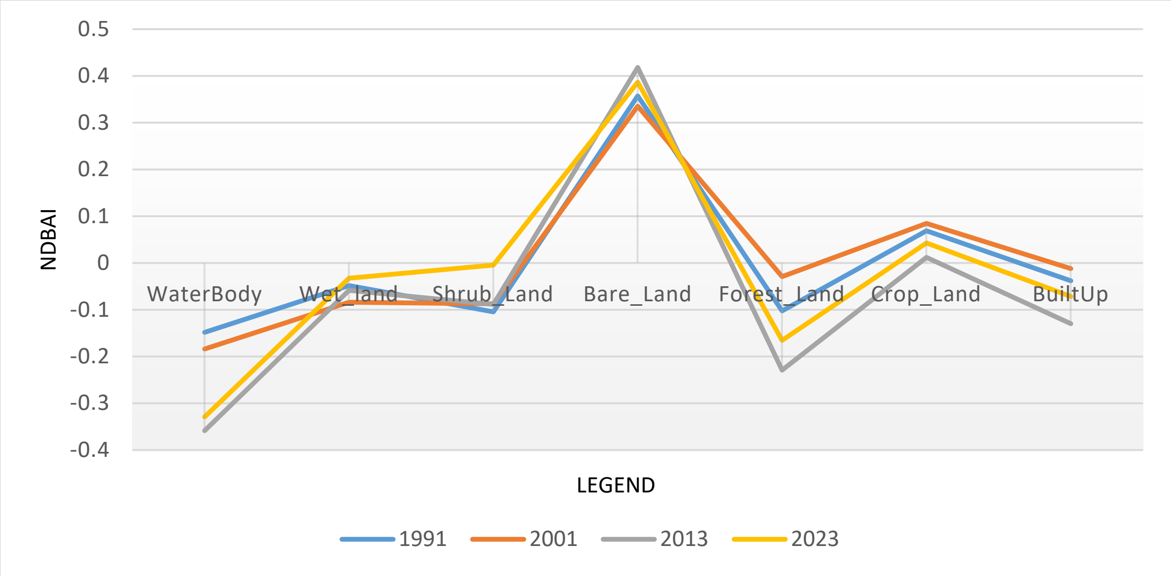

Figure 4.11: Zonal Statistical analysis of NDBaI for the years 1991, 2001, 2013, and 2023 across various LU/LC classes in the study area.

4.9. Normalized Difference Water Index

In 1991 and 2001, water coverage reached its peak as indicated by NDWI values of 0.45 and 0.53, respectively, suggesting substantial aquatic areas. However, in 2013, the NDWI value decreased to 0.23, showing a reduction in water areas, but it slightly rose to 0.26 in 2023 according to the NDWI measurements. These results for the years 1991, 2001, 2013, and 2023 are depicted in Figure 4.12. The data reveals that Gefersa Lake, Legedadi Lake and Drei water refinery exhibited higher NDWI values over these years. The wet land areas reported marginally higher values than other class, which is located in the southern part of the study Area.

Table 4.8: Statistical data on NDWI value for the years 1991, 2001, 2013 and 2023.

Year	Min	Max	Mean	Std
1991	-0.67	0.45	-0.23	8.05
2001	-0.71	0.53	-0.31	8.74
2013	-0.53	0.23	-0.24	6.92
2023	-0.56	0.26	-0.22	7.12

Where, Min = Minimum, Max = Maximum, Std = Standard deviation

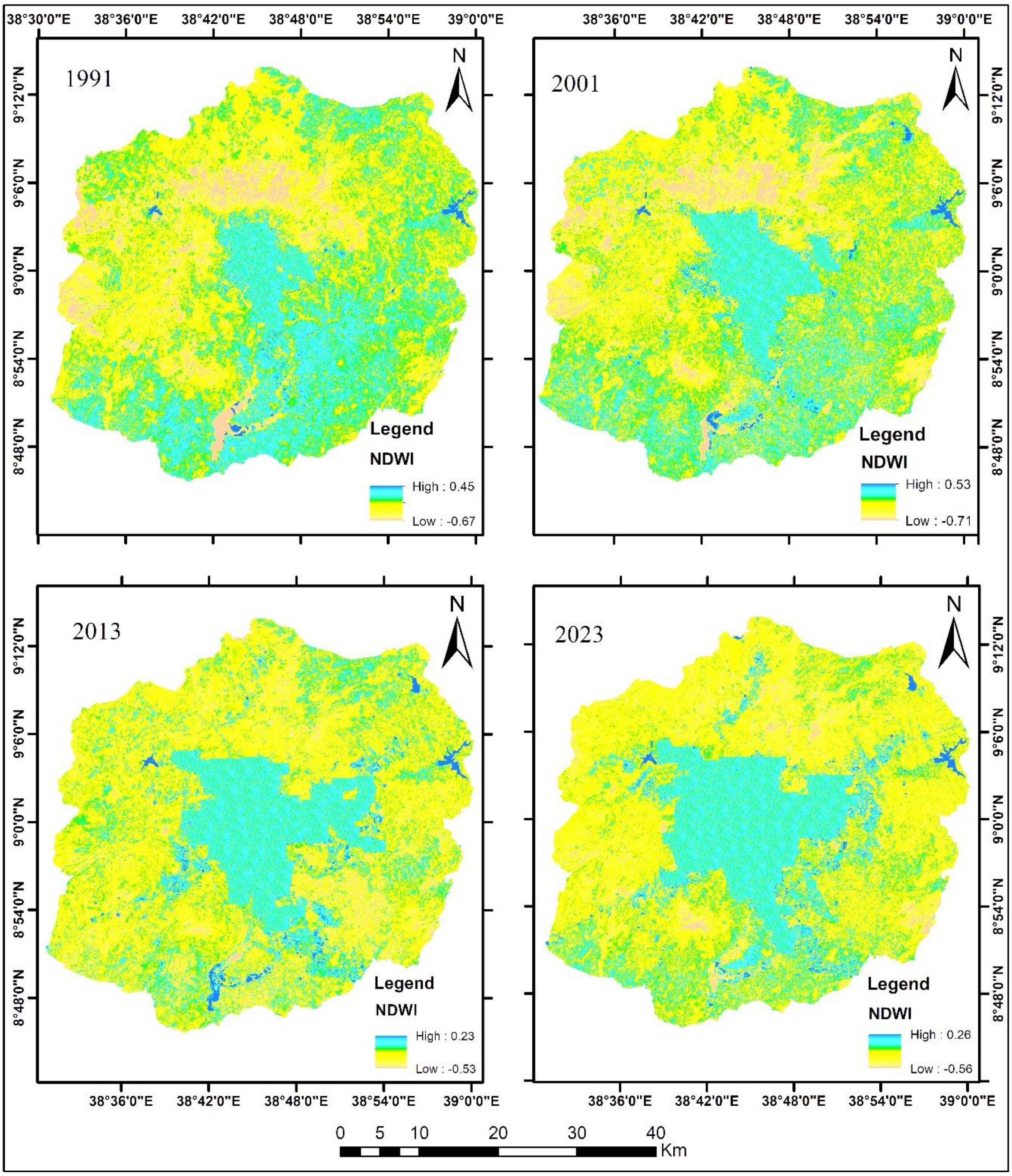

Figure 4.12: Maps of NDWI for the study area in the years 1991, 2001, 2013, and 2023.

4.9.1. Zonal statistical relation LU/LC and NDWI

The study produced maps of the Normalized Difference Water Index (NDWI), which utilizes the green and near-infrared bands. These maps reveal that different types of land use and land cover (LU/LC) display unique NDWI values during the study periods. The NDWI serves as an indicator of water presence and shows variations at various sites based on the water content level there. Typically, areas of water bodies and wetlands record the highest NDWI values compared to other class, as illustrated in Figure 4.13.

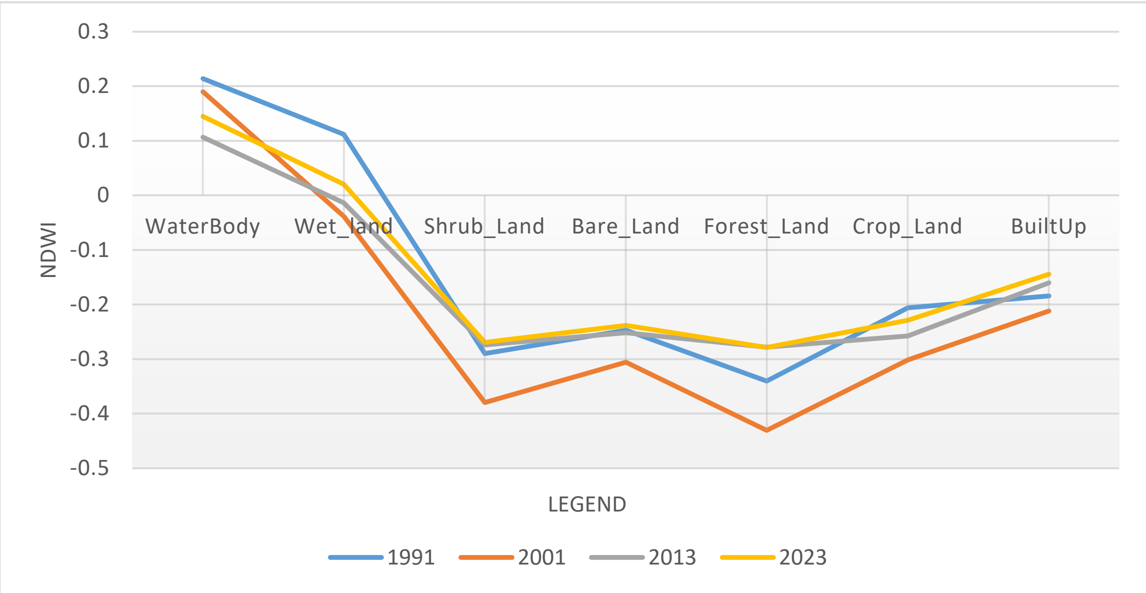

Figure 4.13: Zonal Statistical analysis of NDWI for the years 1991, 2001, 2013, and 2023 across various LU/LC classes in the study area.

4.10. Land Surface Temperature

The study analyzed the spatial distribution of Land Surface Temperature (LST) across the study area using Landsat TM data from the years 1991, 2001, 2013, and 2023 OLI/TIRS thermal bands. The analysis revealed that LST values during the study period varied between 7°C and 41.29°C. High temperatures were notably present in the northwest, southwest, and northeast regions of the area, primarily influenced by factors such as altitude, slope, and land use/land cover types. Conversely, cooler temperatures were recorded in the northern parts of the area, including Entoto, Suba Menagesha Park, and the areas around Geferesa, Legedagi Lake and Drei water refinery. The distribution of LST for each period is depicted in Figure 4.14.

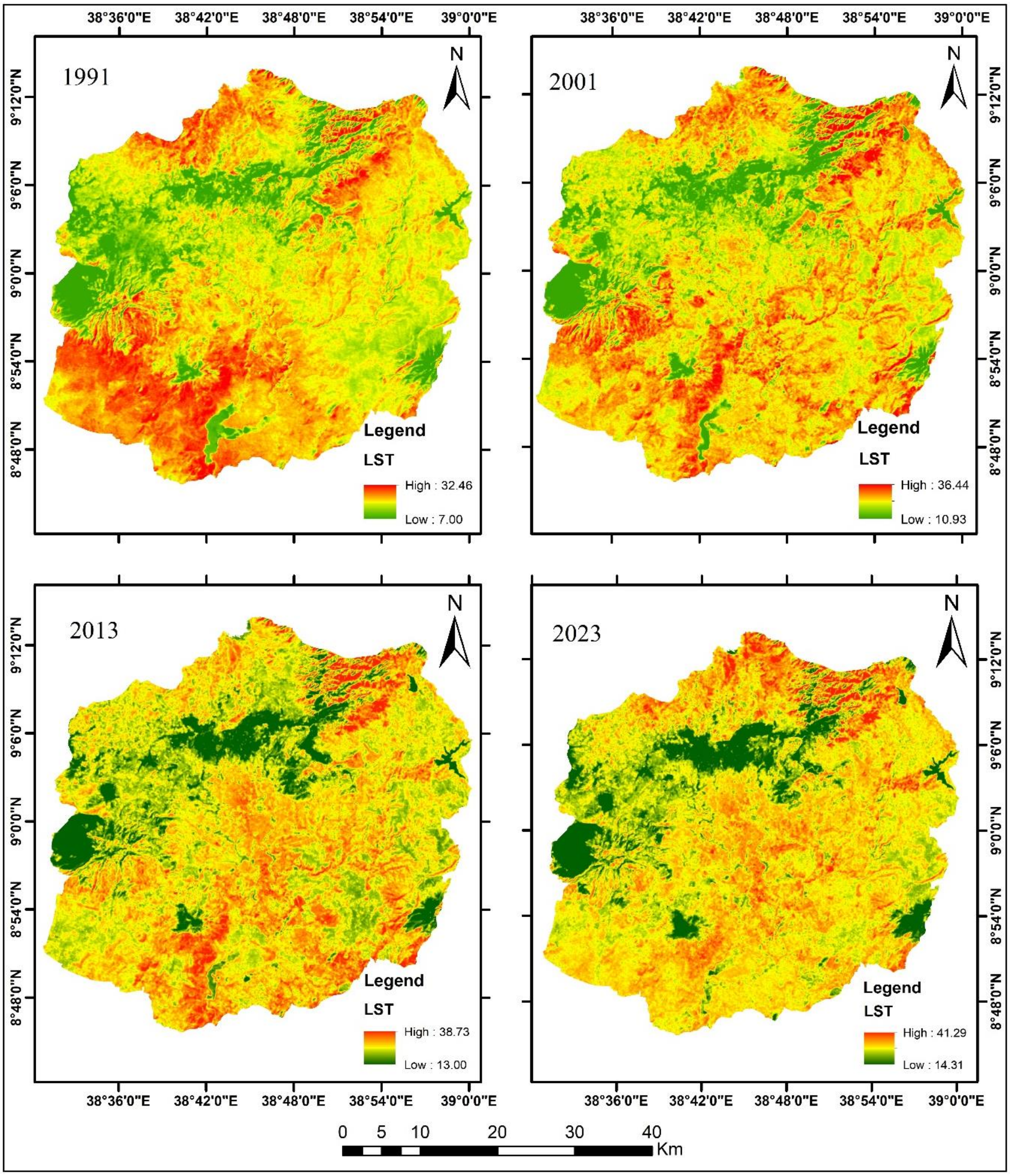

Figure 4.14: Maps of LST for the study area in the years 1991, 2001, 2013, and 2023.

4.10.1. Zonal statistical relation between LU/LC and land surface temperature

The land-use/land-cover and land surface temperature (LST) map of the study area illustrated changes in both the landscape and the corresponding temperatures over the period of study. The lowest temperatures were recorded in areas categorized as water bodies, wetlands, forest land and shrub land, in that order. Both water bodies and vegetated regions were key in reducing LST. Vegetation and tree coverage in various parts of the area provided shade, which helps to decrease surface and air temperatures through the process of evapotranspiration, where plants emit water into the air. Conversely, the highest LST readings were observed in Croplands, Built-up, and bare lands. Notably, LST was particularly elevated in Cropland areas where the imagery capture coincided with the crop harvest period, leaving the land exposed. Between 1991 and 2023, the average land surface temperature (LST) in Addis Ababa, including Sheger, rose by 8.83°C. According to Table 4.9, this increase was observed across all primary land use/land cover class. The highest average LSTs were noted in areas of bare land, crop land, and built-up areas. Conversely, the lowest average LSTs occurred in water bodies, wetlands, forests and shrub land. Figure 4.15 shows comparisons of the mean LST across different LU/LC classes over the period. Overall, the data points to a significant rise in land surface temperature in the study area from 1991 to 2023, as detailed in Table 4.9.

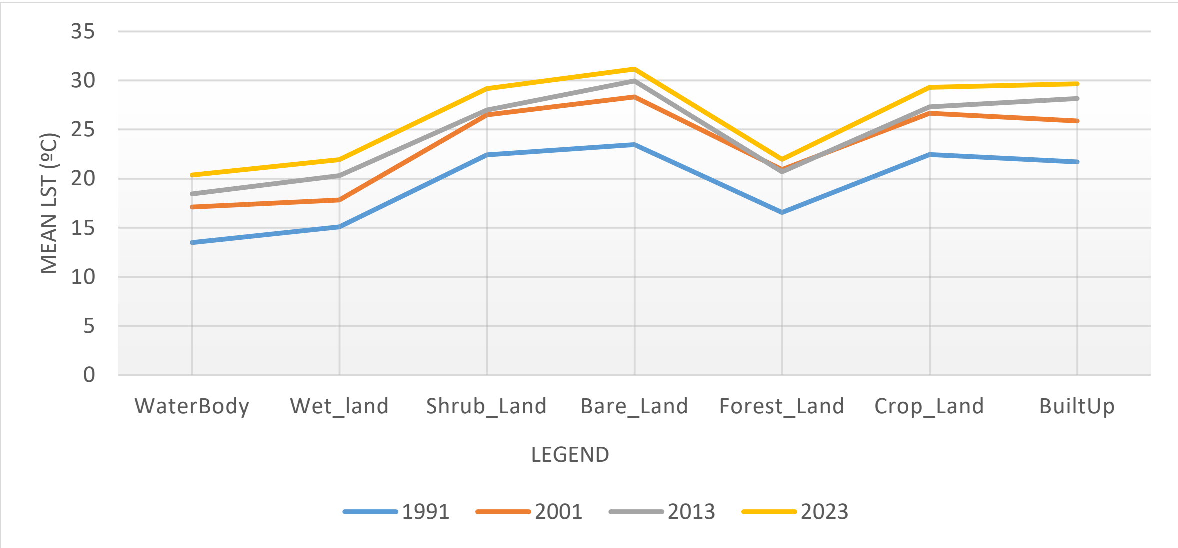

Figure 4.15: Zonal Statistical analysis of LST for the years 1991, 2001, 2013, and 2023 across various LU/LC classes in the study area.

Table 4.9: Mean temperatures for the years 1991, 2001, 2013, 2023 and Changes across various LU/LC classes in the study area.

Class Name	1991 Mean	2001 Mean	2013 Mean	2023 Mean	1991–2001 Change in (ºC)	2001–2013 Change in (ºC)	2013–2023 Change in (ºC)	1991–2023 Change in (ºC)
Waterbody	13.50	17.12	18.44	20.37	3.62	1.33	1.92	6.87
Wetland	15.07	17.83	20.29	21.92	2.76	2.46	1.62	6.85
Shrub Land	22.41	26.51	26.99	29.17	4.10	0.48	2.18	6.76
Bare Land	23.47	28.33	29.96	31.15	4.86	1.63	1.19	7.68
Forestland	16.55	20.94	20.69	21.97	4.38	-0.25	1.28	5.41
Built-up	21.69	25.87	28.15	29.66	4.18	2.27	1.51	7.97
Cropland	22.44	26.66	27.3	29.3	4.22	0.64	2.00	6.86

4.10.2. Analysis of LST Patterns in the Years 1991, 2001, 2013 and 2023

The findings from the study showed a significant increase in the Land Surface Temperature (LST) values throughout the duration of the study. LSTs were categorized into six different ranges spanning from 7°C to 41.29°C. The distribution patterns of LST during the study period presented in Figure 4.16 and Table 4.10.

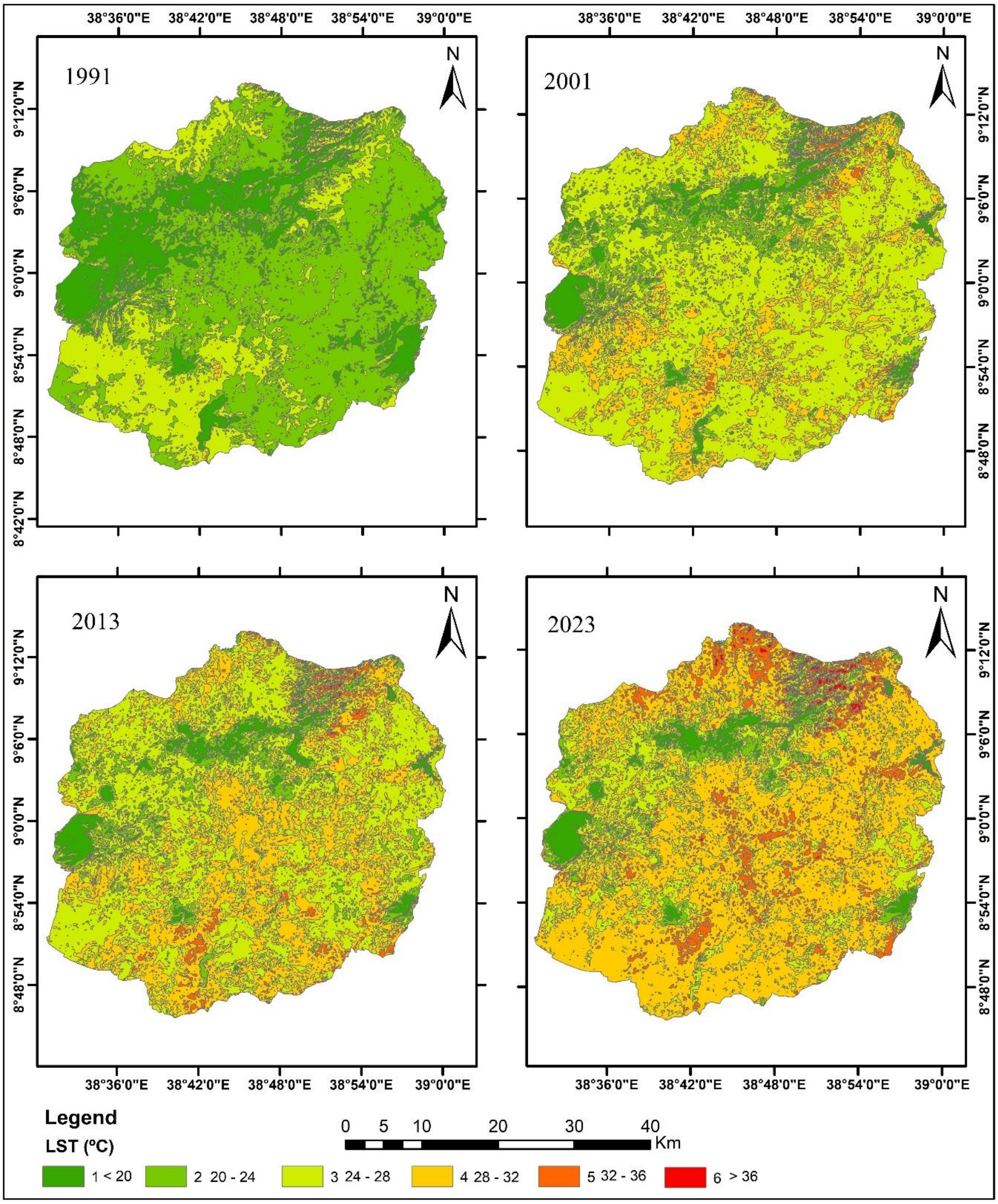

Figure 4.16. Maps of LST distribution for the study area in the years 1991,2001, 2013, and 2023.

Table 4.10: Changes in the pattern of land surface temperatures between 1991 and 2023

LST (ºC)	1991	2001	2013	2023
<20	420.76	109.00	85.04	74.63
20 - 24	1,126.90	228.00	178.32	108.83
24 - 28	481.12	1,266.00	1,026.03	447.07
28 - 32	9.67	415.00	694.17	1,211.89
32 - 36	0.01	20.46	53.42	184.01
>36	0.00	0.00	1.48	12.03
Total	2,038.46	2,038.46	2,038.46	2,038.46

The trend of rising Land Surface Temperature (LST) indicates that in Addis Ababa, including Sheger City, there has been a year-to-year increase in LST. A comparison of the LST distributions for the selected years is presented in Figure 4.17.

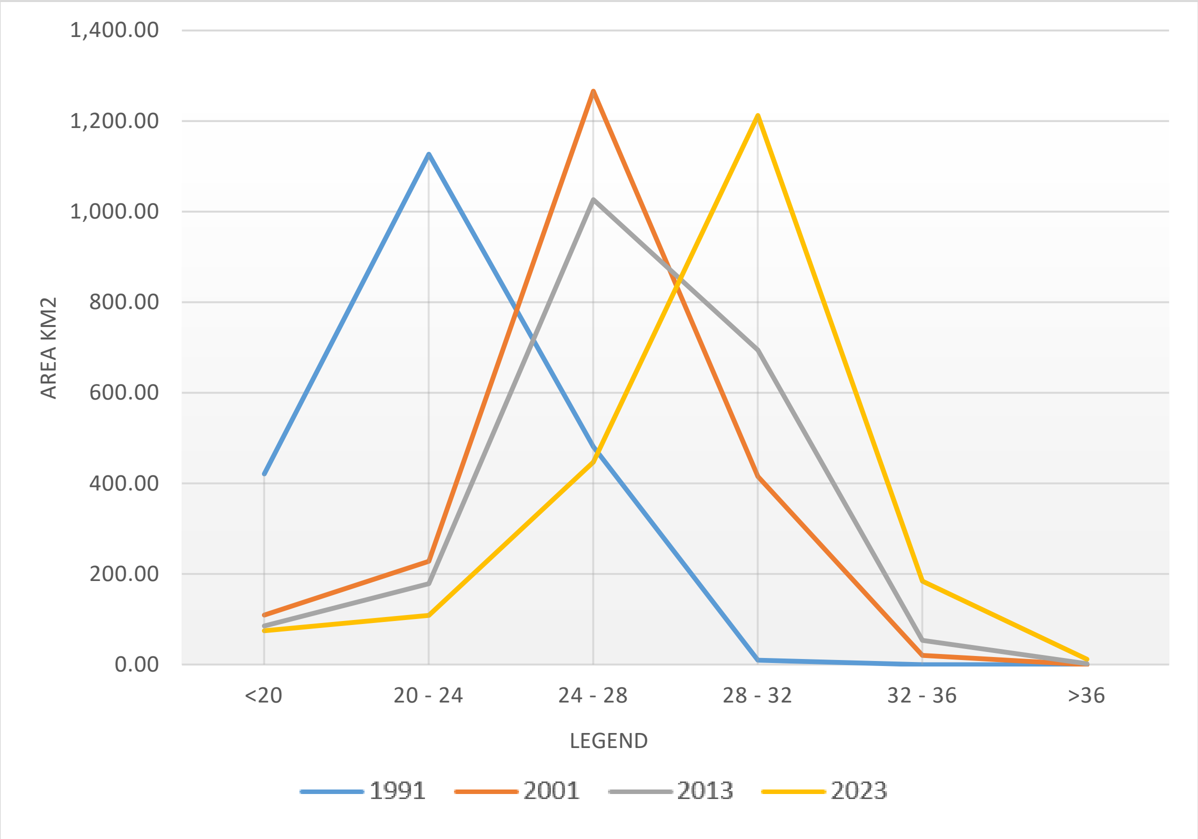

Figure 4.17: Comparative analysis of LST distributions for the years 1991,2001, 2013, and 2023 in the study area.

4.10.3. Land surface temperature Hot Spot Area

This study finds a hot spot Areas in land surface temperature over several years. In 1991, an area of 9.85 km² recorded LST exceeding 28.05°C. By 2001, this increased to an area of 13.48 km² with LSTs over 32.10°C. In 2013, the area where LST surpassed 33.04°C expanded to 22.24 km². However, in 2023, the area with temperatures above 35.32°C decreased slightly to 19.50 km². Although the atmospheric temperature decreases with increasing altitude. High altitude areas such as Hora Kulit and Eka Saden have high prevalence of LST due to bareness of land and also clear skies and high solar radiation in summer, less green space and tree cover, large number of buildings and paved surfaces and low albedo. Floors such as roads and roofs are affect the LST. LST hot spot Area Map Presented in Figure 4.18.

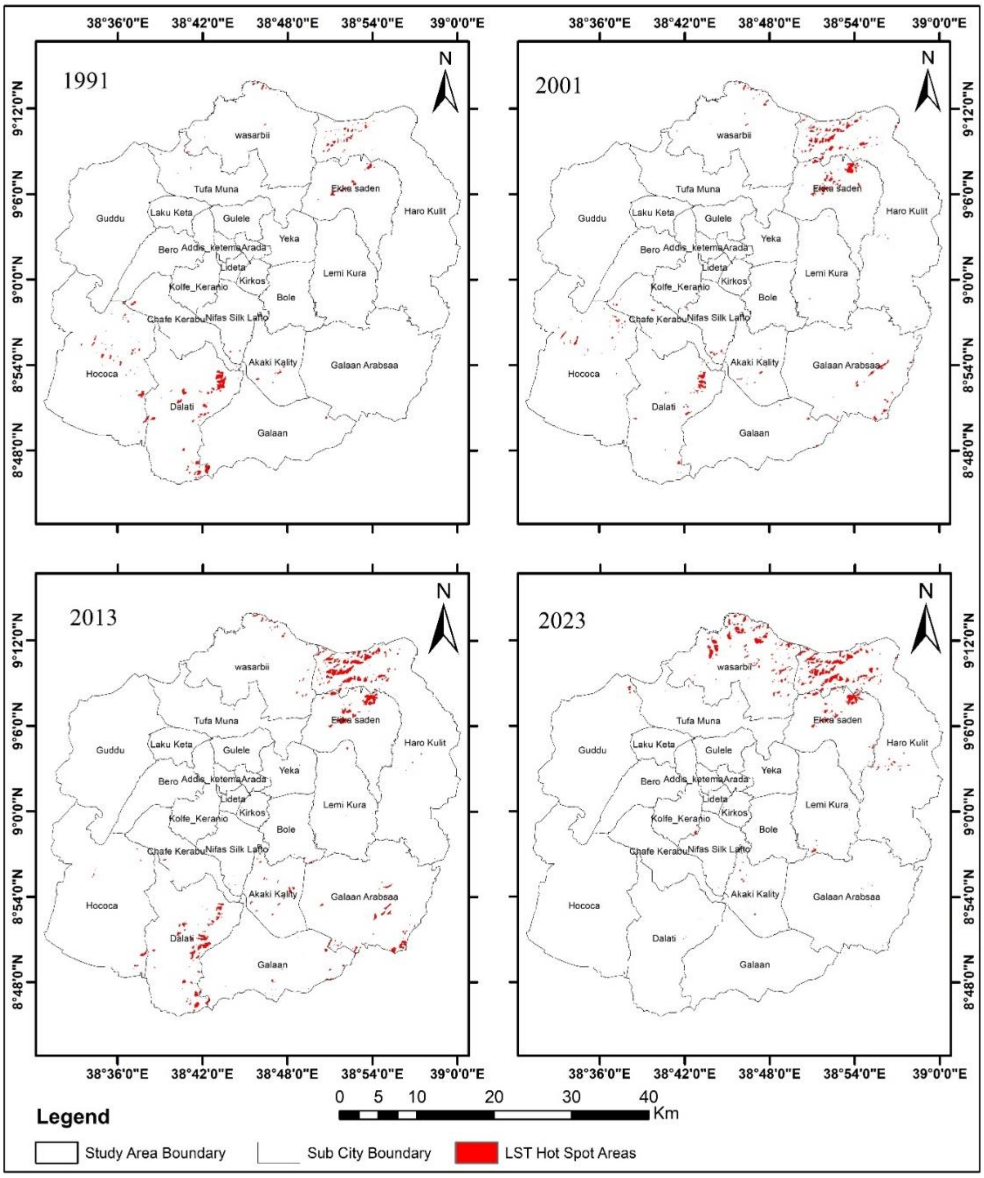

Figure 4.18: Land surface temperature Hot Spot Area.

4.11. Correlation among LST, NDVI, NDBI, NDBaI, and NDWI

In this study, a total of one hundred eighty-eight (188) samples were collected. The correlation analysis was performed using the Pearson correlation coefficient, with a 95.0% confidence interval.

4.11.1. Correlation among LST and NDVI

The Analyzed Landsat images from 1991, 2001, 2013, and 2023 revealed that NDVI and LST share an inverse relationship. Areas with low NDVI values exhibited high LST, while regions with high NDVI values displayed low LST. In contrast, for water bodies, NDVI and LST showed a direct or positive correlation, as both NDVI and LST values were lower for these areas. The correlation coefficients (R^2) between NDVI and LST during the study period were recorded at 84.5%, 85.2%, 87.3%, and 88.4% for the respective years. These figures generally reflect a strong negative correlation between NDVI and LST. The relationship between land surface temperature and NDVI for the years 1991, 2001, 2013, and 2023 are shown in Figure 4.19.

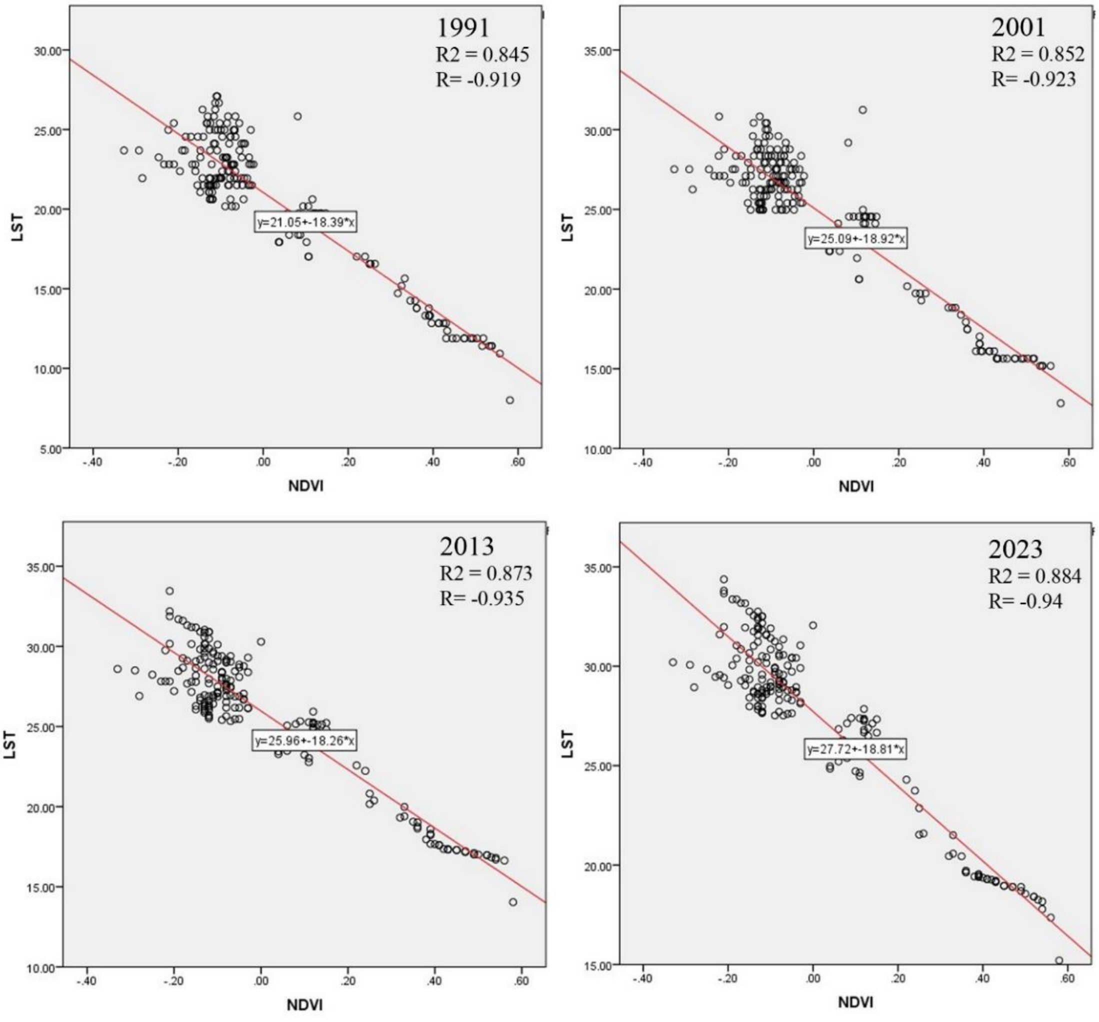

Figure 4.19. Correlation among LST and NDVI.

4.11.2. Correlation among LST and NDBI

The Analyzed Landsat images from the years 1991, 2001, 2013, and 2023 revealed a direct correlation between NDBI and LST, where higher NDBI values are associated with higher LST. The correlation coefficients (R^2 values) for the NDBI-LST relationship during these years were 82.7%, 84.4%, 85.4%, and 89.1% respectively, indicating a consistently strong positive correlation. Figure 4.20 illustrates the correlation between land surface temperature and NDBI for these specific years.

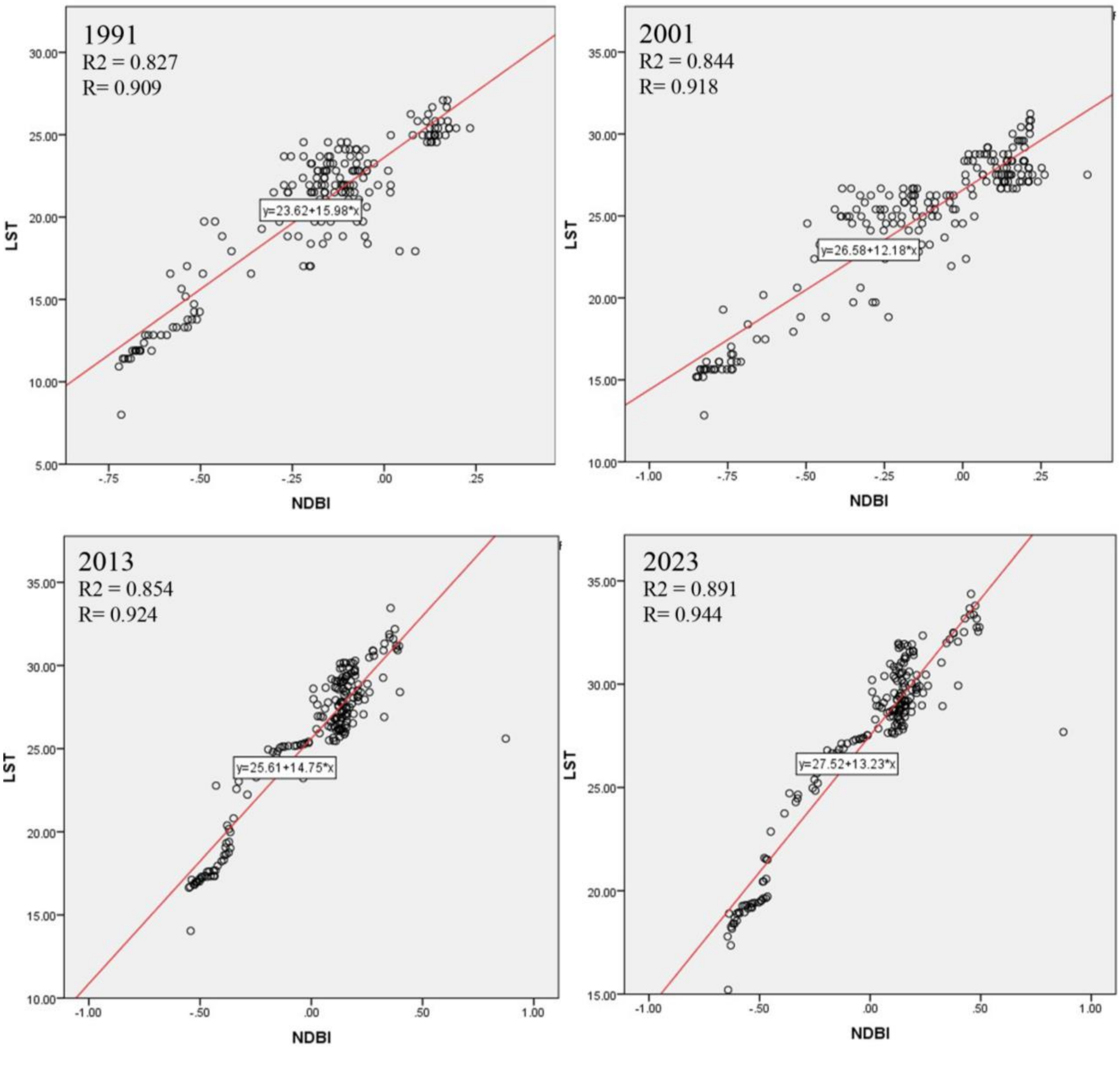

Figure 4.20 Correlation among LST and NDBI.

4.11.3. Correlation among LST and NDBaI

The Analyzed Landsat images from 1991, 2001, 2013, and 2023 revealed a direct association between NDBaI and LST. Higher NDBaI values corresponded to elevated LST levels. The R^2 values for the correlation between NDBaI and LST during the study period were 85.6%, 84.5%, 80.7%, and 80.2%, respectively, indicating a consistently strong positive correlation. Figure 4.21 illustrates the correlation between land surface temperature and NDBaI for the years 1991, 2001, 2013, and 2023.

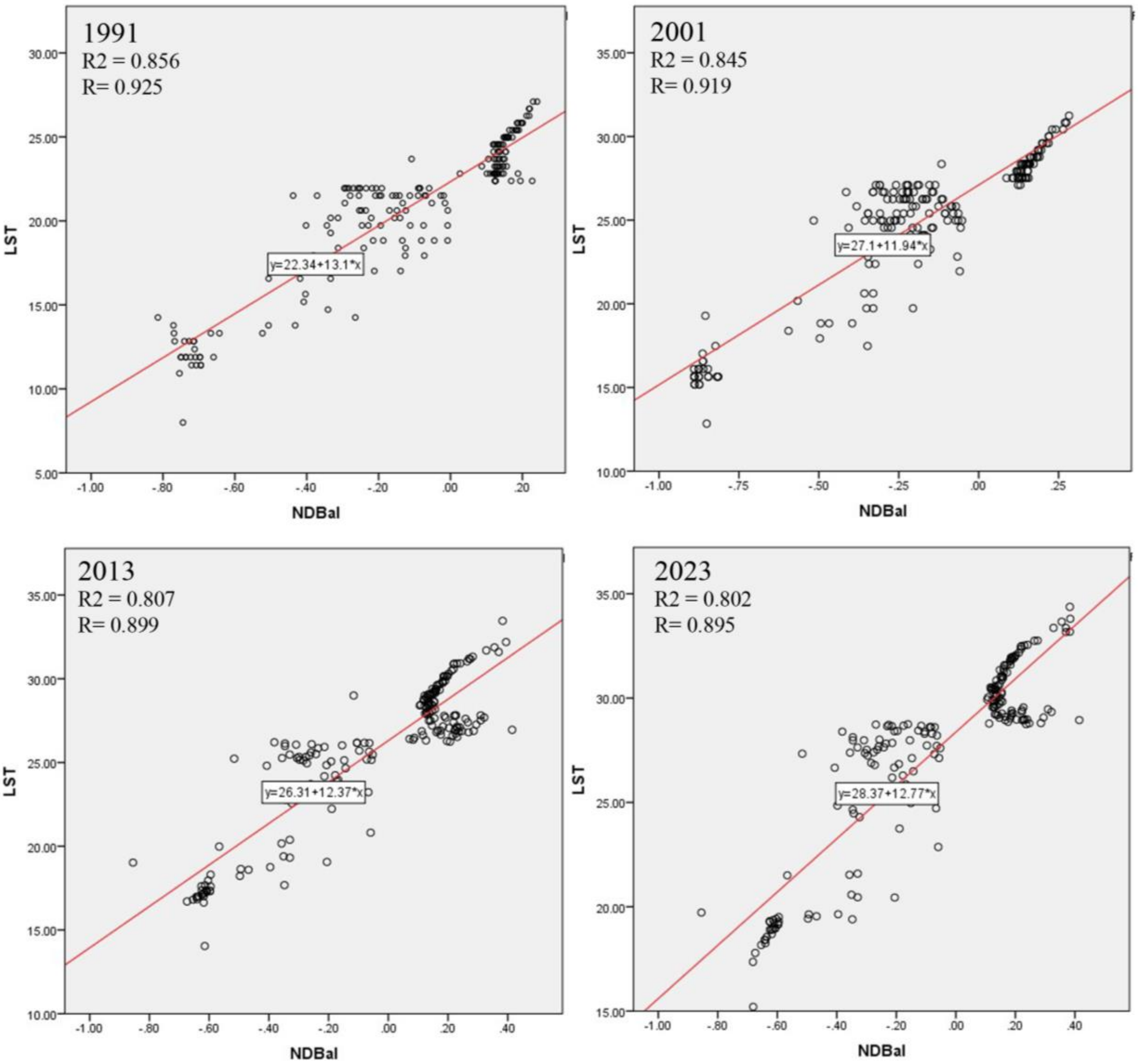

Figure 4.21 Correlation among LST and NDBaI.

4.11.4. Correlation among LST and NDWI

Analysis of Landsat imagery from the years 1991, 2001, 2013, and 2023 reveals a direct correlation between NDWI and LST, where higher NDWI values correspond to higher LST. The strength of this relationship is underscored by R^2 values recorded for these years, at 85.6%, 84.5%, 80.7%, and 80.2% respectively. This indicates a consistently strong negative correlation between NDWI and LST over the study period. The correlation data for land surface temperature and NDWI across these specific years is detailed in Figure 4.22.

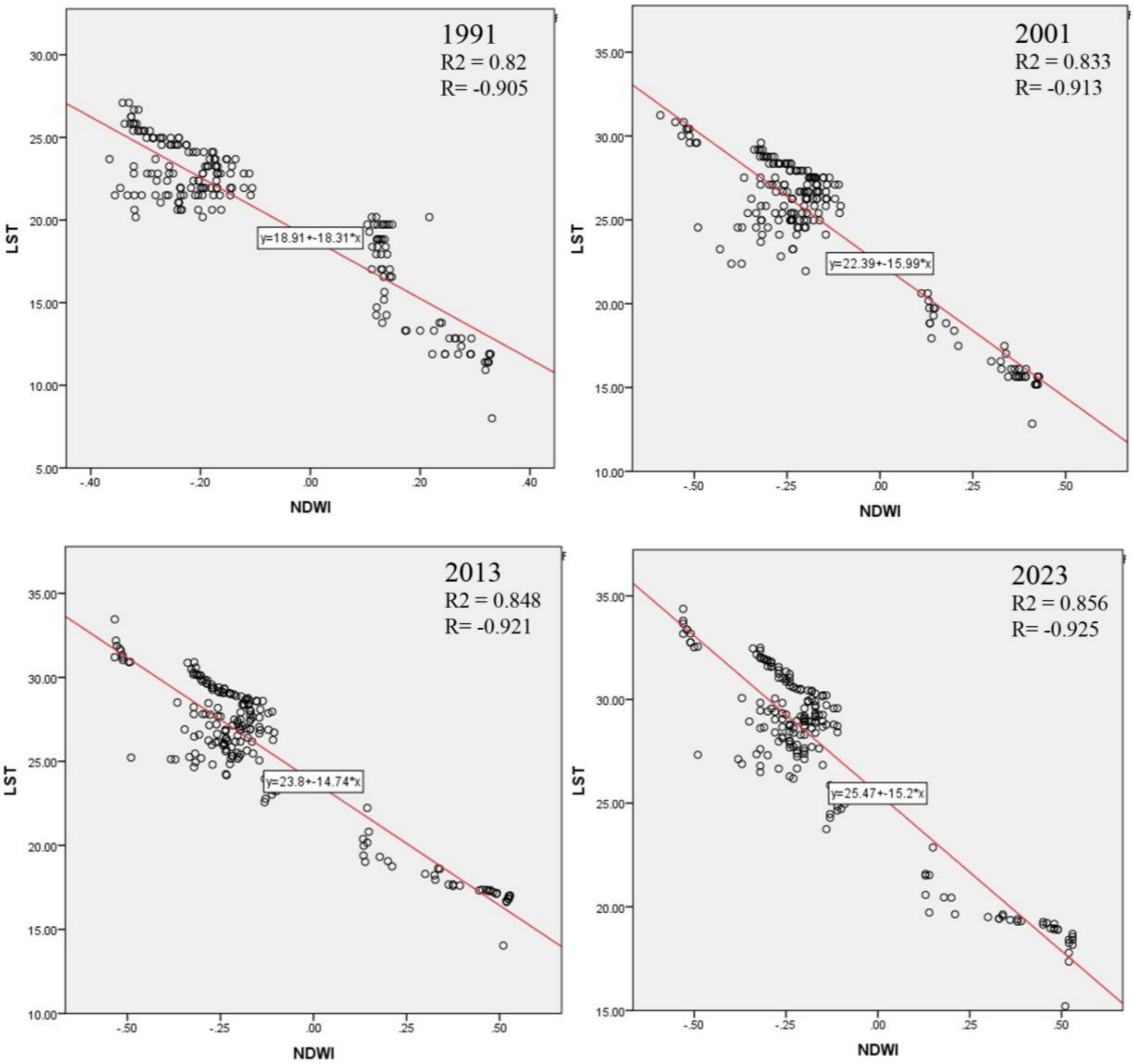

Figure 4.22 Correlation among LST and NDWI

4.12. Confirmation of Land Surface Temperature findings

The study utilized the land surface temperature (LST) derived from the Landsat thermal band and the interpolated atmospheric temperature of the area, revealing a direct correlation between them. However, the LST trends observed were based on Landsat images captured during dry conditions and the harvesting period. Taking into account the prevailing meteorological conditions and the timing of the Landsat data acquisition, the spatial pattern of the LST was confirmed. Land surface temperature was confirmed through meteorological data and land use/land cover (LU/LC) classifications of the study area, verify by GPS points gathered from the field and Google Earth. Temperature data were interpolated using meteorological records obtained from six stations located within and around the study area. These stations included: Addis Ababa Obs, Addis Ababa Bole, Guranda Meta, Sululta, Zequala and Sendafa (Add) a significant correlation exists between land surface temperature (LST) and atmospheric temperature, which has been derived by interpolation from data collected at six stations. LST obtained through remote sensing is highly effective for analyzing and forecasting the spatial and temporal distribution of atmospheric temperatures. As such, LST serves as a reliable indicator of atmospheric temperature. Maps showing interpolated data for atmospheric temperature is given in Figure 4.23.

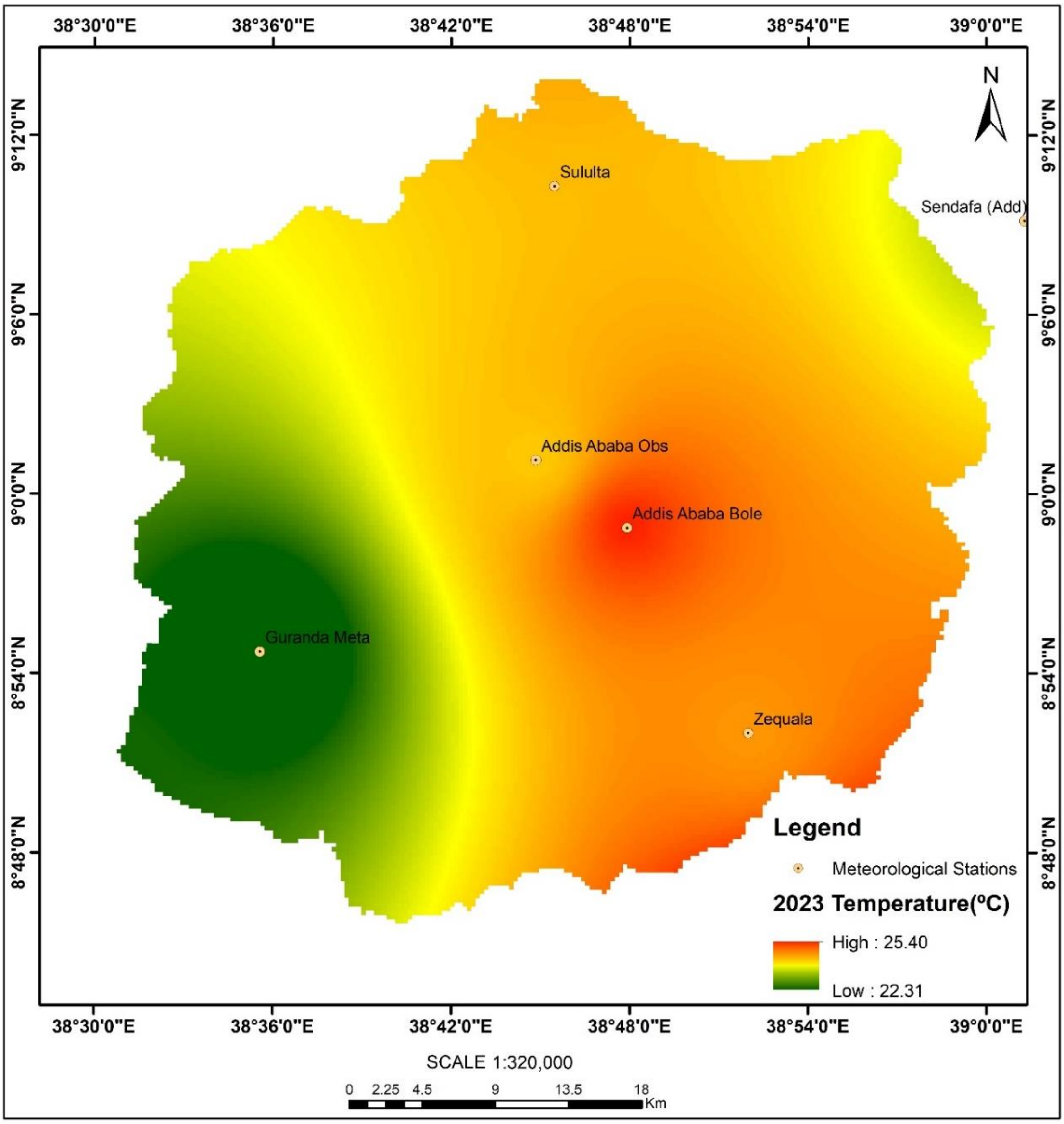

Figure 4.23. Map of interpolated Air temperature of Study Area.

The interpolated map of the study area shows that the central, south east, and southern regions recorded higher temperatures in degrees Celsius compared to the relatively cooler southwest and western parts. The Land Surface Temperature (LST) data, derived from Landsat's thermal bands, showed that during each study period, the highest temperatures were recorded in the northern, northeastern, eastern, and central regions, while the western and southwestern regions experienced the lowest temperatures. LST obtained from the thermal bands at Stations, and the interpolated atmospheric temperatures during the same periods correlation is presented in table 4.11.

Table 4.11: correlation between LST and Air Temperature.

Model Summary

Model	R	R Square	Adjusted R Square	Std. Error of the Estimate
1	.851[a]	.724	.723	1.98293

a. Predictors: (Constant), Air Temperature

4.13. Impact of Land Use Land Cover Change on Land Surface Temperature

The dynamics of land use and land cover significantly influence land surface temperature. Alterations in land use and land cover, especially in built-up, harvested cropland, and bare land, have led to changes in surface temperatures. Specifically, the high land surface temperatures observed in Cropland areas can be attributed to the fact that the imagery analyzed was captured during the harvest season and under dry weather conditions. The LST values for different LU/LC categories differ across locations due to variations in vegetation and climate conditions. Additionally, the transformation of Croplands and other land uses into built-up areas has led to higher LST levels. As shown in Figure 4.4, which documents the outward expansion of built-up areas from the city center between 1991 and 2023 (refer to Table 4.13), there has been a significant increase in built-up area.

Table 4.13: Statistical analysis of LST for the years 1991, 2001, 2013, and 2023 across various LU/LC classes in the study area.

Class Name	1991				2001				2013				2023			
	Min	Max	Mean	Std	Min	Max	Mean	Std	Min	Max	Mean	Std	Min	Max	Mean	Std
Water body	10.93	22.38	13.50	1.93	14.71	25.83	17.12	1.82	16.6	27.8	18.44	1.7	18.1	31.2	20.37	1.9
Wet land	12.84	23.25	15.07	1.39	14.25	28.35	17.83	2.20	17.8	26.2	20.29	2.2	18.1	29	21.92	2.3
Shrub Land	11.89	31.24	22.41	2.26	16.10	34.86	26.51	1.98	17	35.4	26.99	2.2	17	39.5	29.17	2.1
Bare Land	12.36	32.05	23.47	2.83	17.02	36.05	28.33	1.98	20.7	37.1	29.96	2.2	20.3	40.2	31.15	2.3
Forest land	7.00	27.93	16.55	3.01	10.93	32.05	20.94	3.30	13	33.6	20.69	2.7	14.3	34.4	21.97	3.5
Built-up	11.89	30.83	21.69	1.96	14.71	35.65	25.87	1.93	16.6	37.5	28.15	2	15.8	41	29.66	2.1
Crop land	8.98	32.46	22.44	2.44	13.31	36.44	26.66	2.20	15.2	38.7	27.3	2.4	16.7	41.3	29.3	2.4

As the result above shows the thermal band of the Landsat image was crucial for measuring the land surface temperature of the region. In this study, cropland, built-up areas, and bare land exhibited high LST values. This is primarily due to low NDVI and NDWI values, combined with high NDBI and NDBaI values, as the image was captured during the dry season and harvest period in November and December. In Ethiopia, the main harvest season spans November to January. Consequently, cropland, bare land, and built-up areas had high surface reflectance. Following the harvest, the land was extremely dry, leading to increased land reflectance. The Normalized Difference Vegetation Index values are lower for water bodies, wetlands, bare lands, built-up areas, and crop lands. Conversely, forest lands and shrub lands exhibit relatively higher NDVI values. Similarly, the Normalized Difference Built-up Index values are lower for water bodies, wetlands, forest lands, shrub lands, and crop lands, whereas built-up and bare lands show relatively higher values. The Normalized Difference Bareness Index values are lower for water bodies, wetlands, shrub lands, built-up areas, and forest lands, with higher values observed for bare lands and crop lands. The Normalized Difference Water Index values are lower for bare lands, built-up areas, forest lands, shrub lands, and crop lands, while water bodies and wetlands show higher values.

To evaluate the thermal status of the land surface using satellite imagery, understanding the relationship between land use/land cover types and Land Surface Temperature is crucial. NDVI, NDBI, NDBaI, and NDWI play significant roles in assessing and investigating LST. Land surface temperature shows a strong negative relationship with NDVI across different LU/LC Class, except for water bodies, which exhibit low NDVI and LST values. LST has a strong positive correlation with NDBI and NDBaI, while it shows a strong negative correlation with NDBI. The NDVI value and the types of land use/land cover affect the LST value. Nevertheless, this does not imply that land use/land cover type is the sole factor contributing to increase LST. Various other factors contribute to both the rise and fall of LST values. These include soil type, geothermal energy, geological formation, altitude, and local climate conditions.

Various researchers have employed thermal bands to analyze Land Surface Temperature (LST). For instance, (G. Worku et al., 2021) utilized Landsat satellite imagery to examine the LST in Addis Ababa. His study explored the connection between Land Use/Land Cover (LU/LC), LST, and NDVI. They observed a negative correlation between NDVI and

LST values, this study results are disagree with (G. Worku et al., 2021) it is important to note that water bodies should be treated as an exception since they exhibit low NDVI and LST values. The findings of the current study indicate that different types of land use/land cover exhibit varying NDVI and LST values over the study period.

(Maitima et al., 2009; Khin et al., 2012; Kerr et al., 2004)concur that the primary driver for the rise in Land Surface Temperature (LST) in both rural and urban areas is due to land-cover changes and the unplanned utilization of land resources. In less developed regions, the connection between land-cover change, biodiversity loss, and land degradation is particularly strong, as forests and vegetation are converted into human settlements, farmlands, and grazing areas (Maitima et al. 2009). Similar trends in Regarding LU/LC changes in the study area, the expansion of built-up areas has significantly reduced forest land, cropland, shrub land, and bare land. This is particularly noticeable in the city's central part, where small-scale farmers have been displaced by the expanding built-up areas and have begun to settle in open spaces and shrub land.

The normalized difference vegetation index and land surface temperature typically exhibit an indirect or negative relationship. However, this relationship can become positive or direct, particularly in water bodies and areas with high geothermal potential. (Burgan and Hartford,1993) note that negative NDVI values often indicate water, snow, clouds, non-reflective surfaces, and other non-vegetated regions, while positive values are characteristic of reflective surfaces like vegetated areas. Nonetheless, not all negative NDVI values correlate with high LST values. LST is influenced by the reflective properties of the Earth's surface. Generally, areas with non-vegetated, non-reflective surfaces tend to have higher LSTs compared to vegetated areas and water bodies.

The study's findings indicate the presence of seven primary land use/land cover categories, each exhibiting different land surface temperature values. Water bodies, wetlands, forest lands, and shrub lands generally show lower LST compared to built-up areas, croplands, and bare lands. Analysis of spatial and temporal LST distribution from 1991, 2001, 2013, and 2023 reveals significant changes over the study period. In 1991, LST ranged from a minimum of 7ºC to a maximum of 32.46ºC. By 2001, these values shifted to a range of 10.93ºC to 36.44ºC, in 2013 from 13ºC to 38.73ºC, and in 2023 from 14.31ºC to 41.29ºC.

CHAPTER V

5. CONCLUSION AND RECOMMENDATION

5.1. Conclusion

Satellite data serve for various purposes, including LU/LCC detection and environmental management initiatives. Landsat imagery can explore the interactions of land use and land cover and assess the spatial and temporal patterns of LST. This study utilized images from Landsat TM 5 and Landsat 8(OLI/TIRS) to assess and investigate how changes in land use and land cover affect land surface temperature. Information derived from land surface temperature and LU/LC, obtained through this data, is crucial for tracking activities performed by humans and changes to the environment. The study demonstrated that Landsat imagery is highly effective for quantifying and mapping changes in LU/LC, as well as surface temperature (LST), the Normalize Vegetation Index (NDVI), the Normalized Difference Built-up Index (NDBI), the Normalized Difference Bareness Index (NDBaI), and the Normalized Difference Water Index (NDWI) in Addis Ababa including Sheger city. It was found that the LU/LC dynamics in the area are influenced by socio-economic and natural factors over time and across different Area. Among the various classes, water bodies, forests, and wetland exhibit the lowest LST values, while built-up areas, bare lands, and croplands shrub lands record the highest values. In the study area, land-use and land-cover have undergone changes over time. These changes in LU/LC affect the local surface temperatures (LST). Observations from each year indicate that both the minimum and maximum LST have risen. Therefore, the calculated LST plays a crucial role in identifying influence of land-use and land-cover change on the area's temperature conditions. The study revealed an upward trend in the LST of Addis Ababa including Sheger city across the years 1991, 2001, 2013, and 2023. This increase attributed to changes in LU/LC, human activities and climate variability within the city. Notably, the LST showed significant fluctuations among various LU/LC class. Furthermore, the LST measurements extracted from satellite imagery closely matched the temperature data interpolated from nearby weather stations. The NDVI, NDBI, NDBaI, and NDWI values derived from satellite data serve as reliable indicators of the LST status in the study area. Consequently, GIS and RS data explore the variations in LST across different LU/LC classes demonstrates that it offers a rapid and cost-effective method, with the benefit of encompassing a vast area.

5.2. Recommendation

This research aimed to evaluate the impact of LU/LC transformations on LST in Addis Ababa including Sheger City, using Landsat images from the years 1991, 2001, 2013, and 2023. The findings indicated that various shifts between LU/LC types for instance, from forest land to farmland or from farmland to built-up areas resulted in differing LST values for each classes. Despite this, some changes were found to positively influence LST. Menagesha Suba and Entoto Park positively influenced the low LST value. Consequently, this study has led to the following recommendations.

- Both governmental and non-governmental organizations should consider land use and land cover changes when developing effective land use management and environmental control strategies.
- Conservation efforts need to be implemented in both rural and urban green spaces within the study area.
- It is advisable to plant more trees and green spaces, particularly in areas with extensive development and bare land.
- The Green Legacy Initiative has been instrumental in reducing Land Surface Temperature (LST) and enhancing greenery, the government should expand these activities by engaging the community.
- The findings from this study can be utilized as a resource for future researchers interested in exploring the impact of LU/LCC on environmental concerns, in addition to the connections between NDVI, NDBI, NDBaI, NDWI, and LST.

REFERENCES

Alemayehu Mengistu (2008). Climate variability and change in the Ethiopian Journal of Animal Production, 8, (1), 94 to 98.

Aires, F., Prigent, C., Rossow, W. B., and Rothstein, M (2001). A new neural network method that incorporates an initial estimate for the retrieval of atmospheric Water Vapor, cloud liquid water path, surface temperature, and emissivity over land from satellite micro wave observations Journal of Geophysical Research: Atmospheres, 106(D14), 14887-14907

Asubonteng, K.O. (2007) Locating areas of significant change in land use and cover in the Ejisu-Juabeng Woreda, Ghana. Published by the International Institute for Geo-Information Science and Earth Observation in Enschede, Netherlands.

Becker and Li (1990) towards a local Split window method over land surface, published in Remote Sensing, 11, (3), 369-393.

Billah, M., & Rahman, G. A. (2004) land cover mapping of Khulna city using remote sensing techniques. In Proceedings of the 12th international conference on geoinformatics Sweden: Geospatial information Research: Bridging the Pacific and Atlantic, Unversity of Gavle, 707–714.

Bonini, M., Corti, G., Innocenti, F., Manetti, P., Mazzarini, F., Abebe, t., & Pecskay, Z. (2005). Evolution of the Main Ethiopian Rift in the Context of Afar and Kenya rifts propagration. Tectonic, 24, TC1007.

Burgan, R. E., & Hartford, R.A. (1993). Satellite data for monitoring vegetation greenness.

Burriugh, P.A. (1990). Principles of geographic information systems. Oxford University Press, UK. (p. 333)

Buyadi, S. N. A., Mohd, W.M. N. W., and Misni, A. (2013) Effect of land use changes on the surface temperature distribution of the area surrounding the National Botanic Garden, Shah Alam. Procedia-Social and Behavioral Sciences. 101, 516-525.

Chen, X. (2000). Analyzing land cover change and its impacts on regional sustainable development using RS and GIS. International Journal of Remote Sensing, 23(1), 107–113.

Coppin, P. R., & Bauer, M. E. (1996). Digital Change detection in forest ecosystems with remote sensing imagery. Remote sensing Reviews, 13(3-4),207-234.

Central Statistical Agency. (2007). Summary and statistical report of the population and housing census. Addis Ababa, Ethiopia.

Dash, P., Göttsche, F. M., Olesen, F. S., & Fischer, H. (2002). Theory and practice of land surface temperature and emissivity estimation from passive sensor data: current trends. International Journal of Remote Sensing, 23(13), 2563-2594.

Di Gregorio, A., & Jansen, L. J. (2000). Land cover classification: classification concepts and user manual. Rome: Food and Agriculture Organization (FAO) of the United Nations.

Emilio, C. (2008). The Role of Satellite remote sensing in monitoring the global environment. Department of Geography, University of Alkala, Spain. 1-2.

FAO/UNEP. (1999). Terminology for integrated resources planning and management. Food and Agriculture Organization/United Nations Environmental Program. Rome, Italy and Nairobi, Kenya.

Farooq, A. (2012). Landsat ETM+ and MODIS EVI/NDVI data products for climate variation and Agricultural measurements in Holliston Desert. Global Journal of Humanities, social Science: Geography and Environmental Geosciences, 12(13), 111.

Foresman, T. W. (ED.). (1998). The history of geographic information systems: Perspectives from the pioneers. Prentice Hall. From satellites: status and future prospects. Remote Sensing Review, 12, 175–223.

Gallo, K. P., McNab, A. L., Karl, T. R., Brown, J. F., Hood, J. J., & Tarpley, J. D. (1993). The use of NOAA AVHRR data for assessment of the urban heat island effect. Journal.

Gebrekidan, W. (2016, September 23-24). Modeling land surface temperature from satellite data: the case of Addis Ababa. Paper presented at the Eastern Africa Education GIS Conference, Africa Hall, United Nations Conference Center, Addis Ababa. Journal of Applied Meteorology, 32(5), 899-908.

Guha, S., Govil, H., & Mukherjee, A. (2017). A comparative study of land use and land cover change in Kuhar Michael and Lenche Dima of Blue Nile and Awash Basins, Ethiopia. Journal of Environmental Studies, 12(3), 94–98.

Gumindoga, W. (2010). Hydrologic impact of land use change in the upper Gilgel Abay River Basin, Ethiopia: TOPMODEL Application (Doctoral dissertation, M.Sc. Thesis, ITC Netherlands).

Hardegree, L. C. (2006). Spatial Characteristics of the Remotely sensed Surface Urban Heat Island in Baton Rouge, LA: 1988-2003 (Doctoral dissertation).

Houghton, R.A. (1994). The global scale of land use change. BioScience, 44(5), 305-313.

Hulley, G. C., Hughes, C. G., and Hook, S. J. (2017). Quantifying the surface temperature of urban heat islands in Los Angeles using a helicopter-borne thermal infrared hyperspectral scanner. Remote Sensing, 9(10), 1030.

Jiang, J., & Guangjin, T. (2010). Analysis of the impact of land use land cover change on land surface temperature with remote sensing. Procedia Enviromental Sciences, 2, 571-575.

Jin, M., & Dickinson, R. E. (2010). Benefitting from the strengths of satellite observations: land surface skin temperature climotology. Environmental Research Letters, 5(4), 044004.

Kayet, N., Pathak, K., Chakrabarty, A., and Sahoo, S. (2016). Spatial impact of land use land cover change on land surface distribution in Saranda Forest, Jharkhand. Modeling Earth system and environment, 2(3), 1-10.

Kern, A. (2011). Deriviving Normalized Difference Vegetation Index from MODIS and AVHRR remote sensing data (Doctoral dissertation, Eotvos Lorand University).

Khin, M. Y., Shin, D. Y., Park, J. J., & Choi, C. C. (2012). Land surface temperature changes due to land use changes in the inlay Lake area, Myanmar. Department of Spatial Information Engineering Pukyong National University, South Korea.

Kuenzer, C., & Dech, S. (2013). Thermal Infrared Remote Sensing: Sensors, Methods, Applications. Springer Science & Business Media.

Kumar, R., & Singh, S. (2016). Correlation between change detaction analysis and land surface temperature retrieval in the Uttrakhand Region: A Case Study. Imperical Journal of interdisciplinary Research, 2(9).

Lambin, E. F., Turner, B. L., Geist, H. J., Agbola, S. B., Angelsen, A., Bruce, J.W., George, P. (2001). Moving beyond the myths: the causes of land-use and land cover change. Global Enviromental Change, 11(4),261-269.

Li, Z.-L., Tang, B.-H., Wu, H., Ren, H., Yan, G., Wan, Z., Tringo, I. F., & Sobrino, J.A. (2013). Satellite derived land surface temperature: current status and Perspectives. Remote Sensing of Environment, 131, 14-37.

Lillesand, T., Kiefer, R. W., & Chipman, J. (2014). Remote sensing and image Interpretation. New Delhi: John Wiley and Sons.

Liu, L., & Zhang, Y. (2011). Urban heat island analysis using Landsat TM and ASTER data: a case study in Hong Kong. Remote Sensing, 3(7), 1535-1552.

Ma, Y., Kuang, W., and Huang, N. E. (2010). The empirical mode decomposition method: A new approach to nonlinear and non- stationary data modeling. Advances in Adaptive Data Analysis, 1(4), 609-637.

Mallick, J., Kant, Y., & Bharath, B. D. (2008). Estimation of land surface temperature over Delhi using Landsat-7 ETM+. Journal of the indian society of remote sensing, 36(3), 289-296.

McFeeters, S. K. (1996). The delineation of open water features using the Normalized Difference Water Index (NDWI). International journal of remote sensing, 17(7), 1425-1432.

Shahid, L. Md. (2014). Land surface temperature retrieval if Landsat 8 data using split window algorithm: a case study of Ranchi Woreda. International journal of engineering Development and Research, 2(4), 3840–3849.

Mildrexler, D. J., Zhao, M., & Running, S. W. (2011). The cooling effect of forests: global comparison between station air temperatures and MODIS land surface temperatures. Journal if Geophysical research: Bio geosciences, 116(G3).

Mather, A. S., & Needle, C. L. (2000). The relationships between population and forest trends. The Geographical Journal, 166(1), 2–13.

Meyer, W. B., & Turner, B. L. (1992). Human population growth and global changes in land use and land cover. Annual review of ecology and systematics, 23(1),39-61.

Naissan, O.W., & Lily, T. (2016). Effects of climate change on skin. Dermatology News USA. Aesthetic Dermatology.

Nuruzzaman, M. (2015). A Review of urban heat island: causes, effect, and mitigation Measures. International journal of environmental monitoring analysis, 3(2),67.

Nunes, M.C., Vasconcelos, M. J., Penreira, J. M., Dasgupta, N., Alldredge, R. J., and Rego, F.C. (2005). Land cover type and fire in portugal: Selective burning of land cover by fires. Land scape Ecology, 20(6), 661-673.

Oluseyi, I. O., Danlami, M.S., & Olusegun, A.J. (2011). Managing land use transformation and land surface temperature change in Anyigba Town, Kogi State, Nigeria. Journal of Geography and Geology, 3(1), 77.

Orsolya, G., Zalan T., & Boudewijn V.L. (2016). Satellite-based analysis of surface urban heat Island intensity. Journal of environmental Geography, 9(2), 23-30

Paramasivam, C.R. (2016). Remote sensing and Spectral studies of magnesite mining area in Salem, India. Doctoral dissertation, Periyar University, Salem, India.

Peng, S., Piao, S., Ciais, P., Friedlingstein, P., Ottle, C., Breon, F.-M., Nan, H., Zhou, L., & Myneni, R. B. (2012). Surface urban heat island across 419 global Big cities. Environmental Science & Technology, 46(2), 696-703.

Prata, A. J., & Caselles, V. (1995). Thermal remote sensing of land surface temperature.

Rajeshwari, A., and Mani, N. D. (2014). Using Landsat 8 data, Rajeshwari and Mani estimated the land surface temperature of Dinfigul Woreda. International Journal of Research in Engineering and Technology, 3(5), 122–126.

Ratner, B. (2009). The range of the correlation coefficient values: Do they really range between +1 and −1? Journal of Targeting, Measurement and Analysis for Marketing, 17(2), 139-142.

Schwarz, N., Lautenbach, S., and Seppelt, R. (2011). Exploring indicators to quantify surface urban heat Islands in European cities using MODIS land Surface temperatures. Remote Sensing of Enviroment, 115(12), 3175-3186.

Sobrino, J. A., Jiménez-Muñoz, J. C., and Paolini, L. (2004). Retrieval of land surface temperature using Landsat TM 5. Remote Sensing Of Environment, 90(4), 434-440.

Stathopoulou, M., and Cartalis, C. (2009). An application to major cities in Greece: daytime Urban Heat Islands form Landsat ETM+ and corine land cover data. Solar Energy, 83(10), 1871-1883.

Streutker, D. R. (2003). Growth of Houston's urban heat island as measured by satellite. Remote Sensing of Environment, 85(3), 282-289.

Tran, H., Uchihama, D., Ochi, S., & Yasuoka, Y. (2006). Using multi-temporal satellite data to assess urban environmental changes: A study on urban heat islands and vegetation comfort indices in Bangkok, Thailand. Remote Sensing of Environment, 100(3), 387-398.

Voogt, J. A. (2002). Hotter cities: Urban heat island. American Scientist, 90(1), 36-43.

Walsh, C. L., Dawson, R. J W., Barr, S. L., Bristow, A. L., and Tight, M.R (2011). Evaluation of urban Climate Change Mitigation and adaptation strategies. Proceeding of the institution of Civil Engineers - Urban design and Planning, 164(2), 7584.

Weng, Q., Lu, D., and Schubring, J. (2004). For urban heat island studies, the relationship between land surface temperature and vegetation abundance was estimated. Remote sensing of Environment, 89(4), 467-483.

Yue, W., Xu, J., Tan, W., and Xu, L. (2007). Application of remote sensing in examining the relationship between NDVI and Land surface temperature using shanghai Landsat 7 ETM+ data. International journal of remote Sensing, 28(15), 3205-3226.

Zha, Y., Gao, J., Jiang, J., Lu, H., and Huang, J. (2003). The Normalized Difference Haze Index (NDHI): A novel spectral index designed for urban air pollution monitoring. International Journal of Remote Sensing, 33(1). 309- 321

Li, Z., & Zhang, J. (2012). Urbanization's impact on the urban heat island effect. Environmental Research Letters, 14(3), 123-135.

Zubair, A. O. (2006). Change detection in land use/land cover using remote sensing data and GIS: A case study of llorin and its environments in kwara State. University of Ibadan, Department of Geography.

APPENDICES

Appendix 1: Accuracy Assessment Sample Points.

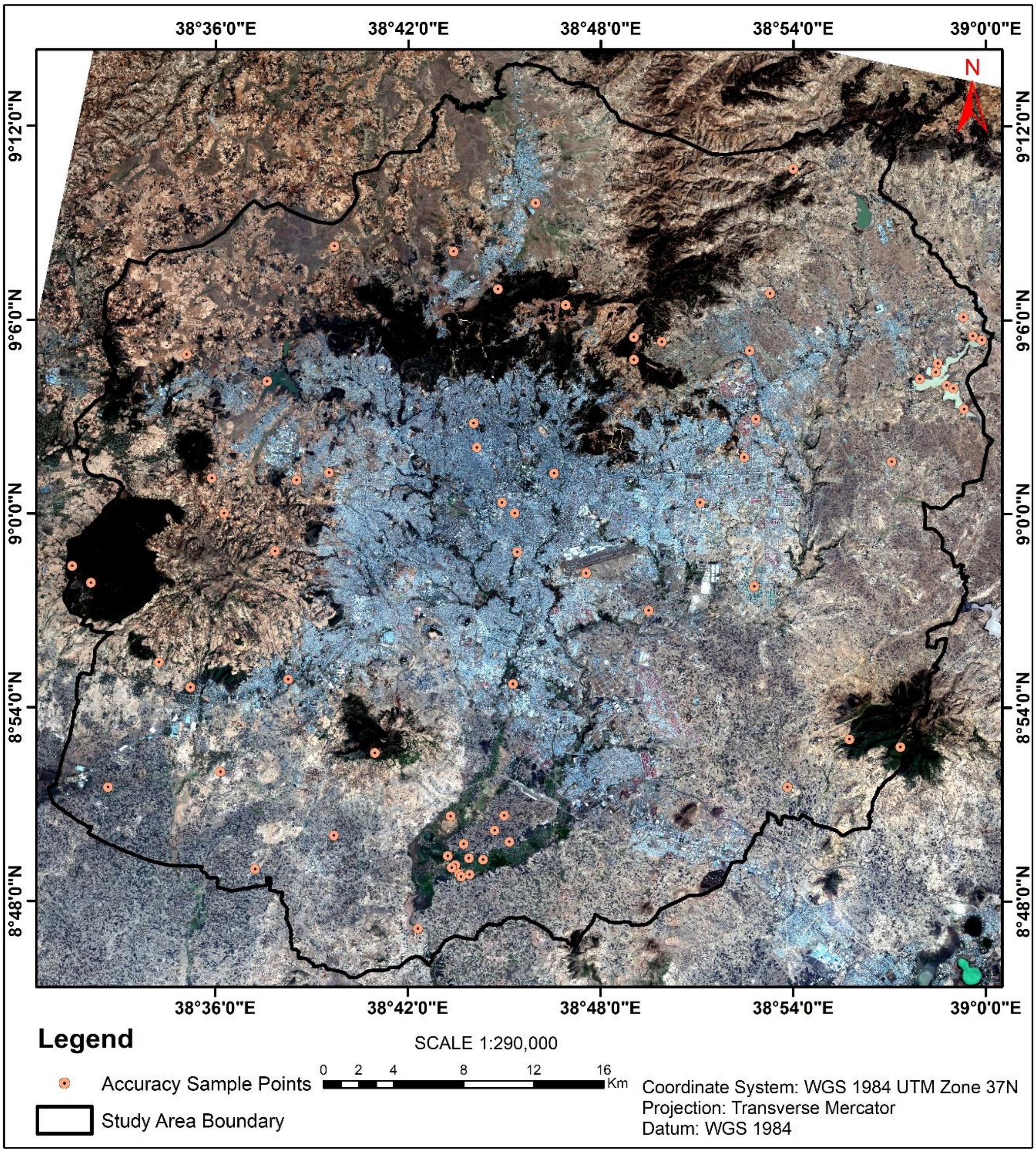

Appendix 2: Sample Points taken for Correlation.

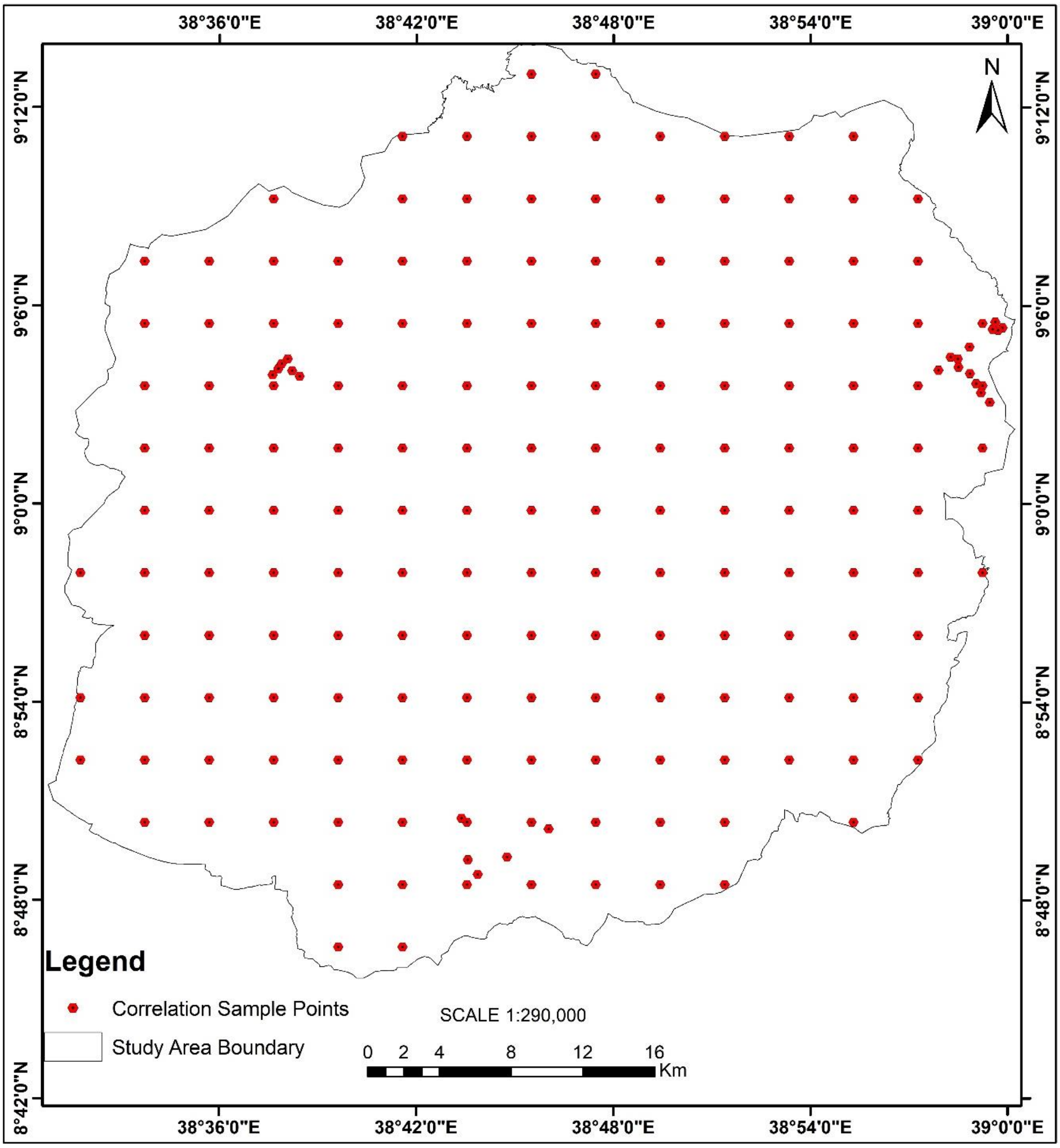

Appendix 3: Meteorological Stations Locational Map.

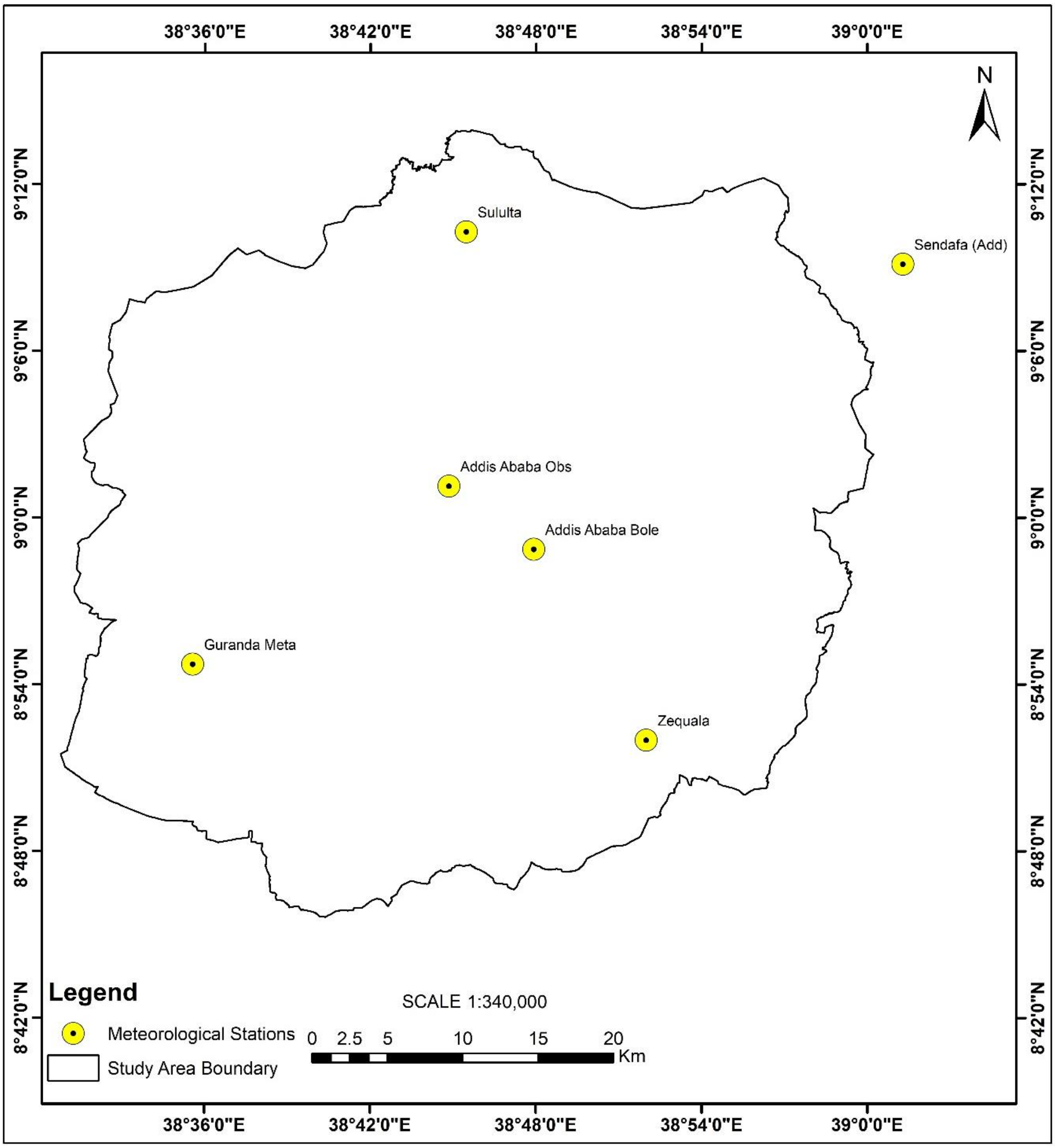

Appendix 4: Sample of different Land use Land Cover image.

Bare Land

Forest Land

Built-Up Area

Shrub Land

Crop Land

Water Body

Wet Land